Membrane Interactions with Membrane Type 1 Matrix Metalloproteinase: Structural Determination Through NMR Directed Studies

A Dissertation presented to the

Faculty of the Graduate School

University of Missouri-Columbia

In Partial Fulfillment

Of the requirements for the Degree

Doctor of Philosophy

By

TARA MARCINK

DR. STEVEN R. VAN DOREN, Dissertation Supervisor

May 2018

The undersigned, appointed by the Dean of the Graduate School, have examined the dissertation entitled

Membrane Interactions with Membrane Type 1 Matrix Metalloproteinase: Structural Determination Through NMR Directed Studies

Presented by Tara Marcink,

a candidate for the Doctor of Philosophy degree,

and hereby certify that, in their opinion, it is worthy of acceptance

_____

Professor Steven R. Van Doren

_____

Professor Lesa Beamer

_____

Professor Peter Cornish

_____

Professor George Davis

ACKNOWLEDGEMENTS

I would like to thank my mentor and principal investigator Dr. Steven Van Doren. He has been supportive of my research and in particular my freedom of scientific expression. He believed in me when I didn't believe in myself. He is very patient, understanding and always available to talk with. It is because of his teaching and work ethic that I have been granted a bright future that I am proud of.

I would like to thank Dr. Linda Randall who has been the most supportive person in my scientific career and personal life thus far. Her poise and approachability have meant everything to me. During some of the hardest times, I have sat down with her and we worked through it together. I can only hope that someday I will have an impact on someone the way she has with me.

I would like to thank my committee members Dr. Peter Cornish and Dr. George Davis for all the insightful and challenging conversation. In particular, I would like to thank Dr. Lesa Beamer who has given me constructive feedback on my work and has always listened to me when I needed someone to talk with.

I would like to thank everyone who has helped me on this MT1-MMP project. Dr. Gregg Fields provided both financial and scientific support for this project. I am extremely grateful to him for the opportunity to work in such an amazing field. Dr. Yingchu Zhao's help with MMP prep and her insight into the MMP field was invaluable. Jayce Simoncic has helped me with fluorescence-based assays. Anna Knapinska provided the data for collagenolysis assays with a triple helical peptide mimic. Dr. Bo An and Dr. Barbara Brodsky provided the bacterial collagen used in my bacterial collagen assays.

I would like to thank Dr. Tommi White for helping me learn the challenging technique of electron microscopy. Her personality and passion are contagious. She has opened the world of scientific possibilities and my career path has since been altered thanks in part to her.

I would like to thank the NMR staff, Dr. Shaokai Jiang and Dr. Wei Wycoff for all their help with my NMR setup and discussions. They were invaluable in my NMR studies.

I want to thank Matt Stanley for his help my molecular dynamics setup on the university computer cluster.

I am appreciative for the members of my lab. Rama Koppisetti and Dr. Steve Prior have been a source of inspiration challenging my ideas and execution. Their contributions have impacted my career development in protein purification and molecular dynamics. Thanks to Dr. Yan Fulcher for all her help and for our wonderful conversations we have had over the years.

Last but not least, I would like to thank my spouse, Jackie Marcink, for encouraging me in every part of this wonderful journey. My kids, Elias and Evie, for giving me the drive needed to finish and succeed. My family has been my rock and my strength and without them, this dream would not have been possible. We got each other so we got this!

This Research was supported by NIH grants R01 GM057289 and CA098799

TABLE OF CONTENTS

LIST OF FIGURES

LIST OF TABLES

LIST OF ABBREVIATIONS

AFM	atomic force microscopy
CMC	critical micelle concentration
CSP	chemical shift perturbation
Col	collagen
CPMG	Carr-Purcell-Meiboom-Gill
DHPC	1,2-diheptanoyl-sn-glycero-3-phosphocholine
DMPC	1,2-dimyristoyl-sn-glycero-3-phosphocholine
DPPC	1,2-dipalmitoyl-sn-glycero-3-phosphocholine
ECD	extracellular domain
ECM	extracellular matrix
EGFR	epidermal growth factor
FID	free induction decay
FRET	Förster resonance energy transfer
GPI	glycosylphosphatidylinosital
HPX	hemopexin-like domain
IANBD	N,N'-dimethyl-N-(iodoacetyl)-N'-(7-nitrobenz-2-oxa-1,3-diazol-4-yl)ethylenediamine
LMC	lipid membrane cage
LUV	large unilamellar vesicles
MD	molecular dynamics
MSP	molecular scaffolding protein

MMP	matrix metalloproteinase
MT1-MMP	membrane type 1 matrix metalloproteinase
MUV	medium-sized unilamellar vesicles
NMR	nuclear magnetic resonance
PC	phosphatidylcholine
PE	phosphatidylethanolamine
ppm	parts per million
PRE	paramagnetic relaxation enhancement
PRO	propeptide domain of MMPs
Scl2	*Streptococcal* collagen-like protein 2
SDFL	site-directed fluor labeling
SDS-PAGE	sodium dodecyl sulfate polyacrylamide gel electrophoresis
sMT1-MMP	water-soluble MT1-MMP without its transmembrane helix
SUV	small unilamaller vesicle
TIMP	tissue Inhibitor of metalloproteinases

ABSTRACT

Membrane type 1 matrix metalloproteinase (MT1-MMP) is essential to a myriad of extracellular activities including tumor cell migration and angiogenesis. At the cell surface, MT1-MMP is a major factor in the proteolysis of receptors, growth factors, and collagen. MT1-MMP extracellular domains bind the cell surface which can be influential in bringing these complexes together. This study uses new techniques to uncover the interactions between MT1-MMP and the cell surface. Described here is the development of techniques in protein and lipid preparations, NMR data acquisition, and structure determination by molecular dynamics simulations. Through these methods, the HPX domain was shown to bind nanodiscs by opposing tips of blade II and blade IV. The protruding part of these tips contain an EPGYPK sequence that are seen dipping into the membrane surface making contact with the lipid head groups. Blade IV membrane binding allows collagen to bind unhindered. Both blade II and blade IV membrane binding structures are shown to be favorable for homodimerization without disruption of the collagen binding site. The catalytic domain is shown to at least transiently bind membranes. This study then hypothesizes and discusses how these interactions impact both future peripheral protein membrane interaction studies and uncover similarities between the MMP family.

I. INTRODUCTION

I:1 THE MATRIX METALLOPROTEINASE FAMILY

I.1.1 Overview

Matrix metalloproteinases (MMPs) are involved in the degradation of the extracellular matrix (ECM) along with proteolysis of ECM related proteins. The ECM is important during cell development and morphogenesis (1). Proteolysis of the ECM allows for cellular migration and modification of signaling molecules (2). MMP substrates, found in the ECM, include, tyrosine kinase receptors, chemokines, peptide growth factors, MMPs, fibronection (3-6).

Although MMPs have proteolytic activity on ECM components, this is not their only function (7). Furthermore, all MMP's contain zinc at their active site and can be inhibited by EDTA along with at least one of the tissue inhibitor of metalloproteinases (TIMPs) (8,9). MMPs can have additional inhibitors such as RECK and alpha2-macroglobulin. MMPs are subdivided into 5 distinct groups: stomelysins, matrilysins, gelatinases, collagenases, and membrane-bound MMPs in which Membrane Type 1 Matrix Metalloproteinase (MT1-MMP), the focus of this study, belongs to (10).

I.1.2 Structural Comparison of MMPs

Matrix metalloproteinases have been studied since the early 1960's with the first biochemical characterization of an MMP from amphibian tissues occurred in 1962 (11,12). Since then it has been discovered that all MMPs are multidomain proteins that start out as zymogens containing at least a zinc dependent catalytic and propeptide (PRO) domain. This PRO domain is cleaved upon activation of the catalytic domain. Most MMPs also contain a hemopexin-like domain (HPX) used in recognition of binding partners. Membrane MMPs have either a single helix spanning transmembrane domain or a glycosylphosphatidylinosital (GPI) anchored domain that tethers the protein to the plasma membrane (Fig I.1A).

There are 6 membrane-bound MMPs that are bound to the cell surface through either through a GPI anchor (MMP -17, -25) or a single spanning transmembrane domain (MMP -14, -15, -16, -24). There is a flexible linker 1 that connects the catalytic and HPX domains along with a linker 2 between the HPX and Transmembrane domains in membrane bound MMPs (Fig I.1B) (13). The transmembrane spanning MMPs share a similar extracellular domain structure as MT1-MMP (fig I.1B).

I.1.3 Sequence Similarity

MMPs share high similarity in their overall structure and primary sequence. In regard to both the catalytic and HPX domain, there is high similarity in the fold when comparing solved structures. In the catalytic domain there is low sequence variability in the active site cleft where the activating zinc atom is coordinated by

three histidines in all structures (Fig 1.2). The active site accommodates a side chain of the many substrates including collagen. The active site size varies between MMPs and helps in substrate specificity (14). While the active site is conserved, the flanking regions have higher variability in residue sequence (Fig I.2).

The hemopexin domain, connected to the catalytic domain by a flexible linker, is composed of a four-bladed propeller structure (15) (Fig. I.2). The hemopexin domain has higher residue variability compared to the catalytic domain and therefore has been targeted for therapeutic selection (16-18) (Fig I.2). Interactions of the HPX domains of MMP-1 (19), MMP-2 (20), MMP-9 (18), and MT1-MMP (21) with the cell surface proteins, such as CD44 or Integrin, indicate a possibility for cell surface localization. MMP-3 (22) and MT1-MMP (23) have also been shown to internalize into the cell, making their way to the nucleus as transcription factors. These MMPs can potentially use the HPX domain interaction with the cell surface as part of the internalization mechanism.

I.2 MT1-MMP

I.2.1 MT1-MMP Role on the Cell Surface

Membrane-type 1 Matrix metalloproteinase (MT1-MMP) is highly expressed in many cell lines and has been implicated in cancer metastasis, angiogenesis, skeletal development and inflammation (24). MT1-MMP drives this cell invasion through activation of proteolytic proteins such as CD44, MMP-2, and MMP-9 (25),(26) (fig I.3). During cell invasion, MT1-MMP is trafficked from late endosomes

to the invadopodia by way of association with phospatidic acid, Phospholipase D_2, and Kinesin-1 (27). MT1-MMP localizes in lipid rafts that are required for invadopodia formation (28). In particular, cholesterol depletion leads to a loss of lipid rafts along with delocalization of MT1-MMP at the invadopodia (29).

I.2.2 Homodimerization of MT1-MMP

Homodimerization of the hemopexin-like domain is required for *in vivo* activation, although the dimer is not readily formed *in vitro* (30). It has been proposed that the transmembrane or cell surface interaction with the cytoplasmic domain is required for dimerization (31). Furthermore, MT1-MMP dimerization and activity was thought to be controlled by cytoskeleton actin reorganization (32) but it is found to be active in exosomes degrading type-1 collagen and activating MMP-2 (33). Despite the lack of actin skeleton, exosomes have the similar lipid raft composition as the lamellipodia (34) where MT1-MMP associates with and is found to interact with lipids that induce cell migration (35) suggesting a lipid dependence on activation. Exosomes help in cell communication, ECM degradation, and have been implicated in the progression of cancer (36). In these processes, MT1-MMP is an integral component degrading the ECM while activating proteins such as MMP-2 (Fig I.4). MT1-MMP in exosomes make their way to ECM through internalization from the surface, trafficked from the Golgi by VAMP3 trafficking or incorporation into late endosomes and released upon binding at the plasma membrane (Fig I.4).

I.2.3 Hemopexin-Like Domain of MT1-MMP

The hemopexin domain of MT1-MMP is of particular interest due to its interaction with multiple binding partners along with having a higher sequence variability among the MMP family compared with the catalytic domain. CD44 has been shown to interact with blade 1 (37) while collagen has been more recently shown to bind between blades 1 and 2 (38). Single chain antibody fragments that target the hemopexin-like domain have reduced the metastasis rate of the cell suggesting a vital role of the hemopexin domain in cancer metastasis (17). Identification of binding sites where the hemopexin-like domain binds membranes would enhance our understanding of the local environment at the cell surface. To study the HPX domain bound to membranes, advanced membrane mimics and NMR techniques were implemented.

I.3 MEMBRANE MIMICS

I.3.1 Overview

Membrane proteins account for around one-third of the human genome code making them an important area of interest (39). These membrane proteins are involved a multitude of pathological processes including transient receptor potential channels and MT1-MMPs role in cancer (40,41), aquaporin's role in cataracts (42) and the CGRP proteins role in headaches (43) just to name a few. For this reason, many membrane-bound and peripherally bound proteins are becoming targets for drug design.

There are many options in membrane mimetic for structural studies including micelles, bilayered micelles (bicelles), nanodiscs, and liposomes (Fig I.5). Shape, curvature, thickness and dielectric constant are just a few of the conditions that determine a binding orientation during structural data collection (44). For example, the dynamics and rigidity of the loops of the integral membrane protein OmpX change upon the addition of micelles (45), bicelles (46), or nanodiscs (47). Discussed here are the three main types of membrane mimics used in the HPX membrane interaction studies.

I.3.2 Small Unilamaller Vesicles

Small Unilamaller Vesicles (SUVs) are spherical vesicles comprised of one or a more combinations of lipids. SUVs have a diameter of up to 100 nm similar to exosomes. These are formed by hydration and either sonication or extrusion methods. SUVs have been used to determine structural information of protein membrane complexes such as cytochrome C membrane interactions (48). SUVs are relatively easy to prepare in large quantities compared to other membrane mimics. For this reason, they are readily used in biochemical assays to help identify binding orientations and affinity of proteins for the membrane (46,49,50).

I.3.3 Bicelles

Phospholipids assemble into bilayer aggregates but are normally far too large for structural studies by NMR. Bicelles consist of long chain phospholipids in

combination with lipids that have both hydrophilic head and hydrophrobic tail regions (amphiphiles). Together these create a disk like shape more suitable for NMR when the ratio of long chain phospholipids to amphiphile (q) factor is below 0.5. These isotropic bicelles reorient themselves on an NMR timescale due to their fast tumbling time. The stability of bicelles in solution is temperature and ionic strength dependent. It has been previously found that DMPC/DHPC bicelles are stable from pH 4.0 – 7.0 (51,52).

Bicelles have been used extensively to solve structures of membrane bound proteins (53-56). Bicelles with very large q-factor magnetically align in the presence of an external magnetic field through which a protein's axis of symmetry in relation to the membrane mimic can be found. This can help determine orientation angles of the protein inserted in the membrane or bound to the surface. Using paramagnetic relaxation enhancement NMR, two peripheral proteins structures have been identified using low q-factor bicelles (46,49). These structures where determined using a DPPC containing a nitroxide probe embedded into a DMPC/DHPC bicelle.

I.3.4 Nanodiscs

Nanodiscs were first characterized by Atomic Force Microscopy (AFM) in the late 1990s (57) and have since then become recognized as highly suitable for membrane protein interactions (58-60). Nanodiscs are composed of two copies of helical membrane scaffold proteins (MSPs) and one or more lipids (61). After self-

assembly, higher aggregates of nanodiscs can be easily removed through size-exclusion. Monodisperse nanodiscs can be made in high enough yields for most biochemical approaches (62).

Nanodiscs can be used in many techniques including electrochemistry, single molecule studies (63), X-ray crystallography (64), electron microscopy (65), and NMR (66) to name a few. Nanodiscs have an advantage over other techniques through their unique MSP protein bound around the edges. This protein is stable at higher temperatures keeping the bilayer shape better than bicelles, SUVs, or micelles. The nanodisc also removes the use of a detergent as in bicelles leading to higher protein stability. The length of the MSP protein directly impacts the diameter of the nanodisc (67) and this allows for precise control over the size of the experiment. Due to these advantages, the nanodisc is a more robust and stabilizing method for protein characterization on the membrane. In particular, NMR methods combined with nanodiscs are allowing for better characterization of membrane bound proteins (66,68,69).

NMR is a precise tool to study dynamics and structure for many of these membrane protein complexes. As a non-invasive technique, proteins and lipid interactions can be probed and understood without perturbing the sample. NMR has the power to elucidate structural and dynamic information of these complexes but is limited by the membrane mimic and protein complex size. Advances in NMR techniques, along with enhancements to membrane mimics have led to more precise membrane protein characterization and one of these advances is discussed here.

I.4 TECHNICAL NMR BACKGROUND

I.4.1 NMR Basics

To determine 3D structures at near atomic or atomic resolution there are only 3 techniques: Nuclear magnetic resonance (NMR) along with X-ray crystallography and cryo-electron microscopy. Since the 1940s NMR has been utilized not only for structure determination but for its powerful application in dynamic and kinetic studies, including the first few NMR studies of an MMP (70-72)

I.4.2 NMR signal

Nuclei that have an odd number of protons, such as ^{1}H, ^{13}C, ^{15}N, ^{19}F among others, produce a non-zero spin that are detected in a magnetic field. In the presence of a magnetic field (B_0) the energy levels of the nuclei undergo Zeeman splitting into high and low energy fields (Fig I.6B) and is described by:

$$\Delta E = h\upsilon = \frac{h\gamma B_0}{2\pi} \qquad \text{Equation I-1}$$

where B_0 is the magnetic field strength, γ is the gyromagnetic ratio, h is Planck's constant, and υ is the Larmor precession frequency. Applying a radiofrequency magnetic field perpendicular to B_0 and the magnetic dipole moments of spins aligned with it, results in the precession of the spins of these nuclei around the magnetic field (Fig I.6A). Once the radiofrequency light is turned off, the magnetization starts decaying back to zero. This change is recorded on the NMR instrumentation and produces a time-dependent sinusoidal free induction decay

(FID). This time domain data can be transformed into a signal in the frequency domain I through Fourier transformation. This is a procedure where the intensity and frequency of each sinusoidal signal is converted into a peak in the NMR spectrum (73). This signal contains chemical shift (peak position), line width, and peak intensity information (Fig I.6C).

I.4.3 Chemical Shift

Along with the external B_0 field, the local electronic environment creates a local magnetic environment that opposes the direction of the applied magnetic field. which is known as shielding and is described by equation I.2:

$$\omega_{obs} = \gamma B_0(1 - \sigma) \qquad \text{Equation I.2}$$

where σ describes the amount of shielding. The shift caused by this environment is what gives rise to the chemical shift. This measurement is independent of the magnetic field and is expressed in parts per million (ppm) relative to a reference standard and described by:

$$\delta = 10^6 \frac{\upsilon - \upsilon_{ref}}{\upsilon_{ref}} \qquad \text{Equation I.3}$$

Chemical shift, δ, is independent of the magnetic field and is represented as a dimensionless quantity, i.e. as a ratio. The chemical shift provides useful nucleus-specific information and can be used as a probe due to its high dependence on the local electromagnetic environment. This can be used, for example, to observe conformational changes in a protein's structure upon ligand and biomolecular interactions (74,75).

I.4.4 Multidimensional NMR

The peaks of individual nuclei can be resolved and enhanced by using more than one dimension. To obtain a 2D spectrum, a transfer from one nucleus to another needs to occur. This is accomplished through a mixing period added in the pulse sequence. After an initial excitation pulse, there is an evolution period where transverse magnetization evolves from both chemical shift and scalar coupling. A mixing period precedes the evolution period and allows for a transfer of magnetization between spins connected to each other through bond or nearby spatially. After the mixing period, an FID is recorded as a function of T_2. Repeating this at equally spaced time intervals of t_1 creates a matrix of FIDs of both the t_1 and t_2 time domains. A Fourier transform of this 2D matrix will correlate the spins in mixing times resulting in coordinated spectral peaks in the two dimensions at the frequency of each nuclear spin (Fig I.6C).

I.4.5 Spin Relaxation

There are two types of spin relaxation that occur in NMR. Spin-lattice relaxation (T_1 or longitudinal relaxation) results from the return to equilibrium at the Larmor precession frequency in the direction of the magnetic field. Transverse relaxation (T_2 or spin-spin relaxation) is a description of the decay of the excited magnetization perpendicular to the applied magnetic field. T_2 occurs from

molecular motions in transient magnetic fields and also coupling constants or chemical shifts from chemical exchange. Any variation in magnetic fields occurring from T_1 relaxation also affects T_2 relaxation but the inverse is not true. This relationship can be exploited to determine protein spherical shape through the determination of rotational correlation time (τ_c) (76,77). Relaxation techniques can also be used to study protein motions through incorporation of paramagnetic compounds causing increased relaxation effects.

I.4.6 Local Environment Changes Upon Macromolecular Associations

An interaction of proteins with other molecular structures often changes the local environment of residues. Being sensitive to local nuclei changes, NMR can be used to understand these interactions through changes in chemical shift or spin relaxation alter the peak location and intensities in the spectra. These interactions can cause chemical exchange.

Chemical exchange is the process where a nucleus can exchange between different environments resulting in NMR relaxation, scalar coupling and/or chemical peak shift (78). This occurs either as a chemical reaction or conformational change. This change is dependent on the time scale of chemical shift differences, which ranges in the milliseconds. For reactions at equilibrium in which the sum of the forward and backward reaction rates is slower than the chemical shift difference, the system is seen as slow exchange and two distinct peaks in the spectra can be seen. If the opposite is true, this is referred to as fast exchange and only one signal will be seen at the average frequency weighted in

proportion to the amount of the two states. If the sum of the forward and backward reaction rates is similar to the chemical shift difference, spectral line widths become larger due to corresponding short t_2 values, a situation known as intermediate exchange

I.4.7 Paramagnetic Relaxation

Paramagnetic relaxation occurs from the larger magnetic moments of unpaired electrons effects on the local fields of a nuclei through its isotropic g-tensor (79). Paramagnetic relaxation effects can occur up to 25 Å for nitroxide labels and up to 35 or 40 Å for lanthanides such as Gd^{3+}. The distance r is between the unpaired electron and nucleus of interest. The strength of the paramagnetic relaxation is inversely proportional in an r^6. This is further described by:

$$r_2 = \frac{K}{r^6}\left(4\tau_c + \frac{3\tau_c}{1+\varpi_h^2\tau_c^2}\right) \qquad \text{Equation I.4}$$

where ϖ_h is the Larmor frequency, K is a collection of physical constants and τ_c is the rotational correlation time (80). This creates an experimental opportunity to measure long-range distances.

Incorporation of a paramagnetic probe can occur from nitroxide spin radicals or metal chelators. Previously, a metal chelator (Gd-EDTA) was used to broaden away surface exposed residue peaks leaving binding site residues unaffected due to their distance from the probe (81). Incorporation of a metal chelator with a disulfide bridge to cysteine residues helped uncover dynamic motions in a protein structure (82). MTSL, a nitroxide spin radical, helped

determine how proteins fold (83). More recently, a nitroxide labeled lipid has been used to determine binding orientations of peripheral proteins bound to membrane mimics (46,49) through the incorporation of a novel pulse sequence.

I.4.8 Paramagnetic Relaxation Enhancement

The paramagnetic relaxation rate (Γ_2) is a measurement of the difference between the T_2 rate without and with the paramagnetic probe and can be described as:

$$\Gamma_2 = R_{2,para} - R_{2,dia} \qquad \text{Equation I.5}$$

Where $R_{2,dia}$ is the diamagnetic state rate and $R_{2,para}$ is the paramagnetic state rate. This equation cancels out all relaxation mechanisms other than the enhanced relaxation from the electron magnetic moment.

PRE-measurements are commonly taken as a method using just the diamagnetic and paramagnetic two-time point approach. This required no fitting and yielded 4 different NMR peak intensities: $I_{dia}(T_a)$, $I_{dia}(T_b)$, $I_{para}(T_a)$, and $I_{para}(T_b)$. Using these, the paramagnetic rate can be calculated as follows:

$$\Gamma_2 = R_{2,para} - R_{2,dia} = \frac{1}{T_b - T_a} ln \frac{I_{dia}(T_b) I_{para}(T_a)}{I_{dia}(T_a) I_{para}(T_b)} \qquad \text{Equation I.6}$$

and the errors propagated in Γ_2 can be calculated by:

$$\sigma(\Gamma_2) = \frac{1}{T_b - T_a} \sqrt{\left\{\frac{\sigma_{dia}}{I_{dia}(T_a)}\right\}^2 + \left\{\frac{\sigma_{dia}}{I_{dia}(T_{ab})}\right\}^2 + \left\{\frac{\sigma_{para}}{I_{para}(T_a)}\right\}^2 + \left\{\frac{\sigma_{para}}{I_{para}(T_b)}\right\}^2} \qquad \text{Equation I.7}$$

where standard deviations from spectral noise in both the diamagnetic and paramagnetic spectra are defined as σ_{dia} and σ_{para} respectively (79).

Visualization of this enhanced decay can be seen in Fig I.7 where residues close to the paramagnetic probe have larger decay rates compared to diamagnetic sample (fig I.7A). In residues identified far away from the probe, there is no difference in the decay rates of the two samples (fig I.7B).

A further enhancement to the PRE data acquisition is the Carr-Purcell and Meiboom-Gill pulse sequence (CPMG), which is used to measure relaxation times effectively. The original Carr-Purcell sequence starts with a polarized 90° pulse with refocusing 180° pulses spaced by a time interval. The CPMG sequence was built upon the original Carr-Purcell sequence and eliminated the amplitude adjustment of the 180° pulses by introducing a 90° phase shift of the first 90° pulse (84). After the refocusing is complete, the signal can be measured (fig I.8). The additional acquisition of spectra at multiple time points allows for better accuracy in determining the decay rates of residues.

I.5 CONCLUSION

This CPMG train has helped the NMR community to uncover dynamic and distance-dependent information on proteins and complexes with lipids, proteins, ligands, and DNA (38,49,85,86). Furthermore, incorporating these techniques into the developments in membrane mimic systems has paved the way to uncover interactions between proteins and the membrane surface.

I.6 FIGURES

Figure I.1 Overall MMP family structure and the structure of MT1-MMP

(A) Overall structural representation of the MMP family grouped by each member's domain similarities. Each member of the MMP family has at least a PRO and Catalytic domain. (B) The extracellular structure representation of MT1-MMP. Catalytic and HPX domains were obtained from crystal structures and collagen binding site is modeled in on the HPX according to previous NMR based experiments (38). The transmembrane domain is connected by a linker at the c-terminal end of the HPX domain. (Panel A used with permission from Parks, W. C., Wilson, C. L., & Lopez-Boado, Y. S., 2004) (87).

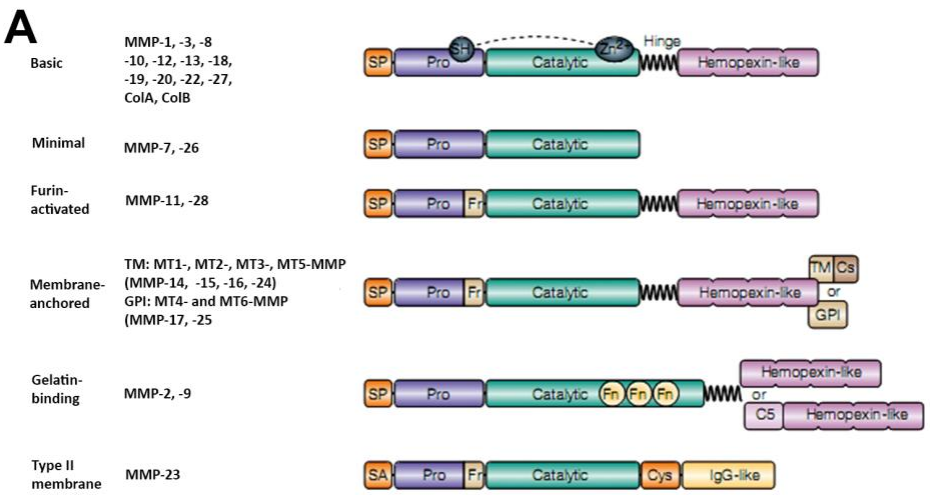
A
Basic
MMP-1, -3, -8
-10, -12, -13, -18,
-19, -20, -22, -27,
ColA, ColB
SP
Pro
SH
Zn2+
Catalytic
Hinge
Hemopexin-like
Minimal
MMP-7, -26
Furin-activated
MMP-11, -28
Fr
Membrane-anchored
TM: MT1-, MT2-, MT3-, MT5-MMP
(MMP-14, -15, -16, -24)
GPI: MT4- and MT6-MMP
(MMP-17, -25
TM
Cs
or
GPI
Gelatin-binding
MMP-2, -9
Fn
C5
Type II membrane
MMP-23
SA
Cys
IgG-like

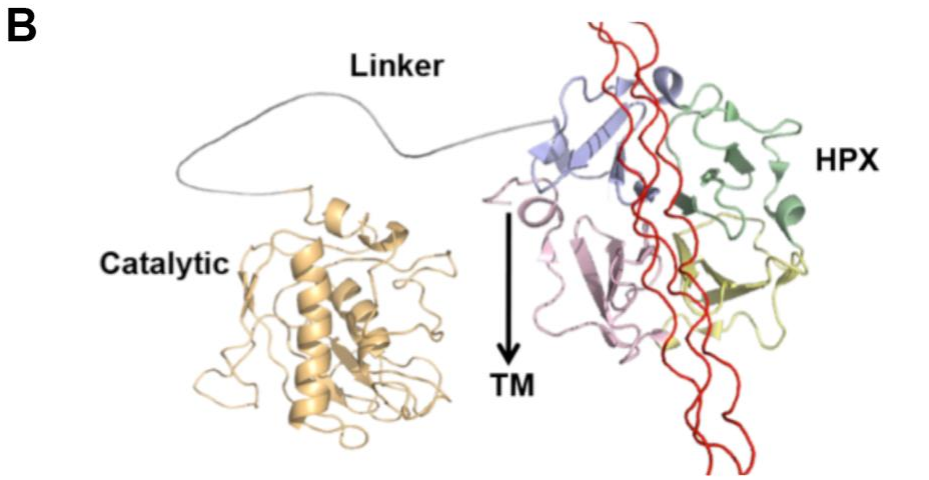
B
Linker
HPX
Catalytic
TM

Figure I.2 Evolutionary Trace of both the catalytic and HPX domain of MT1-MMP.

The Evolutionary Trace was performed through the Litcharge Lab's online ETserver at http://lichtargelab.org/software/ETserver. 202 and 213 sequences were used for the evolutionary trace alignment of the HPX and catalytic domains of MT1-MMP respectively. The sites of high ET coverage are more unique to MT1-MMP while the less sequence variability between MMPs is seen at the low ET percent coverage.

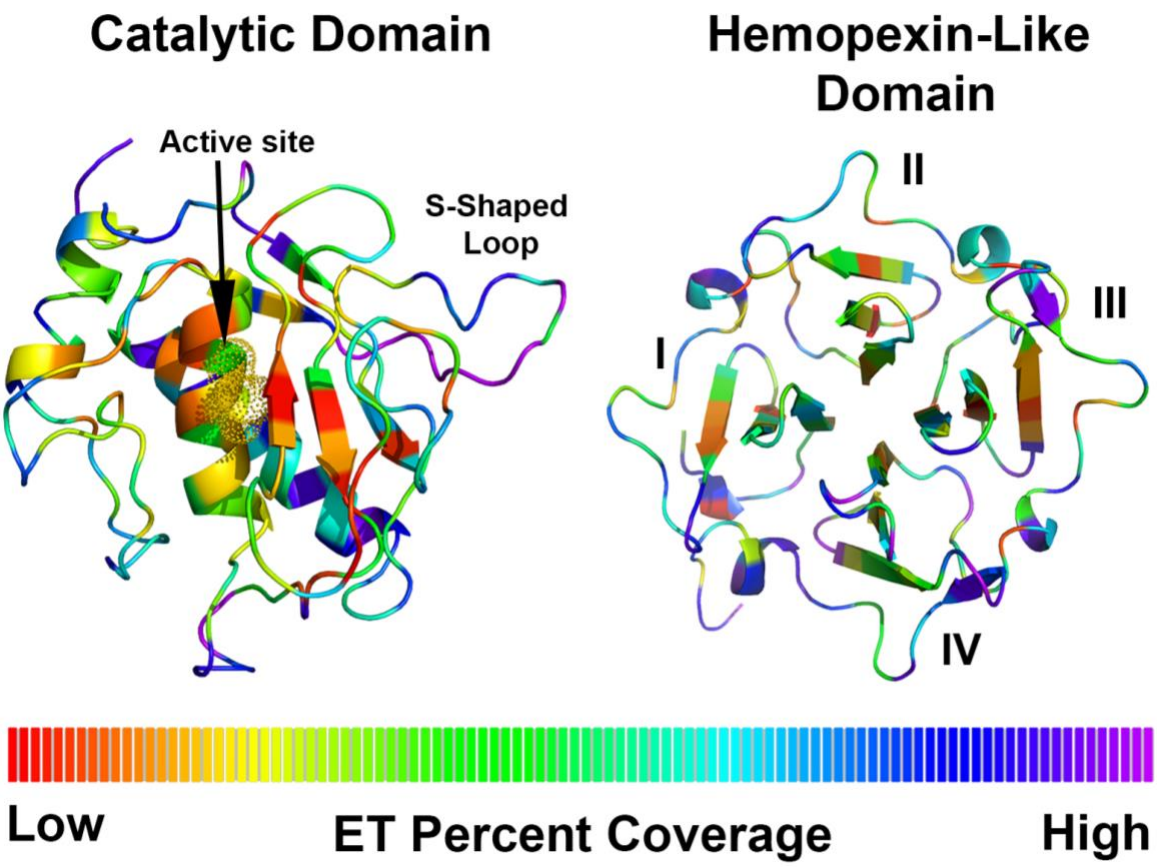

Figure I.3 Various MT1-MMP functions at the cell surface.

MT1-MMP is involved in a multitude of functions on the plasma membrane. Interactions include shedding of CD44, Activation of ProMMP-2, proteolysis of collagen, and internal cell signaling. All of these interactions help advance cell invasion through the ECM. (Figure used with permission from Itoh, Y. and M. Seiki, 2006) (88).

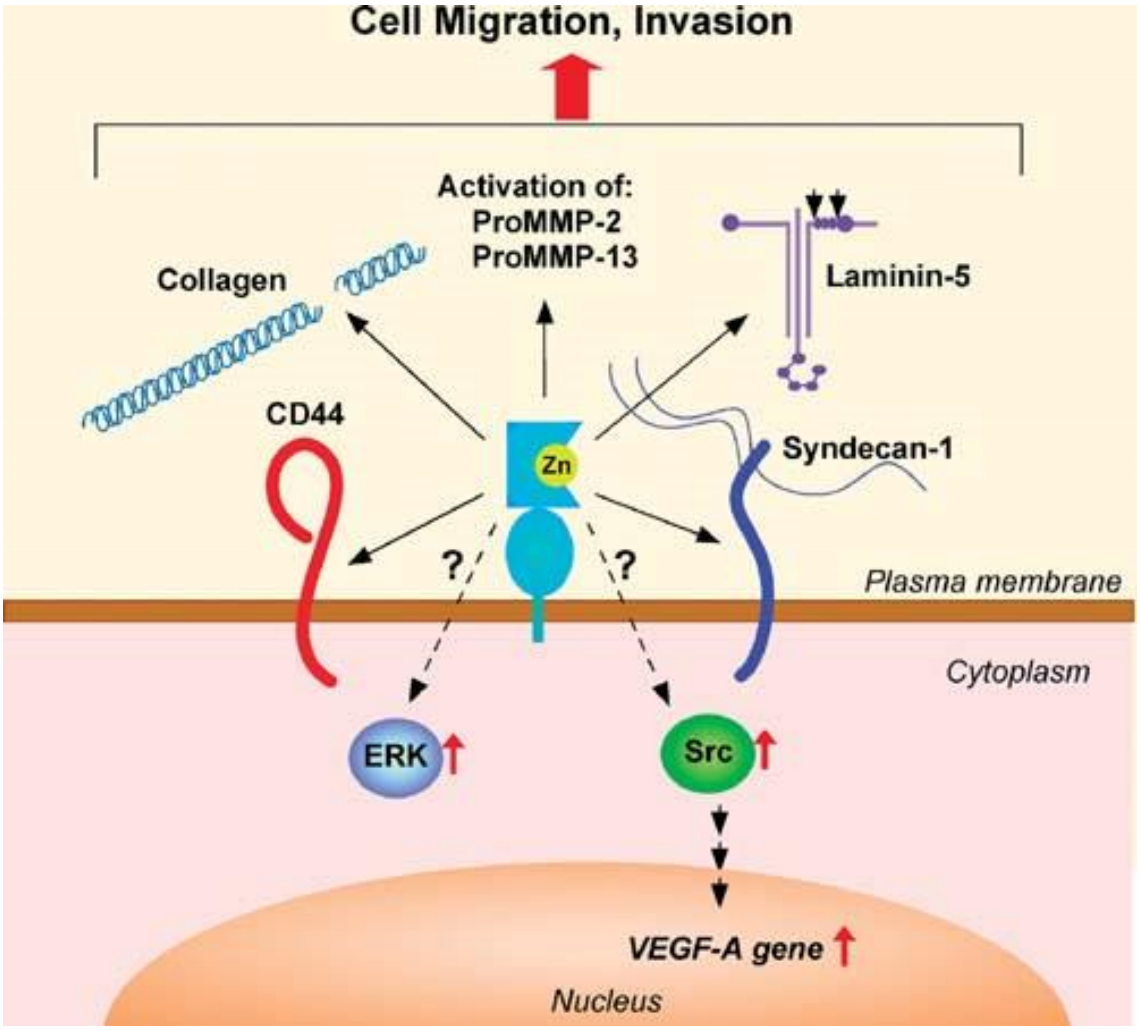

Figure I.4 MT1-MMP's role in exosomal formation and movement

MT1-MMP is found in exosomal vesicles where it has been seen activating MMP-2 and cleaving collagen. MT1-MMP is trafficked in exosomes either by VAMP3 mediated trafficking or incorporation into late endosomes which eventually release exosomes into the extracellular matrix environment. (Figure used with permission from Shimoda, M. & Khokha, R., 2017) (89)

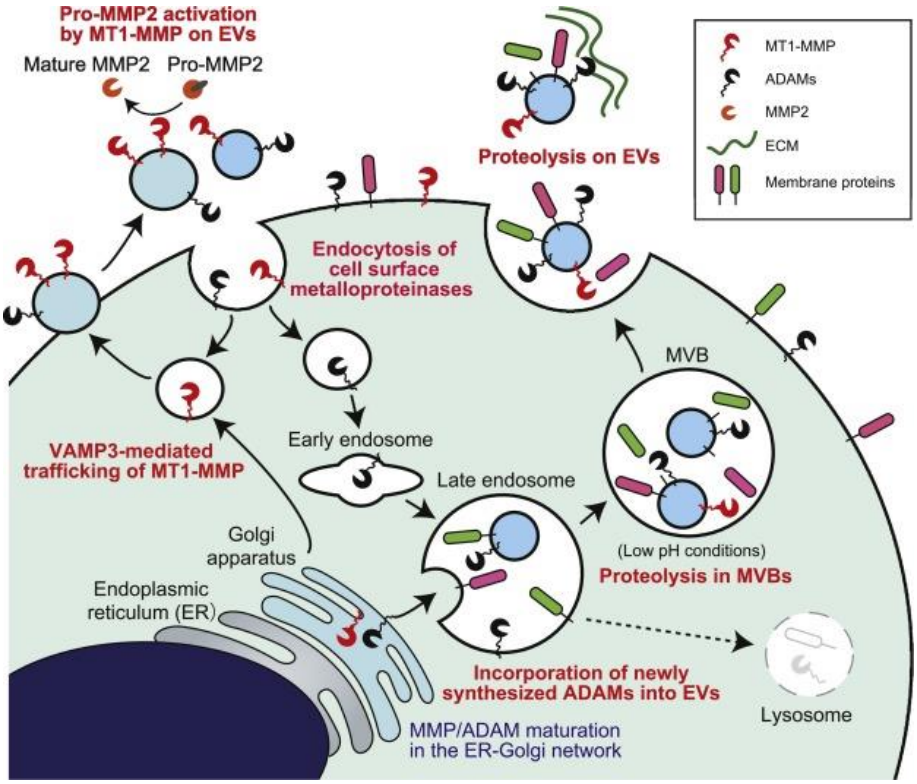
Pro-MMP2 activation
by MT1-MMP on EVs
Mature MMP2
Pro-MMP2
Proteolysis on EVs
MT1-MMP
ADAMs
MMP2
ECM
Membrane proteins
Endocytosis of
cell surface
metalloproteinases
MVB
Early endosome
VAMP3-mediated
trafficking of MT1-MMP
Late endosome
Golgi
apparatus
(Low pH conditions)
Proteolysis in MVBs
Endoplasmic
reticulum (ER)
Incorporation of newly
synthesized ADAMs into EVs
Lysosome
MMP/ADAM maturation
in the ER-Golgi network

Figure I.5 Overview of membrane mimics used in NMR studies.

Of these 4 variations of membrane mimics, this current study used nanodiscs for a majority of the project (90). Liposomes were used in biochemical assays throughout this project.

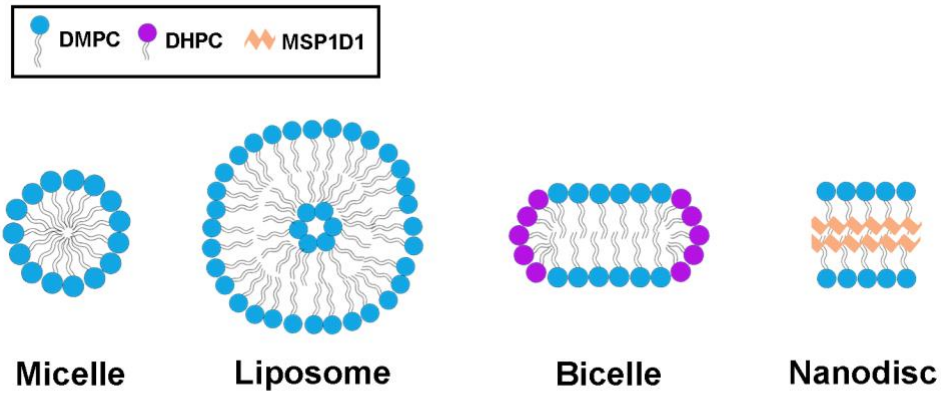

Figure I.6 The Principle of NMR

(A) When protons are placed in a high magnetic field, there magnetic poles align in relation to the magnetic field (H_o) where a radiofrequency pulse is applied, and the resulting pulse is recorded. (B) In the high energy states, they align against the magnetic field and in the low energy states they align with the magnetic field and this difference along with chemical shifts produce different signals. (C) Using a TROSY pulse sequence that applies this radiofrequency pulse along with a transfer of magnetization by another pulse results in a complex output signal (FID). This complex FID can then be Fourier transformed into a 2D spectrum.

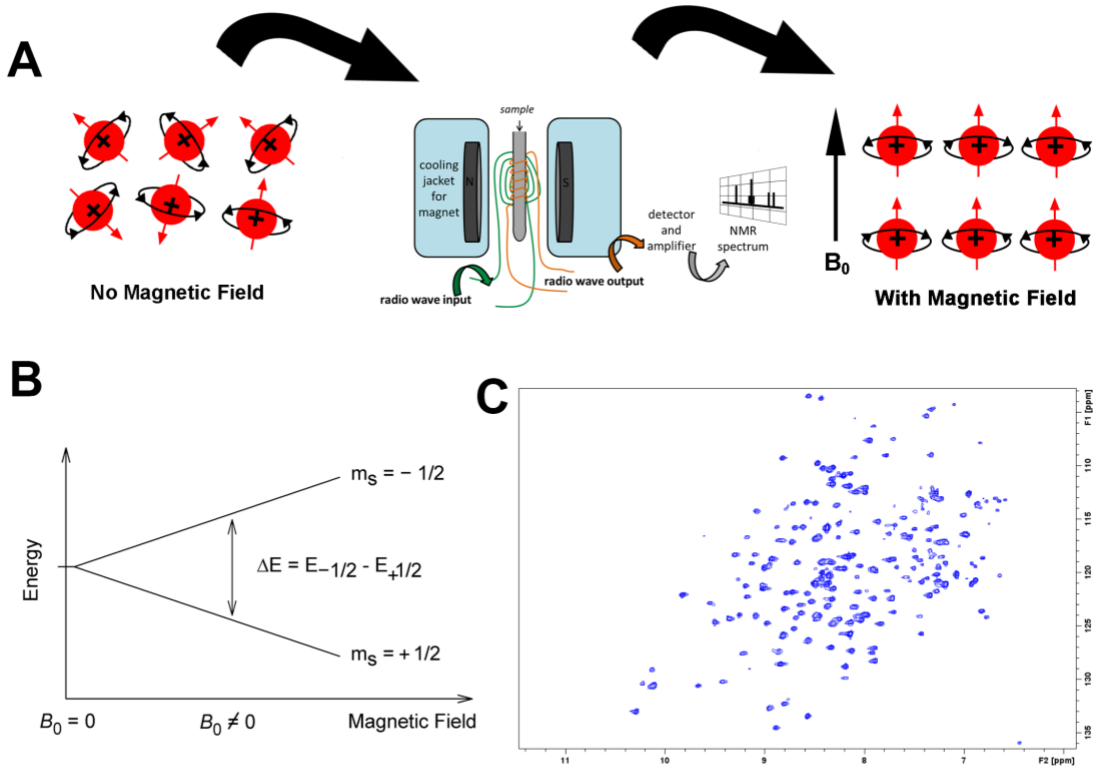

Figure I.7 Paramagnetic relaxation enhancement (PRE) distance dependent effects

(A) Representative PRE and diamagnetic decay curves for a residue in close proximity (X) or distal (Y) from an unpaired electron probe (B) Representation of the proximity of a residue to an unpaired electron lipid probe (green and red spheres) buried in the membrane (grey sticks). For a residue in location X there is a larger decrease in the paramagnetic decay compared to the diamagnetic decay. The opposite is shown where a residue near location Y does not experience the unpaired electron's effects on its decay rate.

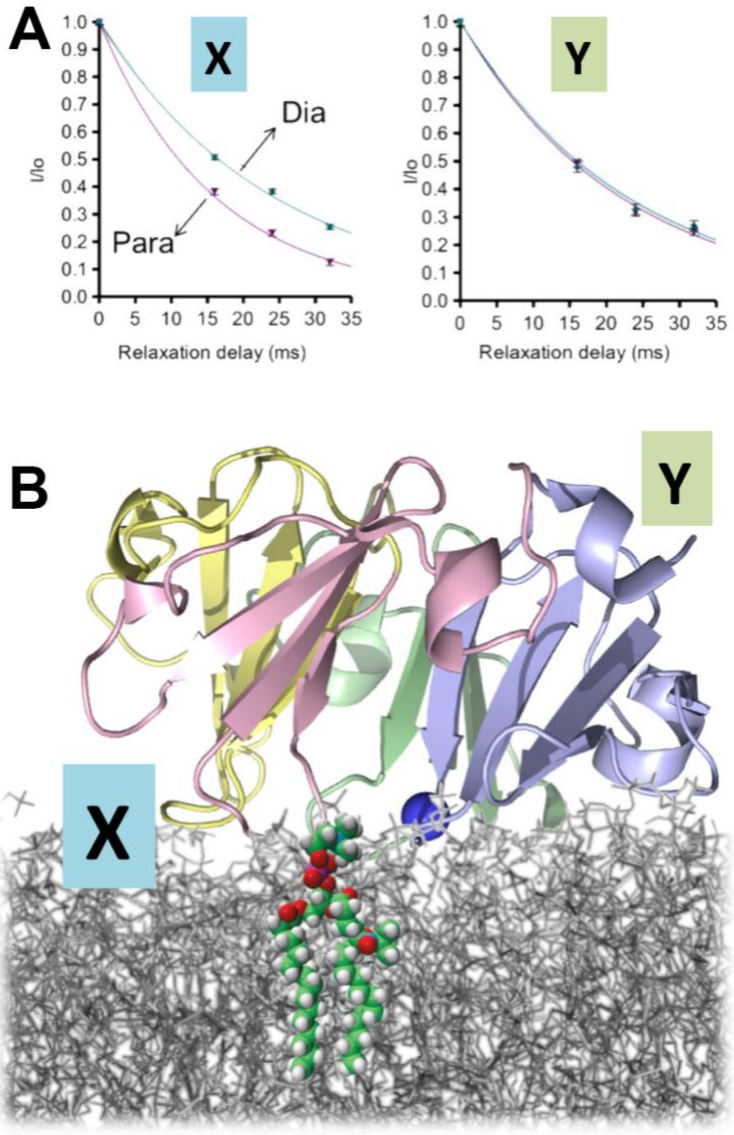

Figure I.8 Basics of the CPMG pulse train, which is used below for measuring PREs

The CPMG pulse sequence is a 90° pulse followed by dephasing period. After this period (τ), a 180° pulse is applied to refocus the signal. After rephrasing (2τ), the NMR signal can be measured. Relaxation delays can be extended by (2τ) through the addition of multiple 180° pulses. Measurement of the residue peak heights of each individual experiment at different CPMG pulse train lengths can then be plotted to obtain a decay curve of each residue.
(This figure was used with permission from:
http://perminc.com/resources/fundamentals-of-fluid-flow-in-porous-media/chapter-3-molecular-diffusion/diffusion-coefficient/measurement-techniques/nmr-method/principles-nmr-processing/spin-echo-cpmg-pulse-sequence/)

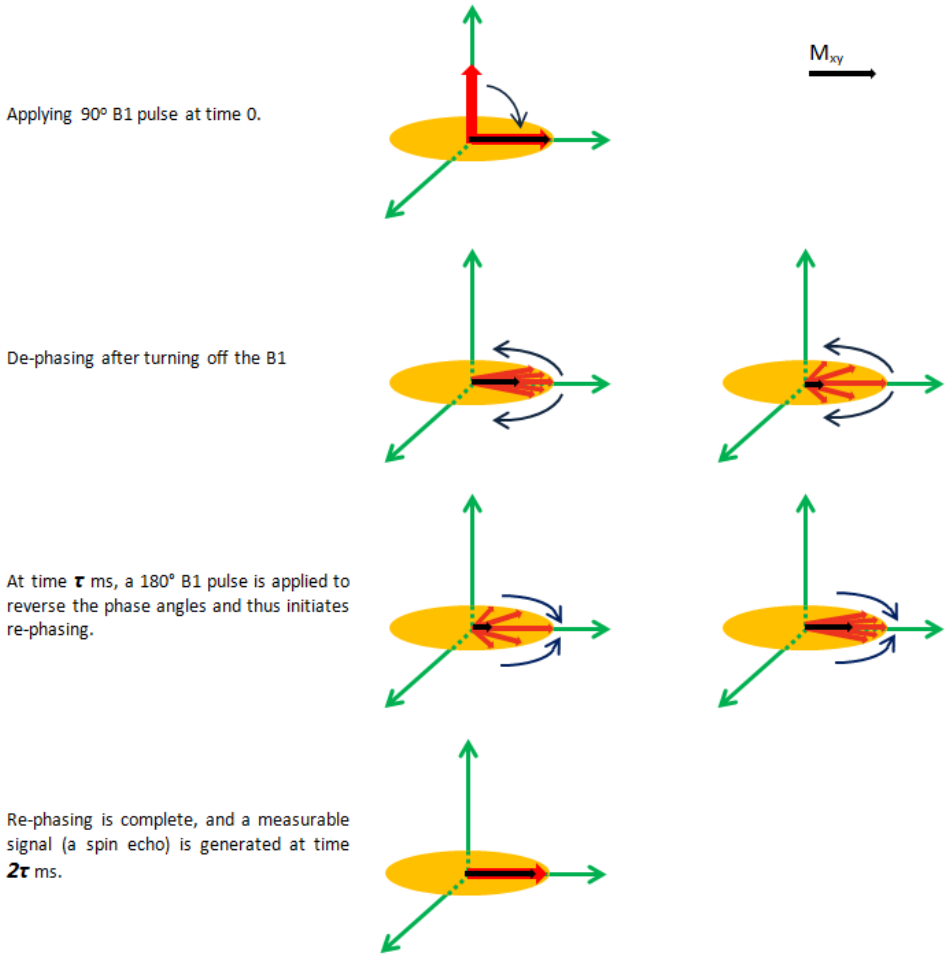

I.6 REFERENCES

1. Willis, A. L., Sabeh, F., Li, X. Y., and Weiss, S. J. (2013) Extracellular matrix determinants and the regulation of cancer cell invasion stratagems. *Journal of Microscopy* **251**, 250-260

2. Sternlicht, M. D., and Werb, Z. (2001) How matrix metalloproteinases regulate cell behavior. *Annu Rev Cell Dev Biol* **17**, 463-516

3. Suzuki, M., Raab, G., Moses, M. A., Fernandez, C. A., and Klagsbrun, M. (1997) Matrix Metalloproteinase-3 Releases Active Heparin-binding EGF-like Growth Factor by Cleavage at a Specific Juxtamembrane Site. *Journal of Biological Chemistry* **272**, 31730-31737

4. Sternlicht, M. D., Bissell, M. J., and Werb, Z. (2000) The matrix metalloproteinase stromelysin-1 acts as a natural mammary tumor promoter. *Oncogene* **19**, 1102-1113.

5. Van Doren, S. R. (2015) Matrix metalloproteinase interactions with collagen and elastin. *Matrix Biol* **44-46**, 224-231

6. Malemud, C. J. (2006) Matrix metalloproteinases (MMPs) in health and disease: an overview. *Front Biosci* **11**, 1696-1701

7. Chakraborti, S., Mandal, M., Das, S., Mandal, A., and Chakraborti, T. (2003) Regulation of matrix metalloproteinases: an overview. *Molecular and cellular biochemistry* **253**, 269-285

8. Woessner, J. F., Nagase, H. (2000) *Matrix Metalloproteinases and TIMPs*, Oxford University Press, New York

9. Iyer, R. P., Patterson Nl Fau - Fields, G. B., Fields Gb Fau - Lindsey, M. L., and Lindsey, M. L. (2012) The history of matrix metalloproteinases: milestones, myths, and misperceptions.

10. Visse, R., and Nagase, H. (2003) Matrix metalloproteinases and tissue inhibitors of metalloproteinases: structure, function, and biochemistry. *Circ Res* **92**, 827-839

11. Gross, J., and Lapiere, C. M. (1962) COLLAGENOLYTIC ACTIVITY IN AMPHIBIAN TISSUES: A TISSUE CULTURE ASSAY. *Proceedings of the National Academy of Sciences of the United States of America* **48**, 1014-1022

12. Nagai, Y., Lapiere, C. M., and Gross, J. (1966) Tadpole Collagenase. Preparation and Purification. *Biochemistry* **5**, 3123-3130

13. Itoh, Y. (2015) Membrane-type matrix metalloproteinases: Their functions and regulations. *Matrix Biol* **44-46**, 207-223

14. Bode, W., Fernandez-Catalan, C., Tschesche, H., Grams, F., Nagase, H., and Maskos, K. (1999) Structural properties of matrix metalloproteinases. *Cell Mol Life Sci* **55**, 639-652.

15. Gohlke, U., Gomis-Ruth, F. X., Crabbe, T., Murphy, G., Docherty, A. J., and Bode, W. (1996) The C-terminal (haemopexin-like) domain structure of human gelatinase A (MMP2): structural implications for its function. *FEBS Lett* **378**, 126-130

16. Andreini, C., Banci, L., Bertini, I., Luchinat, C., and Rosato, A. (2004) Bioinformatic comparison of structures and homology-models of matrix metalloproteinases. *J Proteome Res* **3**, 21-31

17. Basu, B., Correa de Sampaio, P., Mohammed, H., Fogarasi, M., Corrie, P., Watkins, N. A., Smethurst, P. A., English, W. R., Ouwehand, W. H., and Murphy, G. (2012) Inhibition of MT1-MMP activity using functional antibody fragments selected against its hemopexin domain. *Int J Biochem Cell Biol* **44**, 393-403

18. Fields, G. B. (2015) New strategies for targeting matrix metalloproteinases. *Matrix Biology* **44–46**, 239-246

19. Stricker, T. P., Dumin, J. A., Dickeson, S. K., Chung, L., Nagase, H., Parks, W. C., and Santoro, S. A. (2001) Structural analysis of the alpha(2) integrin I domain/procollagenase-1 (matrix metalloproteinase-1) interaction. *J Biol Chem* **276**, 29375-29381

20. Bai, S., Thummel, R., Godwin, A. R., Nagase, H., Itoh, Y., Li, L., Evans, R., McDermott, J., Seiki, M., and Sarras, M. P., Jr. (2005) Matrix metalloproteinase expression and function during fin regeneration in zebrafish: analysis of MT1-MMP, MMP2 and TIMP2. *Matrix Biol* **24**, 247-260

21. Itoh, Y., Ito, N., Nagase, H., Evans, R. D., Bird, S. A., and Seiki, M. (2006) Cell surface collagenolysis requires homodimerization of the membrane-bound collagenase MT1-MMP. *Mol Biol Cell* **17**, 5390-5399

22. Shirvaikar, N., Marquez-Curtis, L. A., Shaw, A. R., Turner, A. R., and Janowska-Wieczorek, A. (2010) MT1-MMP association with membrane lipid rafts facilitates G-CSF–induced hematopoietic stem/progenitor cell mobilization. *Exp Hematol* **38**, 823-835

23. Eguchi, T., Kubota, S., Kawata, K., Mukudai, Y., Uehara, J., Ohgawara, T., Ibaragi, S., Sasaki, A., Kuboki, T., and Takigawa, M. (2008) Novel Transcription Factor-Like Function of Human Matrix Metalloproteinase 3 Regulating the CTGF/CCN2 Gene. *Molecular and Cellular Biology* **28**, 2391-2413

24. Sabeh, F., Shimizu-Hirota, R., and Weiss, S. J. (2009) Protease-dependent versus -independent cancer cell invasion programs: three-dimensional amoeboid movement revisited. *The Journal of Cell Biology* **185**, 11-19

25. Sato, H., Takino, T., Okada, Y., Cao, J., Shinagawa, A., Yamamoto, E., and Seiki, M. (1994) A matrix metalloproteinase expressed on the surface of invasive tumour cells. *Nature* **370**, 61-65

26. Toth, M., Chvyrkova, I., Bernardo, M. M., Hernandez-Barrantes, S., and Fridman, R. (2003) Pro-MMP-9 activation by the MT1-MMP/MMP-2 axis and MMP-3: role of TIMP-2 and plasma membranes. *Biochemical and Biophysical Research Communications* **308**, 386-395

27. Wang, Z., Zhang, F., He, J., Wu, P., Tay, L. W. R., Cai, M., Nian, W., Weng, Y., Qin, L., Chang, J. T., McIntire, L. B., Di Paolo, G., Xu, J., Peng, J., and Du, G. (2017) Binding of PLD2-Generated Phosphatidic Acid to KIF5B Promotes MT1-MMP Surface Trafficking and Lung Metastasis of Mouse Breast Cancer Cells. *Developmental Cell* **43**, 186-197.e187

28. Yamaguchi, H., Takeo Y Fau - Yoshida, S., Yoshida S Fau - Kouchi, Z., Kouchi Z Fau - Nakamura, Y., Nakamura Y Fau - Fukami, K., and Fukami, K. Lipid rafts

and caveolin-1 are required for invadopodia formation and extracellular matrix degradation by human breast cancer cells.

29. Albrechtsen, R., Stautz D, Sanjay A, Kveiborg M , Wewer, U. M. (2015) Extracellular engagement of ADAM12 induces clusters of invadopodia with localized ectodomain shedding activity.

30. Tam, E. M., Wu, Y. I., Butler, G. S., Stack, M. S., and Overall, C. M. (2002) Collagen binding properties of the membrane type-1 matrix metalloproteinase (MT1-MMP) hemopexin C domain. The ectodomain of the 44-kDa autocatalytic product of MT1-MMP inhibits cell invasion by disrupting native type I collagen cleavage. *J Biol Chem* **277**, 39005-39014

31. Itoh, Y., Ito, N., Nagase, H., and Seiki, M. (2008) The second dimer interface of MT1-MMP, the transmembrane domain, is essential for ProMMP-2 activation on the cell surface. *J Biol Chem* **283**, 13053-13062

32. Itoh, Y., Palmisano, R., Anilkumar, N., Nagase, H., Miyawaki, A., and Seiki, M. (2011) Dimerization of MT1-MMP during cellular invasion detected by fluorescence resonance energy transfer. *Biochem J* **440**, 319-326

33. Hakulinen, J., Sankkila, L., Sugiyama, N., Lehti, K., and Keski-Oja, J. (2008) Secretion of active membrane type 1 matrix metalloproteinase (MMP-14) into extracellular space in microvesicular exosomes. *J Cell Biochem* **105**, 1211-1218

34. Skotland, T., Sandvig, K., and Llorente, A. (2017) Lipids in exosomes: Current knowledge and the way forward. *Prog Lipid Res* **66**, 30-41

35. Gingras, D., Michaud, M., Di Tomasso, G., Beliveau, E., Nyalendo, C., and Beliveau, R. (2008) Sphingosine-1-phosphate induces the association of membrane-type 1 matrix metalloproteinase with p130Cas in endothelial cells. *FEBS Lett* **582**, 399-404

36. Sanderson, R. D., Bandari, S. K., and Vlodavsky, I. (2017) Proteases and glycosidases on the surface of exosomes: Newly discovered mechanisms for extracellular remodeling. *Matrix Biology*

37. Mori, H., Tomari, T., Koshikawa, N., Kajita, M., Itoh, Y., Sato, H., Tojo, H., Yana, I., and Seiki, M. (2002) CD44 directs membrane-type 1 matrix metalloproteinase to lamellipodia by associating with its hemopexin-like domain. *Embo J* **21**, 3949-3959

38. Zhao, Y., Marcink, T. C., Sanganna Gari, R. R., Marsh, B. P., King, G. M., Stawikowska, R., Fields, G. B., and Van Doren, S. R. (2015) Transient collagen triple helix binding to a key metalloproteinase in invasion and development. *Structure* **23**, 257-269

39. Fagerberg, L., Jonasson K Fau - von Heijne, G., von Heijne G Fau - Uhlen, M., Uhlen M Fau - Berglund, L., and Berglund, L. (2010) Prediction of the human membrane proteome.

40. Prevarskaya, N., Zhang L Fau - Barritt, G., and Barritt, G. (2007) TRP channels in cancer.

41. Turunen, S. P., Tatti-Bugaeva, O., and Lehti, K. (2017) Membrane-type matrix metalloproteases as diverse effectors of cancer progression. *Biochimica et Biophysica Acta (BBA) - Molecular Cell Research* **1864**, 1974-1988

42. Verkman, A. S., Ruiz-Ederra, J., and Levin, M. H. (2008) Functions of Aquaporins in the Eye. *Progress in Retinal and Eye Research* **27**, 420-433

43. Just, S., Arndt, K., Weiser, T., and Doods, H. (2006) Pathophysiology of migraine: A role for neuropeptides. *Drug Discovery Today: Disease Mechanisms* **3**, 327-333

44. Cross, T. A., Sharma, M., Yi, M., and Zhou, H.-X. (2011) Influence of solubilizing environments on membrane protein structures. *Trends in Biochemical Sciences* **36**, 117-125

45. Lenoir, M., Coskun, U., Grzybek, M., Cao, X., Buschhorn, S. B., James, J., Simons, K., and Overduin, M. (2010) Structural basis of wedging the Golgi membrane by FAPP pleckstrin homology domains. *EMBO Rep* **11**, 279-284

46. Koppisetti, R. K., Fulcher, Y. G., Jurkevich, A., Prior, S. H., Xu, J., Lenoir, M., Overduin, M., and Van Doren, S. R. (2014) Ambidextrous binding of cell and

membrane bilayers by soluble matrix metalloproteinase-12. *Nat Commun* **5**, 5552

47. Frey, L., Lakomek, N.-A., Riek, R., and Bibow, S. (2017) Micelles, Bicelles, and Nanodiscs: Comparing the Impact of Membrane Mimetics on Membrane Protein Backbone Dynamics. *Angewandte Chemie International Edition* **56**, 380-383

48. Da Costa, G., Chevance, S., Le Rumeur, E., and Bondon, A. (2006) Proton NMR Detection of Porphyrins and Cytochrome c in Small Unilamellar Vesicles: Role of the Dissociation Kinetic Constant. *Biophysical Journal* **90**, L55-L57

49. Prior, S. H., Fulcher, Y. G., Koppisetti, R. K., Jurkevich, A., and Van Doren, S. R. (2015) Charge-Triggered Membrane Insertion of Matrix Metalloproteinase-7, Supporter of Innate Immunity and Tumors. *Structure* **23**, 2099-2110

50. Marcink, T. C., Koppisetti, R. K., Fulcher, Y. G., and Van Doren, S. R. (2017) Mapping Lipid Bilayer Recognition Sites of Metalloproteinases and Other Prospective Peripheral Membrane Proteins. in *Matrix Metalloproteases: Methods and Protocols* (Galea, C. A. ed.), Springer New York, New York, NY. pp 61-86

51. Struppe, J., Whiles, J. A., and Vold, R. R. (2000) Acidic phospholipid bicelles: a versatile model membrane system. *Biophysical Journal* **78**, 281-289

52. Glover, K. J., Whiles, J. A., Wu, G., Yu, N., Deems, R., Struppe, J. O., Stark, R. E., Komives, E. A., and Vold, R. R. (2001) Structural evaluation of phospholipid bicelles for solution-state studies of membrane-associated biomolecules. *Biophys J* **81**, 2163-2171

53. Bárány-Wallje, E., Andersson, A., Gräslund, A., and Mäler, L. (2004) NMR solution structure and position of transportan in neutral phospholipid bicelles. *FEBS Lett.* **567**, 265-269

54. Andersson, A., and Maler, L. (2002) NMR solution structure and dynamics of motilin in isotropic phospholipid bicellar solution.

55. Papadopoulos, E., Oglęcka, K., Mäler, L., Jarvet, J., Wright, P. E., Dyson, H. J., and Gräslund, A. (2006) NMR Solution Structure of the Peptide Fragment 1−30,

Derived from Unprocessed Mouse Doppel Protein, in DHPC Micelles. *Biochemistry* **45**, 159-166

56. Cerofolini, L., Amar, S., Lauer, J. L., Martelli, T., Fragai, M., Luchinat, C., and Fields, G. B. (2016) Bilayer Membrane Modulation of Membrane Type 1 Matrix Metalloproteinase (MT1-MMP) Structure and Proteolytic Activity. *Sci Rep* **6**, 29511

57. Carlson, J. W., Jonas, A., and Sligar, S. G. (1997) Imaging and manipulation of high-density lipoproteins. *Biophysical Journal* **73**, 1184-1189

58. Boldog, T., Li, M., and Hazelbauer, G. L. (2007) [14] - Using Nanodiscs to Create Water‐Soluble Transmembrane Chemoreceptors Inserted in Lipid Bilayers. in *Methods Enzymol.* (Melvin I. Simon, B. R. C., and Alexandrine, C. eds.), Academic Press. pp 317-335

59. Kucharska, I., Edrington, T., Liang, B., and Tamm, L. (2015) Optimizing nanodiscs and bicelles for solution NMR studies of two β-barrel membrane proteins. *Journal of Biomolecular NMR* **61**, 261-274

60. Yu, T. Y., Raschle, T., Hiller, S., and Wagner, G. (2012) Solution NMR spectroscopic characterization of human VDAC-2 in detergent micelles and lipid bilayer nanodiscs. *Biochim Biophys Acta* **1818**, 1562-1569

61. Wlodawer, A., Segrest, J. P., Chung, B. H., Chiovetti, R., and Weinstein, J. N. (1979) High-density lipoprotein recombinants: evidence for a bicycle tire micelle structure obtained by neutron scattering and electron microscopy. *FEBS Lett.* **104**, 231-235

62. Denisov, I. G., Grinkova, Y. V., Lazarides, A. A., and Sligar, S. G. (2004) Directed self-assembly of monodisperse phospholipid bilayer Nanodiscs with controlled size. *J Am Chem Soc* **126**, 3477-3487

63. Laursen, T., Singha, A., Rantzau, N., Tutkus, M., Borch, J., Hedegård, P., Stamou, D., Møller, B. L., and Hatzakis, N. S. (2014) Single Molecule Activity Measurements of Cytochrome P450 Oxidoreductase Reveal the Existence of Two Discrete Functional States. *ACS Chemical Biology* **9**, 630-634

64. Rasmussen, S. G. F., Choi, H.-J., Fung, J. J., Pardon, E., Casarosa, P., Chae, P. S., DeVree, B. T., Rosenbaum, D. M., Thian, F. S., Kobilka, T. S., Schnapp, A., Konetzki, I., Sunahara, R. K., Gellman, S. H., Pautsch, A., Steyaert, J., Weis, W. I., and Kobilka, B. K. (2011) Structure of a nanobody-stabilized active state of the β(2) adrenoceptor. *Nature* **469**, 175-180

65. Akkaladevi, N., Mukherjee, S., Katayama, H., Janowiak, B., Patel, D., Gogol, E. P., Pentelute, B. L., Collier, R. J., and Fisher, M. T. (2015) Following Natures Lead: On the Construction of Membrane-Inserted Toxins in Lipid Bilayer Nanodiscs. *J Membrane Biol* **248**, 595-607

66. Zhang, M., Huang, R., Ackermann, R., Im, S. C., Waskell, L., Schwendeman, A., and Ramamoorthy, A. (2016) Reconstitution of the Cytb5-CytP450 Complex in Nanodiscs for Structural Studies using NMR Spectroscopy. *Angew Chem Int Ed Engl* **55**, 4497-4499

67. Bayburt, T. H., Grinkova, Y. V., and Sligar, S. G. (2002) Self-assembly of discoidal phospholipid bilayer nanoparticles with membrane scaffold proteins. *Nano Letters* **2**, 853-856

68. Rouck, J. E., Krapf, J. E., Roy, J., Huff, H. C., and Das, A. (2017) Recent advances in nanodisc technology for membrane protein studies (2012-2017). *FEBS Lett* **591**, 2057-2088

69. Mazhab-Jafari, M. T., Marshall, C. B., Stathopulos, P. B., Kobashigawa, Y., Stambolic, V., Kay, L. E., Inagaki, F., and Ikura, M. (2013) Membrane-dependent modulation of the mTOR activator Rheb: NMR observations of a GTPase tethered to a lipid-bilayer nanodisc. *J Am Chem Soc* **135**, 3367-3370

70. Van Doren, S. R., Kurochkin, A. V., Ye, Q. Z., Johnson, L. L., Hupe, D. J., and Zuiderweg, E. R. (1993) Assignments for the main-chain nuclear magnetic resonances and delineation of the secondary structure of the catalytic domain of human stromelysin-1 as obtained from triple-resonance 3D NMR experiments. *Biochemistry* **32**, 13109-13122

71. Gooley, P. R., Johnson, B. A., Marcy, A. I., Cuca, G. C., Salowe, S. P., Hagmann, W. K., Esser, C. K., and Springer, J. P. (1993) Secondary structure and Zinc Ligation of Human Recombinant Short-Form Stromelysin by Mutidimensional NMR. *Biochemistry* **32**, 13098-13108

72. Moy, F. J., Pisano, M. R., Chanda, P. K., Urbano, C., Killar, L. M., Sung, M. L., and Powers, R. (1997) Assignments, secondary structure and dynamics of the inhibitor-free catalytic fragment of human fibroblast collagenase. *J Biomol NMR* **10**, 9-19

73. Ernst, R. R. (1992) Nuclear Magnetic Resonance Fourier Transform Spectroscopy. *Chem. Int. Ed. Engl.* **31**, 805-930

74. Williamson, M. P. (2013) Using chemical shift perturbation to characterise ligand binding. *Progress in Nuclear Magnetic Resonance Spectroscopy* **73**, 1-16

75. Gobl, C., Madl, T., Simon, B., and Sattler, M. (2014) NMR approaches for structural analysis of multidomain proteins and complexes in solution. *Prog Nucl Magn Reson Spectrosc* **80**, 26-63

76. Kay, L. E., Torchia, D. A., and Bax, A. (1989) Backbone Dynamics of Proteins as Studied by ^{15}N Inverse Detected Heteronuclear NMR Spectroscopy: Application to Staphylococcal Nuclease. *Biochemistry* **28**, 8972-8979

77. Kojima, C., Ono, A., Kainosho, M., and James, T. L. (1999) Quantitative measurement of transverse and longitudinal cross-correlation between 13C-1H dipolar interaction and 13C chemical shift anisotropy: application to a 13C-labeled DNA duplex. *J Magn Reson* **136**, 169-175

78. Čuperlović-Culf, M. (2013) *NMR metabolomics in cancer research*, Woodhead Publishing, Ltd., Cambridge, UK

79. Clore, G. M., and Iwahara, J. (2009) Theory, practice, and applications of paramagnetic relaxation enhancement for the characterization of transient low-population states of biological macromolecules and their complexes. *Chem Rev* **109**, 4108-4139

80. Clore, G. M. (2015) Chapter Seventeen - Practical Aspects of Paramagnetic Relaxation Enhancement in Biological Macromolecules. in *Methods Enzymol.* (Peter, Z. Q., and Kurt, W. eds.), Academic Press. pp 485-497

81. Arumugam, S., Hemme, C. L., Yoshida, N., Suzuki, K., Nagase, H., Berjanskii, M., Wu, B., and Van Doren, S. R. (1998) TIMP-1 contact sites and perturbations of

stromelysin 1 mapped by NMR and a paramagnetic surface probe. *Biochemistry* **37**, 9650-9657.

82. Keizers, P. H. J., Saragliadis, A., Hiruma, Y., Overhand, M., and Ubbink, M. (2008) Design, Synthesis, and Evaluation of a Lanthanide Chelating Protein Probe: CLaNP-5 Yields Predictable Paramagnetic Effects Independent of Environment. *Journal of the American Chemical Society* **130**, 14802-14812

83. Teilum, K., Kragelund, B. B., and Poulsen, F. M. (2002) Transient structure formation in unfolded acyl-coenzyme A-binding protein observed by site-directed spin labelling. *J Mol Biol* **324**, 349-357

84. Meiboom, S., and Gill, D. L. (1958) Modified SpinEcho Method for Measuring Nuclear Relaxation Times. *Rev. Sci. Instrum* **29**, 688-691

85. Assfalg, M., Banci, L., Bertini, I., Ciofi-Baffoni, S., and Barker, P. D. (2001) (15)N backbone dynamics of ferricytochrome b(562): comparison with the reduced protein and the R98C variant. *Biochemistry* **40**, 12761-12771

86. Schurr, J. M., Fujimoto, B. S., Diaz, R., and Robinson, B. H. (1999) Manifestations of slow site exchange processes in solution NMR: a continuous Gaussian exchange model. *Journal of Magnetic Resonance* **140**, 404-431

87. Parks, W. C., Wilson, C. L., and Lopez-Boado, Y. S. (2004) Matrix metalloproteinases as modulators of inflammation and innate immunity. *Nat Rev Immunol* **4**, 617-629

88. Itoh, Y., and Seiki, M. (2006) MT1-MMP: a potent modifier of pericellular microenvironment. *J Cell Physiol* **206**, 1-8

89. Shimoda, M., and Khokha, R. (2017) Metalloproteinases in extracellular vesicles. *Biochimica et Biophysica Acta (BBA) - Molecular Cell Research* **1864**, 1989-2000

90. Hagn, F., Etzkorn, M., Raschle, T., and Wagner, G. (2013) Optimized phospholipid bilayer nanodiscs facilitate high-resolution structure determination of membrane proteins. *J Am Chem Soc* **135**, 1919-1925

II. MT1-MMP Binds Membranes by Opposite Tips of its β-Propeller to Position it for Pericellular Proteolysis

Tara C. Marcink, Jayce A. Simoncic, Bo An, Anna M. Knapinska, Gregg B. Fields, Steven R. Van Doren – In Submission

II.1 SUMMARY

Critical to migration of tumor cells and endothelial cells is the proteolytic attack of membrane type 1 matrix metalloproteinase (MT1-MMP) upon collagen, growth factors, and receptors at cell surfaces. Lipid bilayer interactions of the substrate-binding hemopexin-like (HPX) domain of MT1-MMP were investigated by paramagnetic NMR relaxation enhancements (PREs), fluorescence, and mutagenesis. The HPX domain binds bilayers by blades II and IV on opposite sides of its β-propeller fold. The EPGYPK sequence protruding from both blades inserts among phospholipid head groups in PRE-restrained molecular dynamics simulations. Bilayer binding to either blade II or IV exposes the CD44 binding site in blade I. Bilayer association with blade IV allows the collagen triple-helix to bind without obstruction. Indeed, vesicles enhance proteolysis of collagen triple-helical substrates by the ectodomain of MT1-MMP. Hypothesized side-by-side MT1-MMP homodimerization would allow binding of bilayers, collagen, CD44, and head-to-tail oligomerization.

Summary Highlights

- Blades II and IV insert into lipid head groups a loop characteristic of some MT-MMPs
- Basic side chains at the bilayer binding sites are drawn to lipid phosphoesters
- Vesicles enhance digestion of collagen-like substrates by the MT1-MMP ectodomain
- Binding of bilayers, collagen, CD44, and one mode of dimerization are compatible

II.2 INTRODUCTION

Membrane type 1 matrix metalloproteinase (MT1-MMP or MMP-14) was discovered as triggering invasion by tumor cells via proteolytic processing of proMMP-2 to MMP-2 on cell surfaces (1). MT1-MMP supports cell invasion in cancer metastasis, angiogenesis, and skeletal development (2,3). It is the pericellular collagenase required for invasion of 3D collagen matrices by tumor cells and endothelial cells forming capillary tubes (4-9). Cell motility dependent upon epidermal growth factor (EGF) receptor (ErbB) is promoted by MT1-MMP-catalyzed release of an EGF-like fragment from laminin 5 (10,11) and proteolysis of heparin-binding EGF (12). Cell motility is also promoted by MT1-MMP shedding of cell adhesion molecules from cell surfaces (3), e.g. hyaluronan receptor CD44 (13), syndecan-1 (14), αV integrin (15), and intracellular adhesion molecule-1 (16).

MT1-MMP can be internalized from the plasma membrane into endosomes and then be recycled back to the cell surface or to exosomes released from cells (17). CD44 may recruit MT1-MMP to lamellopodia (18). During cell invasion, MT1-MMP-containing intracellular vesicles are trafficked to invadopodia by kinesin-1 recruited to the vesicles by its affinity for phosphatidic acid (19). MT1-MMP localizes to cholesterol-containing lipid rafts required for formation of invadopodia (20,21). MT1-MMP is exposed on the surface of extracelluar vesicles such as exosomes (17,22). Secretion of exosomes promotes development of invadopodia, while invadopodia in turn secrete exosomes (23).

The positioning of MT1-MMP upon membrane bilayers has the potential to influence its pivotal proteolytic activities. Its soluble extracellular domains comprise the catalytic domain (a zinc hydrolase), flexible linker, and the hemopexin-like (HPX) domain which adopts a β-propeller fold with four pseudo-symmetric blades (24). MT1-MMP is the only membrane type MMP with a crystal structure available for the HPX domain (25). Both the HPX and catalytic domains were shown to bind peripherally to membrane mimics (26,27). This suggests that the soluble domains may reside on membranes at least transiently, despite widespread depictions of them extending away from the membrane.

The soluble ectodomain of MT1-MMP (sMT1-MMP in which the transmembrane helix is removed) is active in collagenolysis and is monomeric, as is its HPX domain (26,28-30). PISA analysis of the small interfaces in the asymmetric unit of crystals of the HPX domain (25)(PDB: 3C7X) deems it a monomer in solution. The HPX domain was dispensable for cellular collagenolysis

by MT1-MMP, but membrane anchoring was required (31). Other cellular assays implicated symmetric homodimerization about blades II and III in proMMP-2 activation and collagenolysis (25). However, another study disputed this mode of homodimerization (32). The discrepancies in reported requirements for the HPX domain in collagenolysis were attributed to differences in the constructs used (32,33). The bulges emanating from blades I and IV were implicated in activation of proMMP-2, cell migration, lung metastasis, and formation of new blood vessels (32). Dimerization of MT1-MMP occurs at the leading edge (invadopodia) but not trailing surfaces of migrating cells (34-37). Homodimerization via the transmembrane helix supports proMMP-2 activation (38). The intracellular C-terminus also participates in dimerization (36), potentially by its anchorage to the cytoskeleton in invadopodia via palladin (39). Structural analysis of MT1-MMP interactions with membranes could provide insight into the modes and probabilities of enzyme dimerization and association with other cell surface molecules.

Careful appraisal of the proximity of MT1-MMP to lipid bilayers is warranted by its relevance to the digestion of collagen, pro-growth factors, and receptors on cell membranes, and to the sites of action of prospective therapeutics reported to target the HPX domain of this protease (32,40,41). We implemented two key tools in our investigation. First, nanodiscs have emerged as the gold standard of bilayer mimics for structural and biophysical studies of membrane-associated proteins. Nanodiscs encircle disk-like bilayers with two chains of molecular scaffolding protein (MSP). This confers advantages of long-term stability, homogeneity, planarity, and fluidity at high concentrations (42,43). Second, paramagnetic NMR

has successfully docked GTPases peripherally to nanodiscs containing a paramagnetic ion conjugated to a lipid head group (44,45). NMR has also measured soluble protein proximity to bilayer mimics containing the paramagnetic spin label on the fatty acyl chains within the bilayer, which provides detailed structural orientations upon fluid bilayer assemblies (46-50). We show NMR and other lines of evidence that both blades II and IV, on opposite sides of the HPX domain, probably insert their protruding loop peptide sequences of EPGYPK in among the phospholipid head groups of nanodisc bilayers. With blade IV bound to the bilayer, the HPX domain appears free to bind the collagen triple-helix. Indeed, we observe that sMT1-MMP proteolysis of collagen-mimicking substrates is retained and enhanced in the presence of vesicles.

II.3 RESULTS

II.3.1 Nanodiscs Associate with Blades II and IV of the HPX Domain

Equimolar mixtures of DMPC nanodiscs with the HPX domain from human MT1-MMP display high quality NMR spectra upon addition of NaCl to 300 mM (Fig. S1). The HPX domain interacting with the nanodiscs tumbles with a rotational correlation time τ_c around 21 ns at 30°C in 300 mM NaCl. This is almost twice the τ_c of the free state (29) and 3- to 4-fold less than the τ_c of integral membrane proteins in nanodiscs of similar composition (51). These observations and the sharpening of NMR peaks upon salt addition suggest that increased salt weakens the association of nanodiscs with the HPX domain, presumably by diminishing the

electrostatic attraction. High salt may shorten the residence time of the HPX domain upon a nanodisc, resulting in faster tumbling and better spectra of the HPX domain.

To locate binding sites for a lipid bilayer on the HPX domain, nanodiscs were prepared for paramagnetic NMR measurement of proximity by incorporating nitroxide spin-labeled DPPC at a mole fraction of 0.025 of the DMPC. A 5-doxyl substituent was positioned on the acyl chain under the phospholipid head groups whereas a 10-doxyl substituent was positioned deeper inside the bilayer. The resulting paramagnetic relaxation enhancements (PREs given as Γ_2) were measured on Ile, Leu, and Val methyl groups as exponential decay curves that could differ between paramagnetic (spin-labeled) and diamagnetic (unlabeled) nanodiscs (Fig. S1C). The most significant PREs with $\Gamma_2 > 30$ s^{-1} localize to the blades II and IV of the β-propeller (Fig. 1A,B). The nanodiscs induced small amide chemical shift perturbations (CSPs) in blades I, II, and IV (Figs. 1C,D and S1E) that agree with the explicit measurements of proximity that the PREs represent. A mixture of bilayer binding to opposite sides of the HPX domain agrees with negative staining electron microscopy evidence that addition of sMT1-MMP at low [NaCl] draws nanodiscs together into stacks (Fig. S2A,C).

II.3.2 Nanodisc Docking to Opposite Sides of the HPX Domain

The PREs and CSPs measured by NMR were separated into groups on opposite sides of the domain: one in or near blade II and the other in or near blade

IV (Fig. 1B,D). Explicit distances from the PRE-broadened methyl groups to the approximate depth of the 5-doxyl or 10-doxyl groups in the nanodisc bilayer level were estimated from the Γ_2 values (Fig. 1A) and τ_c using eq. 3. Nanodisc-induced peak shifts (CSPs) and broadenings added supplementary but ambiguous restraints on proximity to the surface of the nanodisc (Table 1). These were used as distance restraints in initial HADDOCK rigid body docking (47,48,52), followed by restrained molecular dynamics (MD) simulations using NAMD and the CHARMM36 force field (53). From 4-ns segments of the restrained MD trajectories with blade II or IV at the nanodisc interface, 15 snapshots of the complexes of lowest energy and full consistency with the distance restraints were collected into structural ensembles (Fig. 2A,B,D,E with PDB IDs 6CM1 and 6CLZ). The RMSD values to the mean were around 1.18 and 1.24 Å for the backbone atoms (Table 1).

II.3.3 Protein-Bilayer Interfaces

In both complexes with nanodiscs, 13 residues contact phospholipid head groups throughout each ensemble. Central to the interface in both modes of binding is the outer β-strand and β-bulge of that blade with sequence L/VEPGypK, where the “yp” is recessed from the interface (Fig. 2). This loop motif exhibits similar behavior at the two interfaces. In both cases, the side chain of the central proline and the methylene group of the glycine insert far enough to contact fatty acyl chains and displace head groups to form a small bowl in the bilayer surface

(Fig. 2C,F). The lipids around this bowl in the heart of the interface are more ordered in the MD simulations than those lipids that are more distant from protein.

The net positive charge is greater in the blade IV interface where six side chains are positively charged and one negatively charged. In contrast, the blade II interface has four basic side chains and two acidic side chains in contact with the head groups. The positively charged side chains tend to be drawn into salt bridges to phosphoester linkages in the lipid head groups. This is true of three of the four basic residues in the blade II interface and five of the six basic residues in the blade IV interface (Table S1). The interface centered at blade II includes apparent bilayer contacts of Lys362, the sequence ^{393}ASLEPGYgK^{401} bulging from blade II, Glu405 and Arg408 of blade II, and Leu442 and Arg443 at the edge of blade III closest to blade II. The interface centered at blade IV includes apparent bilayer contacts with Lys454 and G458 at the near edge of blade III, the central bulging blade IV sequence ^{490}KLKVEPGypK^{499}, and Lys482, Arg503, and Ser510 also from blade IV.

The overall tilt of each mode of binding appears to differ. The binding mode at blade II has the collagen-binding face tilted modestly toward the bilayer, possibly due to electrostatic attractions of Arg374 and Lys378 (from the first β-hairpin loop of blade II) to phosphoester groups on that side. A loop from each of blades I and III each join the two loops of blade II in contact with lipid head groups. In contrast, the mode of binding at blade IV tilts in the opposite direction with the collagen-binding face tipped *away* from the bilayer and the “exit” side tilting slightly towards the bilayer. (The exit side refers to the central channel between blades which binds

Cl^- and Na^+ ions (25)). Electrostatic attractions on the exit side of Lys454 and Lys482 to phosphoesters (Table S1) might account for this apparent tilt. The blade III β-hairpin that presents Lys454 and the central EPGYPK motif that inserts partly into the bilayer have counterparts with the blade II interface. However, the two other β-hairpin loops at the blade II interface have no apparent counterparts in the blade IV interface.

II.3.4 Fluorescent Lipid Interactions Probed by Mutations

Due to the pseudo four-fold symmetry of the β-propeller fold and the recent proposal that bilayer binding is centered upon blade III (26), we examined bilayer binding by independent means. We sought to perturb bilayer binding by introducing site-directed Ser substitutions of basic residues placed strategically in the four blades of the β-propeller (Fig. 3A) of the sMT1-MMP (catalytic – linker – HPX) construct. We monitored FRET quenching of intrinsic Trp fluorescence by Pyrene-PE incorporated into small unilamellar vesicles (SUVs) (54,55). Addition of SUVs to wild-type sMT1-MMP attenuated Trp fluorescence emission by nearly 30% (Fig. 3B). Neither the K414S nor the K434S substitution in blade III interfered with fluorescence quenching by pyrene-labeled SUVs (Fig. 3B). Ser substitution for the Lys at the end of the EPGYPK motif of either blade II or IV, i.e. K401S or K499S, respectively, diminished the quenching of Trp fluorescence emission by SUVs containing the Pyrene-PE quencher (Fig. 3B). The R362S variant responded similarly, but to a lesser degree. The mutational evidence of electrostatic attraction

of Arg362, Lys401, and Lys499 to SUVs corroborates the paramagnetic NMR-based proposal that lipid bilayers do recognize blades II and IV (Figs. 1, 2).

Another approach led to a similar conclusion. The HPX domain was specifically labeled with a membrane-responsive fluor at single Cys substitutions (47,48,56). One site was placed in each of blades I, II, and IV, while three sites were selected in blade III (Fig. S3). Each single Cys was condensed with the iodoacetamide-substituted NBD fluorescent probe that responds to a hydrophobic environment with increased fluorescence emission (56). Addition of SUVs to the IANBD conjugate at blade I (at D351C) or blade III (at N424C, N433C, or N446C) failed to increase significantly the fluorescence emission from the NBD (Fig. S3). Addition of SUVs to the HPX domain with IANBD conjugated to D385C in blade II or to D471C in blade IV increased the fluorescence emission significantly by 2.05-fold and 1.36 fold, respectively (Fig. S3). The greater increase from the label at D385C than from D471C is attributable to Asp385 being situated closer to the bilayer than is Asp471 in the structural models of Fig. 2.

II.3.5 MT-MMPs Are Distinguished by their EPGYPK/R Loops

A phylogenetic tree, constructed from each complement of MMP sequences obtained from 10 diverse vertebrate species, separates MT-MMPs from soluble MMPs (Fig. S4A). Evolutionary Trace analysis (57) of this collection finds that most of the MT-MMPs containing a transmembrane helix (MT1-, MT2-, MT3- and MT5-MMP) also share in blades II and IV the hydrophobic PGYP loop motif flanked by polar residues (Figs. 3D, S4B). A majority of MMPs contain the GYP motif in blade

II (Figs. 3D, S4B). In blade IV, MT1-MMP and most MT2-MMP sequences widen the motif to the full bilayer-binding EPGYPK peptide sequence, which is modified in MT3- and MT5-MMP sequences by an Arg replacement of the Lys (Figs. 3D, S4B). The crystal structure of the HPX domain of MT1-MMP differs from those of soluble MMPs in this loop bulging out from outer β-strand 4 of blade IV (Fig. 3C). The membrane-binding EPGYPK/R motif in blade IV appears to be a distinguishing characteristic of those MT-MMPs that possess a transmembrane helix.

II.3.6 Vesicles Enhance Digestion of Collagen Triple-Helix

Streptococcal collagen–like protein 2 (Scl2) was engineered by inserting the collagenase-susceptible sequence from the α1 chain human collagen II (Fig. 4A), in a similar fashion as a collagen III sequence was inserted previously (58). Addition of SUVs increased sMT1-MMP proteolysis of the Scl2-collagen α1(II) by 30% of the total of this substrate at 6 h and 18 h after initiation of the reactions (Fig. 4B,C). For perspective, the coordinates of a collagen triple-helical peptide (THP) bound to the HPX domain (29)(PDB: 2MQS) have been superimposed on the complexes with nanodiscs. Concurrent binding of the HPX domain to collagen triple-helix and membranes appears to be accommodated by blade IV being oriented toward the lipid bilayer (Fig. 5A).

We tested the effects of collagen-like THP and vesicles upon the interactions of each with sMT1-MMP. Addition of SUVs enhanced the initial velocity of sMT1-MMP digestion of the THP by 1.4-fold (Fig. S5A). Additions of the THP to excess interfered in the proximity of sMT1-MMP to the SUVs, as observed

by the FRET assay of quenching of Trp emission by Pyrene-PE in the SUVs (Fig. S5B). Perhaps the excess THP out-competed the SUVs for binding blade II where steric hindrance is expected (Fig. 5B).

II.3.7 Compatibility of Bilayer and Collagen Binding to Hypothesized HPX Dimers

The pericellular collagen digestion by MT1-MMP, characteristic of tumor cell invasion, has been reported to require membrane anchoring (31,59) and could be facilitated by dimerization (37). Consequently, we considered the potential dimers and their compatibility with bilayer binding and collagen triple-helix binding, or lack thereof. For potential modes of dimerization with the largest of the small interfaces identified by PISA in the crystallographic asymmetric unit of the HPX domain (PDB: 3C7X), we considered the possibility of concurrent binding of a membrane to both protomers. A symmetric mode of dimerization, shaped like a “V”, is favored by one mutagenesis study (25) and disputed by another (32). The prospective “side-by-side” mode of dimerization appears to be compatible with the mapping of interactions by Zarrabi et al. (32) but an evaluation of the possibility of side-by-side dimerization has not been reported. We evaluated these two prospective modes of dimerization for compatibility with the proximity of the HPX domain to nanodiscs, which has been detected by paramagnetic NMR. We subjected each dimer to MD simulations with PRE-based distance restraints to a nanodisc (Table 1). We restrained one protomer via the PRE-based restraints which drew blade II to the bilayer. We simultaneously restrained the other protomer to the PREs placing

blade IV at the bilayer. MD simulations of the symmetric dimer defended by Tochowicz et al. (25) using the same PRE-based restraints caused the partial unfolding of both blades II and IV (Fig. S6). The binding path of the collagen triple-helix reported previously (29) also clashes with the bilayer in the simulated assembly of the symmetric dimer with the nanodisc (Fig. S6A). Consequently, the symmetric dimer is probably not able to bind both collagen and membranes simultaneously via the HPX domain. On the other hand, the corresponding PRE-restrained MD simulation of the potential side-by-side dimer encountered neither structural perturbations nor violations of the intermolecular distance restraints from Table 1 based on PREs. In the experimentally restrained simulation of the hypothetical side-by-side dimer, the protomer with blade IV at the bilayer presents an open binding site for the collagen triple-helix, without obstruction by the nanodisc (Fig. 5C and Movie S3).

II.4 DISCUSSION

II.4.1 A New View of MT-MMP HPX Domains Positioning at Membranes

These and recent measurements assert that the HPX domain of MT1-MMP occupies lipid bilayers at least transiently (26,27). The flexible linker-2 sequence of 14 residues connecting the HPX domain to the transmembrane helix of MT1-MMP (3) is long enough to reach the transmembrane helix for either mode of bilayer binding by the HPX domain observed herein. The distance from HPX

domain to transmembrane helix is noticeably shorter, however, with blade IV bound to the membrane. Since the catalytic domain can also bind lipid bilayers (27), it may join the HPX domain transiently on bilayers, placing it strategically for proteolytic attack upon proteins anchored to plasma membranes or exosomes. This suggests that the common portrayal of the soluble domains of MT1-MMP radiating away from the membrane (60,61) should be revised. The recent structural question has been about the orientations between the soluble domains and bilayers, which is relevant to recognition of substrates and partners at plasma membranes.

The HPX domain of MT1-MMP was recently proposed to bind bilayered micelles (bicelles) primarily at blade III, based on the broadened NMR peaks of blade III but reaching as far as blade IV residues Lys490 and Glu494 (26). The results herein confirm that Lys490 and Glu494 lie at an interface with bilayers. However, the previously hypothesized docking site does not agree with our new results. Instead, the previous model is centering upon blade III, resulting in greater steric conflict between the binding of bilayer and collagen. The previous modeling appears to rotate the HPX domain at least 50° away from the blade IV-centered complex herein (PDB: 6CLZ) and at least 150° from the blade II-centered complex herein (PDB: 6CM1). The negatively charged Ser-Glu sequence bulging from blade III is also quite unlikely to penetrate the phospholipid bilayer to the region of the phosphoesters and fatty acyl chains reached by the Pro-Gly motif from the EPGYPK sequence of blades II and IV. Two technical aspects of the previous work (26) render it preliminary: 1) The enrichment in CHAPS detergent and less defined

morphology of those bicelles introduce complications; they fall short of the integrity enjoyed by nanodiscs for structural and biophysical studies (42,43,62). 2) Reliance only upon NMR peak perturbations for interface mapping can be subject to systematic errors. The perturbations can propagate far beyond the interface (63,64). Peak perturbations occasionally are much larger *outside* the interface (65). That literature demonstrated the higher accuracy of direct measures of interfacial contact.

The PRE NMR approach employed here, implicating blades II and IV as the interfaces (Figs. 1, 2), provides direct and sensitive measures of intermolecular distances in the 12 to 25 Å range (Fig. S1D), even in cases of partial occupation of the sites (47,66-68). Site-specific labeling with a membrane-responsive fluor provides independent proximity information (47,48,56) ruling an involvement of blade III in binding vesicles as unlikely, and corroborating the close proximity of blades II and IV to the vesicles (Fig. S3). Site-directed mutants found that uncharged replacements of lysine side chains in blades II and IV interfered in association with vesicles while those in blade III did not (Fig. 3A,B). This evidence for electrostatic attraction corroborates the appearance of multiple salt bridges from blade II or IV to lipid phosphoester linkages persisting through the NMR-restrained MD simulations (Table S1).

II.4.2 Potential Scope of Bilayer Binding by MMP HPX Domains

The membrane-binding EPGYP peptide motif of blades II of the MT-MMPs possessing a transmembrane helix distinguishes them from most other MMPs

(Figs. 3D, S4B). The known structures of soluble MMPs lack such a loop bulging from blade IV (Fig. 3C), rendering them unlikely as candidates to be able to insert blade IV into lipid bilayers. However, the APGYP motif in blade IV of the GPI-anchored MT4-MMPs shares sufficient similarity to the EPGYP motif to hypothesize that MT4-MMPs may also be able to penetrate membrane surfaces. Likewise, the SPGFPK/M motif in blade II of soluble MMP-19s (groups 16 and 17 in Fig. S4B) might have the ability to insert among phospholipid head groups. The EPNYPK motif of blade II of soluble MMP-12 (Fig. 3D) also suggests the capacity for membrane association, though its polar Asn is less likely to penetrate as far as the acyl chains.

The MMP-12 HPX domain binds and kills bacteria using its KDEK loop in mice (KDDK in humans) located in blade II (69). This β-hairpin loop is in close proximity to the EPNYPK loop which we hypothesize to bind bilayers. The ^{375}KDGK^{378} peptide sequence of MT1-MMP shares homology with the bactericidal KDEK loop in blade II of MMP-12. Lys378 forms a salt bridge with the Glu396 of the EPGYP motif throughout the structural ensemble in which blade II of MT1-MMP is bound to the nanodisc. Asp376 and Lys378 of this loop in MT1-MMP approach a choline head group throughout the ensemble. Consequently, the corresponding bactericidal KDE/DK loop of MMP-12 can be hypothesized to contact bilayer or protein components of bacterial envelopes.

II.4.3 Membrane Positioning and Partner Interactions

Addition of a 20-fold excess of the collagen-mimicking THP competes out about 25% of the association of sMT1-MMP with vesicles (Figure S5B). This partial competition can be explained by steric interference of bound THP with blade II binding of bilayers, along with retention of blade IV binding of bilayers (Fig. 5A,B). This suggests the orientation of Fig. 5A to be the more likely during collagenolysis.

In invadopodia, the anchorage of MT1-MMP to the actin cytoskeleton (39) might promote its dimerization or oligomerization there. Considering the lower likelihood of HPX domain dimerizing in solution, it is unknown whether addition of nanodiscs or vesicles fosters dimerization of the HPX domain. If the HPX domain does homodimerize on the surface of model membranes, the side-by-side positioning in the crystallographic asymmetric unit is clearly the hypothetical mode of homodimerization that is fully compatible with the measured proximity to bilayers and with binding of the collagen triple-helix (Fig. 5C). Thus, it appears to be the potential mode of homodimerization more plausibly capable of supporting collagenolysis very near plasma membranes. If there is side-by-side dimerization, it could place blade I of one protomer together with blade III of the next protomer in a head-to-tail fashion that could propagate to add more protomers. This could potentially offer a mechanism that might explain the homo-oligomerization of MT1-MMP on cells that was reported (36,70). Such head-to-tail homodimerization via blades I and III (Fig. 5C) would provide the accessibility of the outer β-strand and bulge of blade I needed for both proMMP-2 activation and homodimerization by MT1-MMP (32).

The β-bulges on the surfaces of blades I and IV of MT1-MMP support tumor cell migration, invasion, and angiogenesis (32). The β-bulge of blade I is exposed to binding partners when bound to bilayers, regardless of homodimerization of the HPX domain (Figs. 1B, 2D, 5C, S6A). Blade I is the site of heterodimerization with CD44 (32). Since CD44 is a transmembrane proteoglycan and substrate of MT1-MMP, the positioning of the HPX domain on the plasma membrane by either blade II or IV could facilitate the association leading to shedding of CD44 and its reported activation of EGFR signaling in cell migration (32). Alteration of the outer strand of blade IV interfered with proMMP-2 activation, cell migration, EGFR signaling, and metastasis, which was attributed to disruption of homodimerization (32). However, the defects do not seem attributable directly to interference in homodimerization because the outer strand of blade IV is not part of either dimer interface suggested by crystallography. Nonetheless, the outer strand of blade IV now appears to be critically for positioning of the HPX domain via its shallow insertion into membranes (Figs. 2D-F). This makes binding sites on the HPX domain accessible for interaction with key substrates in cell migration and metastasis, i.e. CD44, collagen (Fig. 5A), and presumably others such as syndecan-1.

II.5 ACKNOWLEDGMENTS AND CONTRIBUTIONS

This work was supported by NIH grant R01 CA098799. B.A. was supported by R01 GM60048. The 800 MHz spectrometer was purchased by NIH grant S10 RR022341 and funds from the University of Missouri. We are most grateful to

Barbara Brodsky for the bacterial collagen substrate, Tommi A. White for providing training in negative staining EM, and Alexander W.E. Franz for detailed comments on the manuscript.

T.C.M., S.V.D, and G.B.F. designed the research. T.C.M., J.C.S, B.A., A.M.K., and S.V.D performed the research. T.C.M. and S.V.D. wrote the manuscript. G.B.F. attracted grant support and critiqued and revised the manuscript.

II.6 ACCESSION NUMBERS

Atomic coordinates and restraints were deposited in the PDB under accession code 6CLZ for the complex with blade IV bound to the nanodisc and 6CM1 for the complex with blade II bound to the nanodisc. Chemical shift assignments of NMR peaks of these complexes were deposited in the BioMagResBank under accession codes 30425 and 30426, respectively.

II.7 STAR METHODS

II.7.1 Preparation of sMT1-MMP and its HPX Domain

Soluble MT1-MMP constructs were expressed and labeled as described (29). Samples for NMR PRE experiments were grown in a $^{13}C/^{1}H$-labeled deuterated *E. coli* culture using an established protocol (71). 50 mg/L of α-ketobutyrate and 100 mg/L of α-ketoisovalerate were added 1 h prior to induction for $^{13}C/^{1}H$-labeling of isoleucine, valine, and leucine methyl groups in a $^{2}H/^{15}N$ background. The culture was optimized by the addition of 2% $^{2}H/^{15}N$ rich labeling

media (ISOGRO, Sigma-Isotec). Post-induction growth was continued for 8 h and then cells were harvested and sonicated to collect the pellet of inclusion bodies.

Inclusion bodies containing the His-tagged HPX domain or sMT1-MMP were dissolved with 6 M GuHCl, dialyzed overnight with 6 M Urea, and spun down to remove any precipitates. The His-tagged HPX domain was bound to a nickel-nitriloacetic acid (NTA) affinity column in 20 mM Tris-HCl (pH 7.2), 1 M NaCl, and 6 M urea and washed with 20 mM imidazole. Folding occurred while bound to the nickel-NTA affinity resin during a linear gradient to change the 6 M urea into a final buffer containing 20 mM Tris-HCl, 1 M NaCl, and 20 mM imidazole at pH 7.2. The flow rate was 1 ml/min. The HPX domain was eluted with 300 mM imidazole and dialyzed overnight to remove imidazole and NaCl.

His-tagged sMT1-MMP was purified in 6M urea using nickel-NTA affinity resin and then folded by stepwise denaturant removal by dialysis in 3 M, 1 M, and then 0 M urea containing 20 mM Tris-HCl (pH 7.2), 10 mM $CaCl_2$, and150 mM NaCl and later made active by the addition of 5 mM $ZnCl_2$.

II.7.2 Preparation of Nanodiscs for NMR

Nanodiscs were formed with MSP1D1 scaffolding protein and 1,2-dimyristoyl-sn-glycero-3-phosphocholine (DMPC, Avanti) as described (72-74). When used, 5- or 10-doxyl DPPC was incubated with DMPC prior to forming nanodiscs in order to ensure full incorporation of the spin label. Samples were prepared for NMR in 20 mM Tris (pH 7.2) and 300 mM NaCl to diminish the affinity of HPX domain for nanodiscs.

II.7.3 NMR Spectroscopy and Paramagnetic Relaxation Enhancements

Spectra were recorded using Bruker shaped tubes to optimize sensitivity by mitigating the dielectric effects of the high [NaCl]. Spectra were acquired at 30°C on a Bruker Avance III 800 MHz Spectrometer with a TCI cryoprobe.

PREs emanating from nitroxide spin-labels were recorded in the presence of 5- or 10-doxy-substituted DPPC. Five relaxation time points were collected at 4 ms intervals using a CPMG pulse train inserted into a ^{13}C HMQC (or ^{15}N TROSY) pulse sequences as described (47). The peak heights were normalized to those of the diamagnetic control using the signal to noise ratio of each spectrum. Curve fitting of the 5-point decays accounted for the 6.8 ms of relaxation delays during the HSQC pulse sequence and prior to the CPMG pulse sequence (Fig. S1C). This decreased systematic fitting error, thereby increasing apparent accuracy of the quantification of the PREs. Exponential decays were measured and compared to diamagnetic controls without spin label in order to estimate the PRE as:

$$\Gamma_2 = R_{2,\,paramag} - R_{2,diamag} \quad (1)$$

The amide chemical shift perturbations are expressed as a radius with the ^{15}N peak shifts normalized to the scale of ^{1}H peak shifts:

$$\Delta\omega_{HN} = \sqrt{\Delta\omega_H{}^2 + (\Delta\omega_N/5)^2} \quad (2)$$

II.7.4 Calculations to Dock the HPX domain to Bilayer Models

The HPX domain and phospholipids were docked as rigid bodies with HADDOCK 2.1 (75) using explicit distance restraints from PREs and ambiguous distance restraints from CSPs and line broadenings as done previously (47). That is, the apparent averaged distance *r* between the methyl group detected by NMR and the nitroxide spin label generating the PRE was estimated by the approximate relationship:

$$\Gamma_2 = 4\kappa\tau_c / r^6 \quad (3)$$

where κ =1.23e-44 $m^6 s^{-2}$ and τ_c is the rotational correlation time which calibrates the relationship of the PRE to the distance *r*. In order to estimate τ_c, we measured the average of the amide ^{15}N NMR transverse cross-correlation rates η_{xy}https://www.nature.com/articles/ncomms6552 - ref60 using the pulse sequence of (76) implemented as a exponentially decaying series of 1D spectra which we integrated and fitted to η_{xy}. This η_{xy} yielded the approximate τ_c using spectral density equations available (77). The uncertainty of each distance restraint was set to range from a lower bound of the closest possible contact of hard spheres up to an upper bound 10% above the apparent distance plus 2.9 Å of additional uncertainties from the depth of the doxyl spin label and ambiguity in *proR* vs. *proS* methyl groups of the Val and Leu side chains.https://www.nature.com/articles/ncomms6552 - ref60

The best-converged structural models from rigid body docking calculations in HADDOCK were used for MD refinement. Nanodiscs were aligned to the phospholipids and used as the starting structural model for refinement by

restrained MD simulations using the CHARMMM_GUI website (78) in NAMD (79). Restraints were implemented using xy-plane harmonic values and colvar distances enforced. 2 ns of minimization and equilibration along with 4 ns of production time were run at 310K with rectangular boxed solvent and ions using NAMD 2.1 with CUDA GPU processing (79). The lowest energy structures were selected from 1 ns segments of the equilibrated trajectories, provided the frames were separated by at least 20 ps. The trajectories were run for another 5 ns without restraints for a total of 11 ns at 310 K to verify stability of the assembly. Models of hypothetical dimers of the HPX domain docked with nanodiscs were prepared by alignment with the lowest energy structural models with blade II and IV at the interface. These starting dimer models were minimized and equilibrated for 4 ns. Lowest energy structures from the subsequent equilibrated 4 ns of the trajectory were used for visualization.

II.7.5 Intrinsic Tryptophan Quenching Assays of Membrane Proximity

Single site-directed mutations were made in sMT1-MMP via QuikChange with PCR master mix (Agilent Technologies).

Small unilamellar vesicles (SUVs) were prepared by suspending DMPC monomers in 20 mM Tris (pH 7.2), with or without addition of lipid probes. After an hour of incubation at 37°C, the hydrated lipids were subjected to multiple freeze-thaw cycles in liquid nitrogen, forming large unilamellar vesicles. Subsequent sonication of these large unilamellar vesicles led to the formation of SUVs. Binding of sMT1-MMP (1 μM) to SUVs of DMPC was determined through the decrease of

the intrinsic tryptophan emission (λ_{ex} = 285 nm, λ_{em} = 315 nm) in the absence and presence of a lipid probe. 1,2-dioleoyl-*sn*-glycero-3-phosphoethanolamine-N-(1-pyrenesulfonyl) lipid (Pyrene-PE, Avanti) was incorporated as a quencher of protein intrinsic emission. All experiments were performed on a BioTek Synergy MX plate reader. Emission was measured after an incubation period and background fluorescence was corrected through subtraction of just Pyrene-PE liposomes in buffer.

II.7.6 Site-Directed Fluorescence to Probe Bilayer Proximity

Site directed cysteine mutations were introduced in sMT1-MMP via QuikChange with PCR master mix (Agilent Technologies). Conjugation of the fluor sensitive probe IANBD (Invitrogen) to the single Cys proceeded by incubating a 10-fold excess of IANBD to overnight at 25°C in a vacuum chamber. Unreacted IANBD was removed by desalting with Sephadex G-25 resin (GE Healthcare). Completion of conjugation was monitored by absorbance.

The fluorescence assays used 10 nM of the IANBD-conjugated sMT1-MMP with SUVs that were 250 μM in DMPC monomers. The fluorochrome was excited at 478 nm and detected at 541 nm in a BioTek Synergy MX plate reader. Emission was measured after 1 h of incubation with the SUVs and normalized by the emission without SUVs.

II.7.7 Preparation and Proteolysis of Bacterial Scl2 Collagen-like Substrate

The recombinant bacterial collagen with its domain structure of V-CL-CL and inserted sequence from type II collagen is illustrated in Figure 4A. The six GXY triplets with the sequence GPPGPQG^LAGQRGIVGLP from the human collagen α1(II) chain were inserted between two collagen-like (CL) domains of the Streptococcal Scl2 protein, with the caret sign denoting the site for hydrolysis by collagenolytic MMPs. This six-triplet sequence corresponds to residues 769–786 of the triple-helical region in human type II collagen α1 chain. An N-terminal octa-His tag was included for purification. It is followed by the natural trimerization V domain of the bacterial collagen. The expression construct was obtained by inserting the annealed oligonucleotide encoding the MMP-cleavable collagen α1(II) sequence between the DNA sequences of the two CL domains using *SmaI* and *ApaI* restriction sites. The inserted human MMP-cleavable site is flanked by bacterial collagen sequences of GKD-GKD-GQP-GKP on the N-terminal side and GPR-GEQ-GPT-GPT on the C-terminus (58). The resulting DNA sequence was confirmed by sequencing. Recombinant protein was expressed using the cold-shock vector system in the *E. coli* BL21 strain, as reported (80).

The sMT1-MMP was activated for use in proteolysis assays by introducing the Zn^{2+} and Ca^{2+} ions required for activity. 20 nM sMT1-MMP was incubated at 30°C for 30 min in 20 mM Tris (pH 7.2), 150 mM NaCl, 10 mM $CaCl_2$, and 100 μM ZnCl both in the presence and absence of SUVs (250 μM in DMPC monomers). The proteolysis reactions were started by adding the aforementiond recombinant bacterial Scl II - collagen α1(II) substrate to 20 μM to the activated sMT1-MMP (20

nM). Aliquots were removed from the proteolysis mixture at several time points and analyzed by SDS-PAGE. Intact bands migrating with similar mobility as the 74 kDa marker were analyzed using ImageJ software. Background noise was subtracted and the initial time point provided the reference intensity.

II.7.8 Kinetics of sMT1-MMP Hydrolysis of Collagen Triple-Helical Peptide

The proenyzme form of sMT1-MMP (pro-sMT1-MMP) was obtained from R&D Systems (catalog # 918-MP) and activated by incubation with 1 mg/mL of activated rhTrypsin-3 (Sigma-Aldrich) for 1 h at 37˚C in TS buffer, i.e., 50 mM Tris (pH 7.5), 50 mM NaCl, 10 mM $CaCl_2$, 0.05% Brij-35. After MT1-MMP activation, the remaining trypsin-3 activity was quenched by addition of 1 mM AEBSF (R&D Systems) and incubation for 15 min at room temperature. Activated enzyme was aliquoted and stored at -80˚C for further use. The triple-helical substrate fTHP-9 [$(Gly\text{-}Pro\text{-}Hyp)_5$-Gly-Pro-Lys(Mca)-Gly-Pro-Gln-Gly~Cys(Mob)-Arg-Gly-Gln-Lys(Dnp)-Gly-Val-Arg-$(Gly\text{-}Pro\text{-}Hyp)_5$-$NH_2$, where Hyp = 4-hydroxyproline, Mca = (7-methoxycoumarin-4-yl) acetyl, Mob = 4-methoxybenzyl, and Dnp = 2,4-dinitrophenyl] was synthesized as described previously (81,82)

Enzyme kinetics were measured in a BioTek H1 plate reader running Gen5 2.09 software using λ excitation = 324 nm and λ emission = 393 nm as described previously (83,84). To allow the proper folding of the peptide triple-helix, substrate fTHP-9 was diluted in TS Buffer and left overnight at 4 °C. The next day, 1 mM DMPC stock was prepared in TS buffer for the assay and further diluted into 50 µl reactions over a series of concentrations. The sMT1-MMP was added to each tube

containing DMPC and incubated for 1 h at room temperature. All enzymatic assays were performed in a black, low-volume 384 well plates. 10 µL of activated sMT1-MMP + DMPC (or sMT1-MMP + TS buffer as control) was added to each well and then 5 µL of substrate fTHP-9 was dispensed into each well. Final enzyme and substrate concentrations were 1.8 nM and 1.7 µM, respectively. The assays were performed in the absence and presence of SUVs ranging from 100 to 800 µM DMPC monomers. The plate was immediately read to obtain fluorescence in relative fluorescence units (RFUs). The fluorescence was monitored continuously for 180 min to determine initial reaction rates. The kinetic protocol at 25 °C used 30 s of shaking followed by reading each well every 30 s. Plates were stored at ambient temperature for 24 h before a final reading. All measurements were performed in triplicate. Kinetic parameters were calculated by Lineweaver-Burke linear regression analysis by GraphPad Prism 7.03.

II.7.9 Assays of Competition between THP and SUV Binding to sMT1-MMP

A similar THP, but without fluor or quencher, was synthesized with the sequence of ((Gly-Pro-Hyp)$_4$-Gly-Pro-Gln-Gly-Ile-Ala-Gly-Gln-Arg-Gly-Val-Val-Gly-Leu-Hyp-(Gly-Pro-Hyp)$_4$-Gly-Tyr-NH_2)$_3$ as described (85). It is designated α1(I)772–786 THP because it corresponds to residues 772–786 of the type I collagen α1 chain.

α1(I)772–786 THP was added to excess (1, 2, or 4 µM) over the sMT1-MMP (200 nM) used in assays of membrane proximity measured by intrinsic tryptophan

quenching by Pyrene-PE, performed as described above. The SUVs had a DMPC monomer concentration of 250 μM and the Pyrene-PE quencher present at 5 μM.

II.7.10 Negative Stain Electron Microscopy

500 nM sMT1-MMP was mixed 1:1 with nanodiscs composed of DMPC and MSP1D1 in 20 mM Tris (pH 7.2), 10 mM $CaCl_2$, and 100 μM ZnCl. 5 μl of this sample was added to 200 mesh copper carbon film grids. 5 μl Nano-W stain (Nanoprobes) was used to affix the samples. These grids were then imaged on a JEOL JEM 1400 Transmission Microscope and analyzed further using ImageJ.

II.7.11 Evolutionary Trace Analysis

Sequences spanning the HPX-like domains of MMPs were acquired and aligned from Blastp https://blast.ncbi.nlm.nih.gov/Blast.cgi?PAGE=Proteins, using the blastp algorithm and spanning 10 diverse species of vertebrates. After the removal of redundancies and truncated sequences, 102 aligned sequences were submitted to the Evolutionary Trace server at http://mordred.bioc.cam.ac.uk/. The resulting phylogenetic tree was subdivided into 15 trace levels that separate the branches of the tree by progressively high sequence identity within each branch. Residues conserved within a subfamily at a selected trace level were recorded.

II.8 FIGURES

Table II-1 NMR Structural Statistics.

	Blade II in interface	Blade IV in interface
PDB accession code	6CM1	6CLZ
RMSD deviations [a]		
Avg. RMSD (Å) for backbone	1.18 ± 0.28	1.27 ± 0.26
Distance Restraints		
Lipid – protein methyl PREs, explicit	3*7	3*4
Lipid – amide shifts, broadenings, ambiguous	11	3
Restraint violations > 0.5 Å		
Protein-lipid PREs	0	0
Protein-lipid ambiguous residues	0	0
Structural quality		
Procheck G-factor (all dihedrals)	-0.55	-0.53
Molprobity score [b]	1.11	1.10
Most favored Ramachandran plot residues (%) [c]	84.7	85.3
Allowed Ramachandran plot residues (%) [c]	11.0	12.3
Buried surface area (Å²) [d]	1225 ± 90	1423 ± 68
CH_3 groups with PREs from 5-doxyl DPPC [e]	357δ, 380γ, 389γ 395δ, 442δ	473γ, 493γ
CH_3 groups with PREs from 10-doxyl DPPC [e]	357δ, 380γ, 389γ	473γ, 493γ
Amide groups perturbed by Nanodiscs	330 [f], 342, 377, 379, 386, 387 [f], 396, 422, 428	459, 489, 499

[a] calculated from the ensemble of 15 lowest energy structures
[b] Combines the clash score, rotamers, and Ramachandran evaluation into a single score
[c] From Procheck-NMR
[d] Average buried surface area from the ensemble of 15 structures
[e] Leu methyl groups are denoted δ and Val methyl groups γ
[f] amide NMR peak undergoes both a shift and broadening

Figure II.1: MT1-MMP Associates with Nanodiscs on Opposite Sides of the HPX Domain

(A) Bilayer proximities of Ile/Leu/Val side chains were measured to DMPC nanodiscs encircled by MSP1D1 (72) doped with an average of two nitroxide spin-labeled phosphatidylcholine (PC) molecules per leaflet. The resulting PREs were plotted as $\Gamma_2 = R_{2,\ paramag} - R_{2,diamag}$, the difference between methyl proton relaxation rates with and without doxyl-substituted DPPC. Γ_2 values resulting from addition of 10-doxyl PC or 5-doxyl PC are plotted in pink triangles and green spheres, respectively. The symbols are filled where $\Gamma_2 > 30/s$.
(B) Ile/Leu/Val side chains with $\Gamma_2 > 30/s$ are marked on the crystal structure of the HPX domain (PDB: 3C7X) with spheres which are pink for proximity to 10-doxyl PC and green to 5-doxyl PC. The blades of the β-propeller are colored blue for I, green for II, yellow for III, and pink IV, respectively, and throughout this article.
(C) Addition of the nanodiscs to the HPX domain in a 1:1 molar ratio induced the radial chemical shift perturbations (CSPs), quantified using eq. 2. CSPs exceeding 0.03 ppm are highlighted in orange.
(D) Sites of the larger CSPs ($\Delta\omega_{HN} > 0.03$ ppm) are plotted as spheres on the backbone.

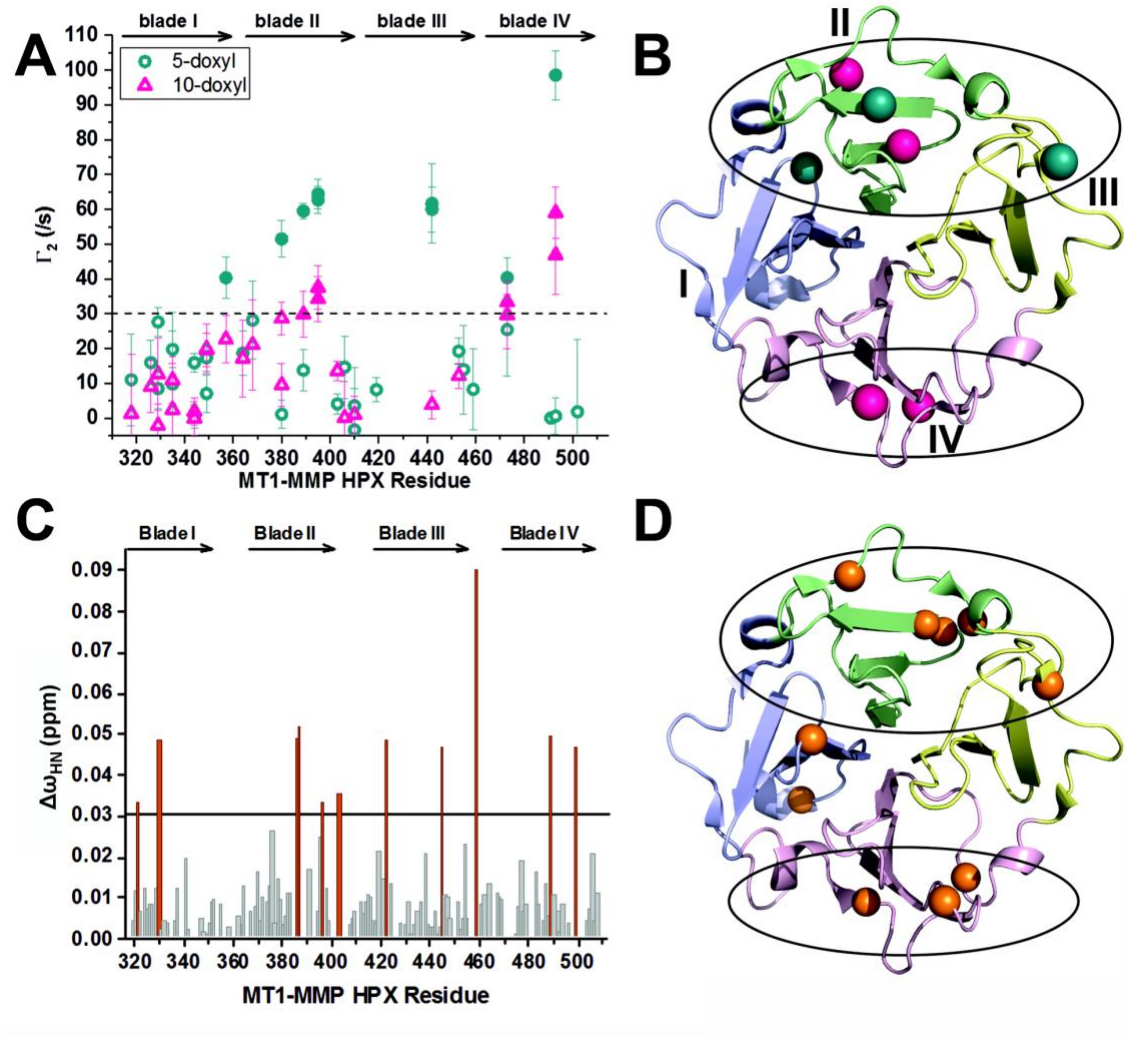
A
blade I
blade II
blade III
blade IV
5-doxyl
10-doxyl
Γ2 (/s)
MT1-MMP HPX Residue
B
II
III
I
IV
C
Blade I
Blade II
Blade III
Blade IV
Δω_HN (ppm)
MT1-MMP HPX Residue
D

Figure II.2: Modes of Nanodisc Binding to Blades II and IV

(A, B) An ensemble of 15 HPX structural models positioning blade II upon a nanodisc model was drawn from a 4-ns MD trajectory restrained by NMR PRE-based distances and shown in Movie S1. The structures were selected for lowest energy and minimal violation of the NMR restraints. The viewing angle differs by 90° between panels. The inset displays HPX residues in contact with the nanodiscs, with polar residues purple and hydrophobic residues green.
(C) Partial insertion of the EPGYPK loop of blade II among the phospholipid head groups is shown, with lipid oxygen atoms pink and carbon white.
(D, E) The PRE distance-restrained ensemble of 15 HPX structural models positioning blade IV on a nanodisc model was selected from another 4-ns MD trajectory shown in Movie S2.
(F) Insertion of the EPGYPK loop of blade IV among the phospholipid head groups is shown. See also Table S1 cataloguing protein contacts with the bilayer.

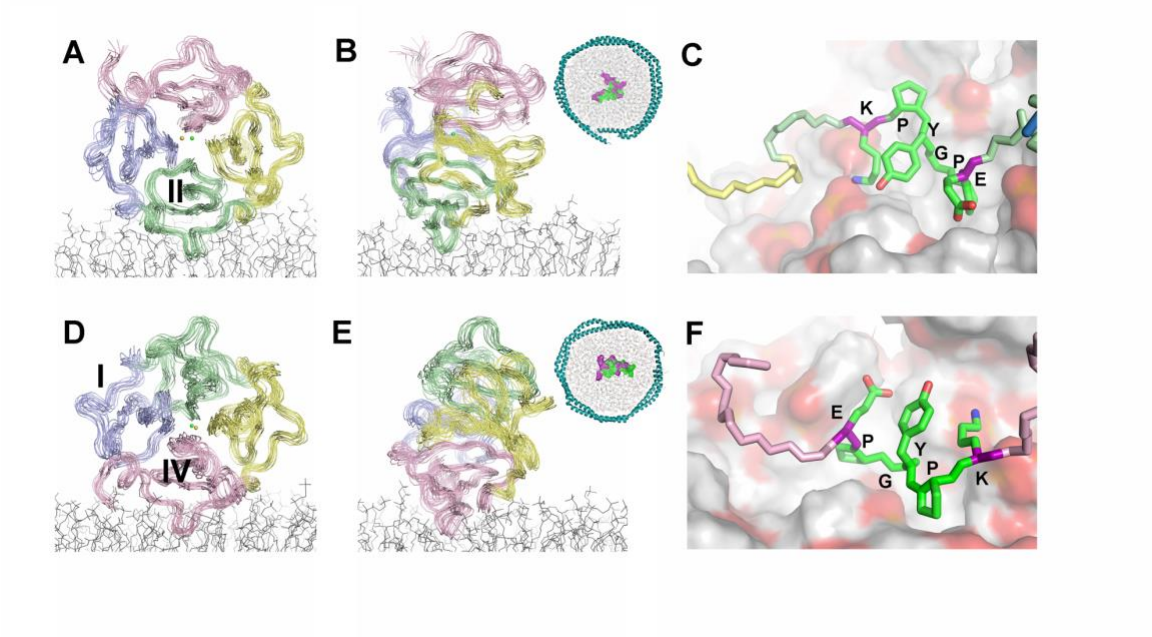

Figure II.3: Basic Residues at the Bulges from Blades II and IV that Support Binding of Soluble MT1-MMP to Membrane Vesicles

(A) Orange spheres identify the locations of Ser substitutions for Lys or Arg in the four blades.
(B) Quenching of Trp fluorescence from sMT1-MMP (orange with addition of doped SUVs and purple without) by addition SUVs composed of DMPC doped with Pyrene PE depends upon the point mutation. The background fluorescence from SUVs only was subtracted from the fluorescence of the mixtures as described (54).
(C) The crystallographic structures of HPX domains of MMPs are superposed. Blade IV of MT1-MMP (green) is distinctive in projecting the EPGYPK loop that is missing from the structures of soluble MMP-1 (red), MMP-2 (yellow), MMP-9 (pink), MMP-13 (purple), and MMP-12 (orange).
(D) Alignment of all human MMP sequences finds that the blade IV loop characteristic of membrane type MMPs is missing from the soluble MMPs. Parts of the corresponding loop from blade II can, however, be found in all MMPs.

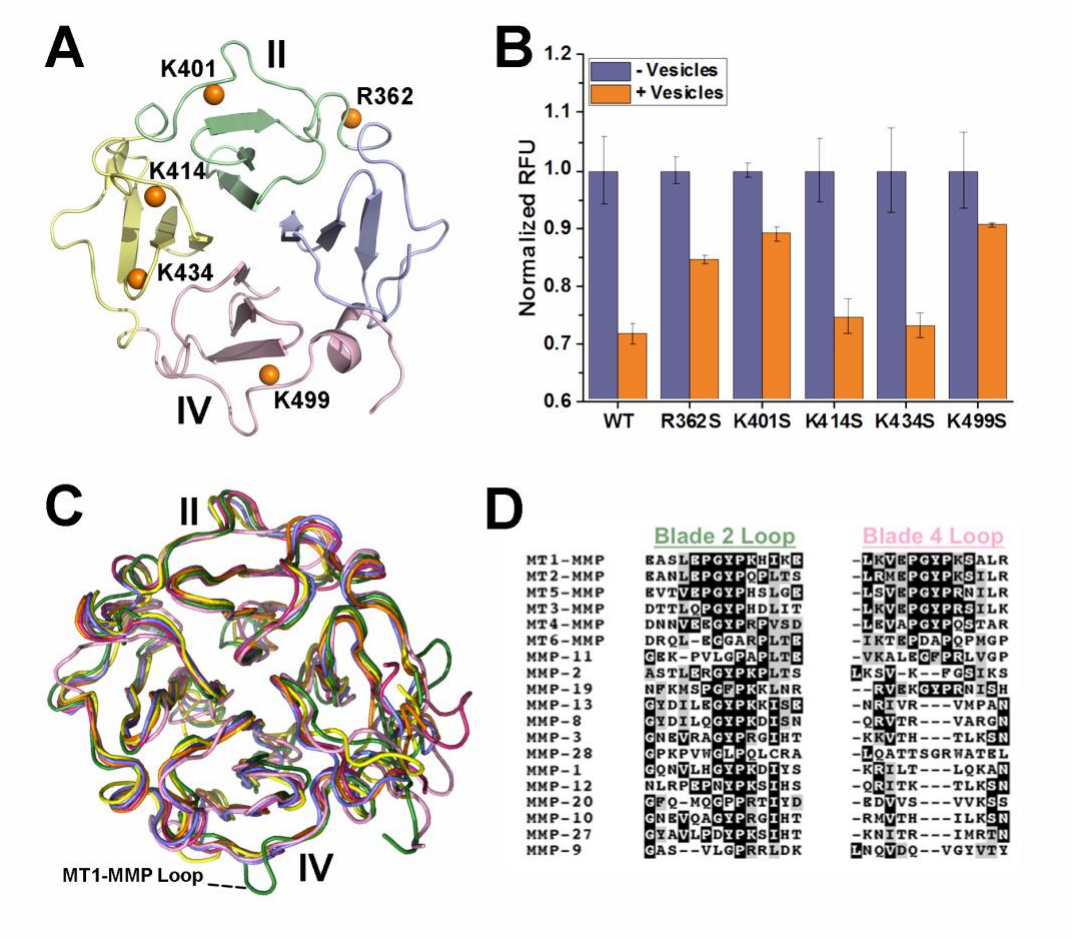

Figure II.4: Vesicles Enhance Digestion of Engineered *Streptococcus* Collagen–Like Protein by the Ectodomain of MT1-MMP

(A) The collagen mimic Scl2 comprises the trimerization domain V at the N-terminus and two *S. pyogenes* collagen-like CL domains. Six triplets from the α1 chain of human collagen II harboring the MMP-cleavable peptide bond (marked by ^) were inserted between the CL domains.
(B) The time course of the digestion of Scl2-collagen α1(II) substrate (20 μM) by sMT1-MMP (20 nM) in the presence of SUVs (with 250 μM DMPC monomers) at 30°C was monitored by SDS-PAGE.
(C) The percentage of the Scl2-collagen α1(II) hydrolyzed in the absence or presence of the SUVs is plotted over time using open circles or triangles, respectively.

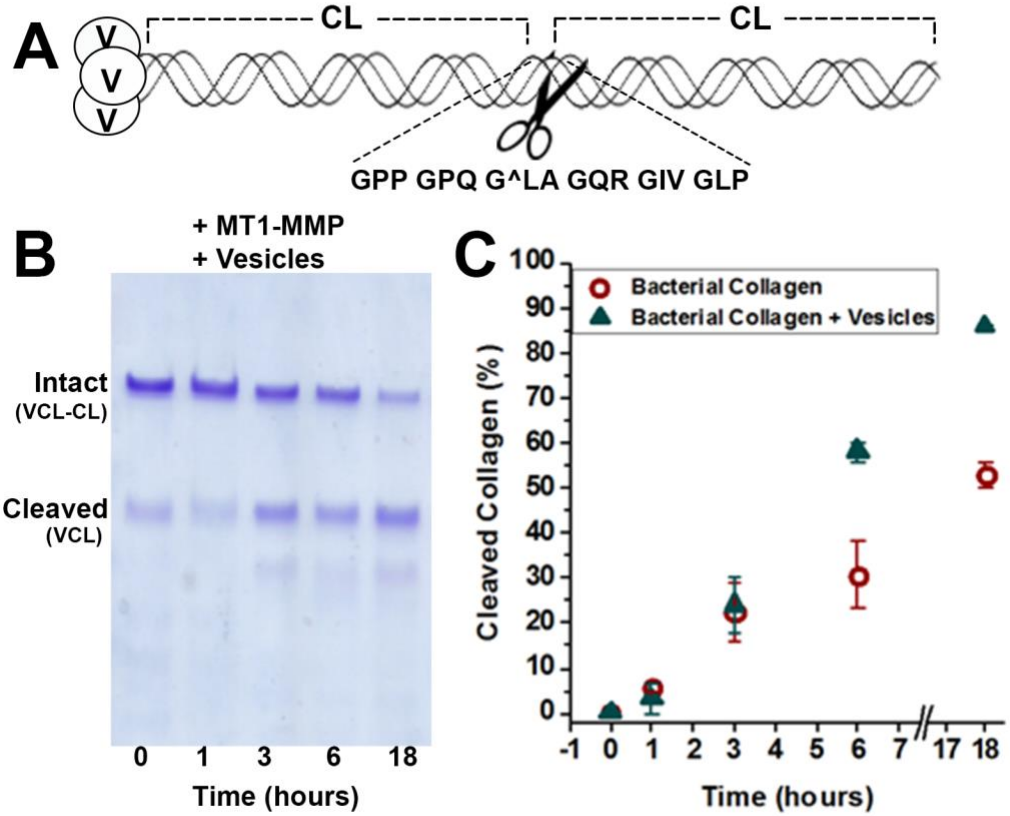

Figure II.5: Potential Assemblies of the HPX domain with Both the Collagen Triple-Helix and Lipid Bilayers

The solution structural model of the complex of a collagen triple-helical peptide with the HPX domain of MT1-MMP (29) is superimposed on the PRE-based structural models presented in Fig. 2 that have blade IV in contact with the bilayer. The compatibility of bilayer and triple-helix binding favor this type of “ternary” complex.
The superposition with experimental model with blade II in contact with the bilayer is plotted. The steric clash between bilayer and triple-helix disfavor formation of this type of “ternary” complex.
(C) Binding of triple-helix to blade IV and bilayers to both the blade II and IV interfaces appears compatible with the “side-by-side” dimer in the crystallographic asymmetric unit of 3C7X.pdb. This compatibility could favor this as a potentially functional dimer and complex. Green dots mark locations of outermost motifs of blades I and IV required for cell migration and proMMP-2 activation (32).

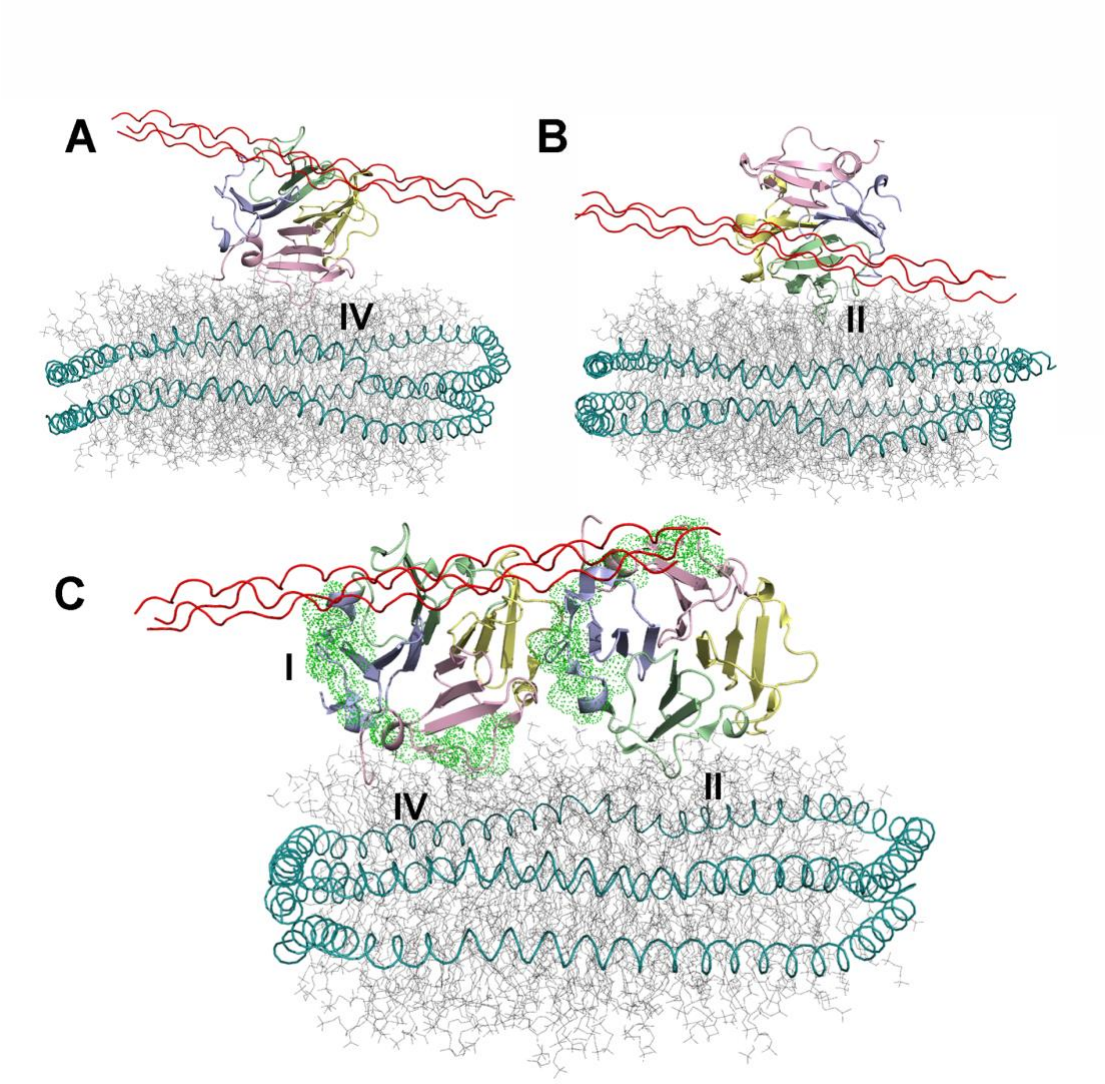

Figure II.6: Graphical Abstract

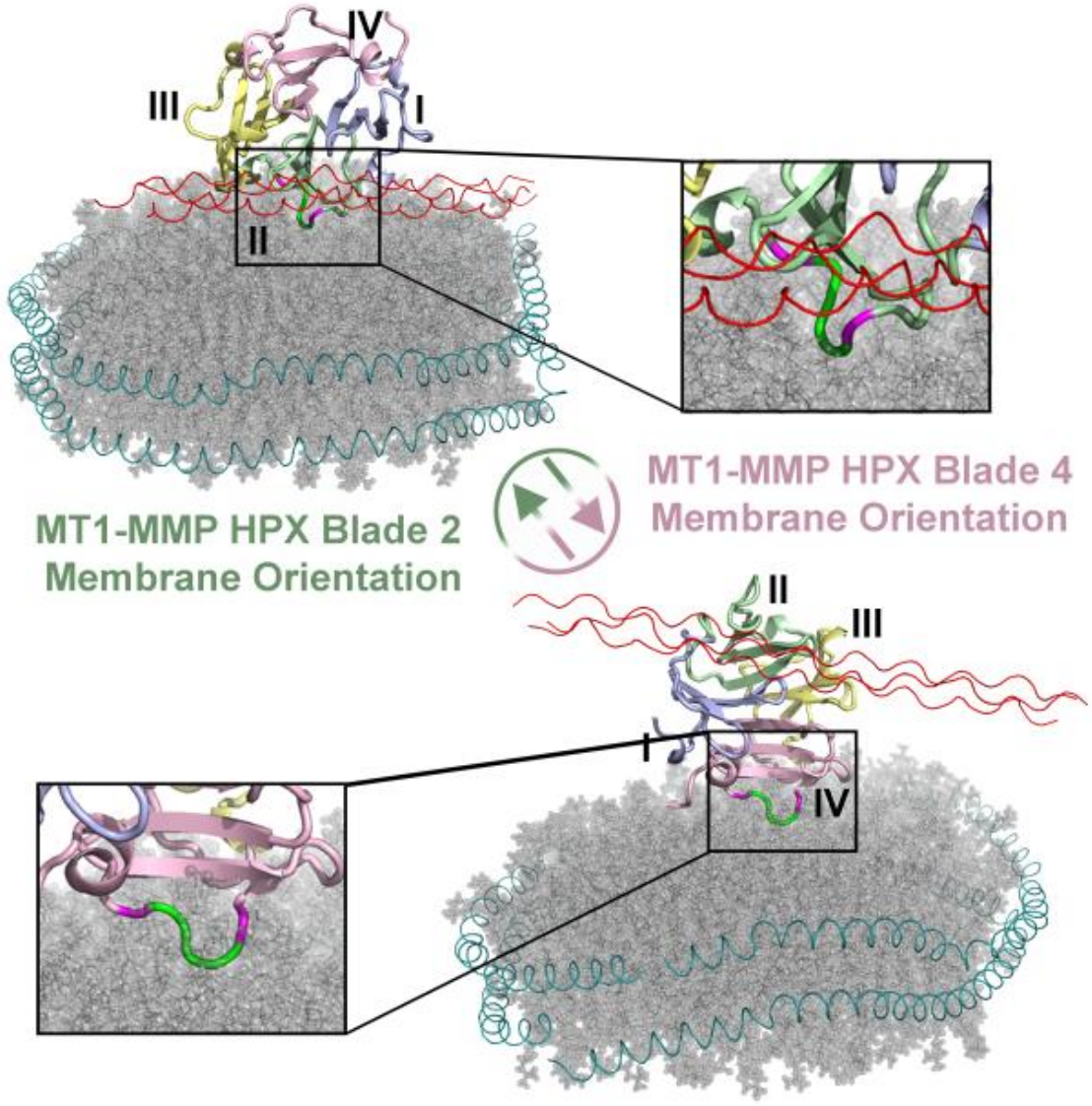

II.9 SUPPORTING FIGURES

Figure II.7 (S1) NMR Spectra, PREs, and Spectral Changes of the HPX Domain of MT1-MMP with Nanodiscs

(A,B) The Leu/Val methyl region of the ^{13}C HMQC spectrum of the HPX domain of human MT1-MMP is shown after addition of nanodiscs of DMPC and MSP1Da without (A) or with paramagnetic spin-label of 5-doxyl DPPC (B). Methyl peaks that experience broadening from the 5-doxyl DPPC are enclosed in dashed boxes.
(C) The raw data defining Γ_2 (the PRE) at Val493 are illustrated. The exponential decay of a methyl NMR peak of Val493 are shown in the presence of paramagnetic and diamagnetic nanodiscs. (The peak heights are measured as a function of the length of the CPMG portion of the NMR pulse sequence.)
(D) The exponential dependence of Γ_2 (the PRE) upon the distance r between the hydrogen atom detected and the unpaired electron is illustrated for globular assemblies with rotational correlation times of 10, 21 and 30 ns. See equation 3.
E) ^{15}N TROSY spectra in the absence (blue) and presence (red) of nanodiscs. CSPs with largest changes identified with arrows in orange dashed boxes.

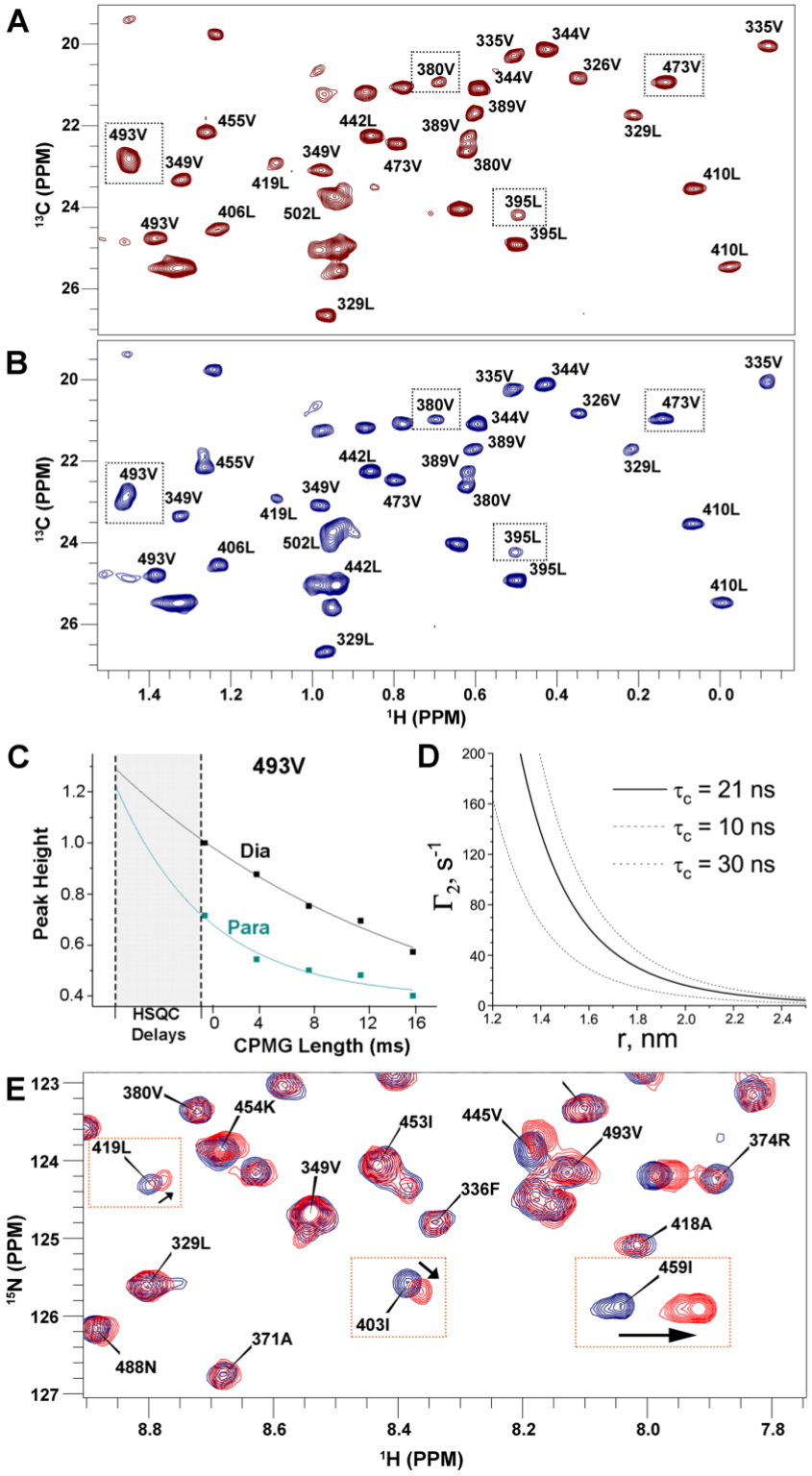
A
B
C
D
E
^{13}C (PPM)
^{1}H (PPM)
493V
Peak Height
Dia
Para
HSQC Delays
CPMG Length (ms)
τ_c = 21 ns
τ_c = 10 ns
τ_c = 30 ns
Γ_2, s^{-1}
r, nm
^{15}N (PPM)

Figure II.8 (S2) Spectroscopy and Negative Staining Electron Microscopy Imply Two Peripheral Membrane Binding Surfaces on Soluble MT1-MMP.

(A) Both modes of peripheral membrane binding by the HPX domain discovered by paramagnetic NMR and fluorescence proximity assays are superimposed. The blade II-proximal association colors lipids in green. The blade IV-proximal association colors lipids in pink. (B) The recent proposal of binding instead at blade III (26)(yellow) is plotted with the HPX domain in the same orientation in order to illustrate the difference in orientations evident from direct measurements of proximity to nanodiscs. (C) An image from electron microscopy is shown of mixtures of sMT1-MMP with nanodiscs negatively stained with methylamine tungstate (Nano-W®). Representative single nanodiscs are outlined in blue, stacked nanodiscs in pink, and higher order stacking in red.

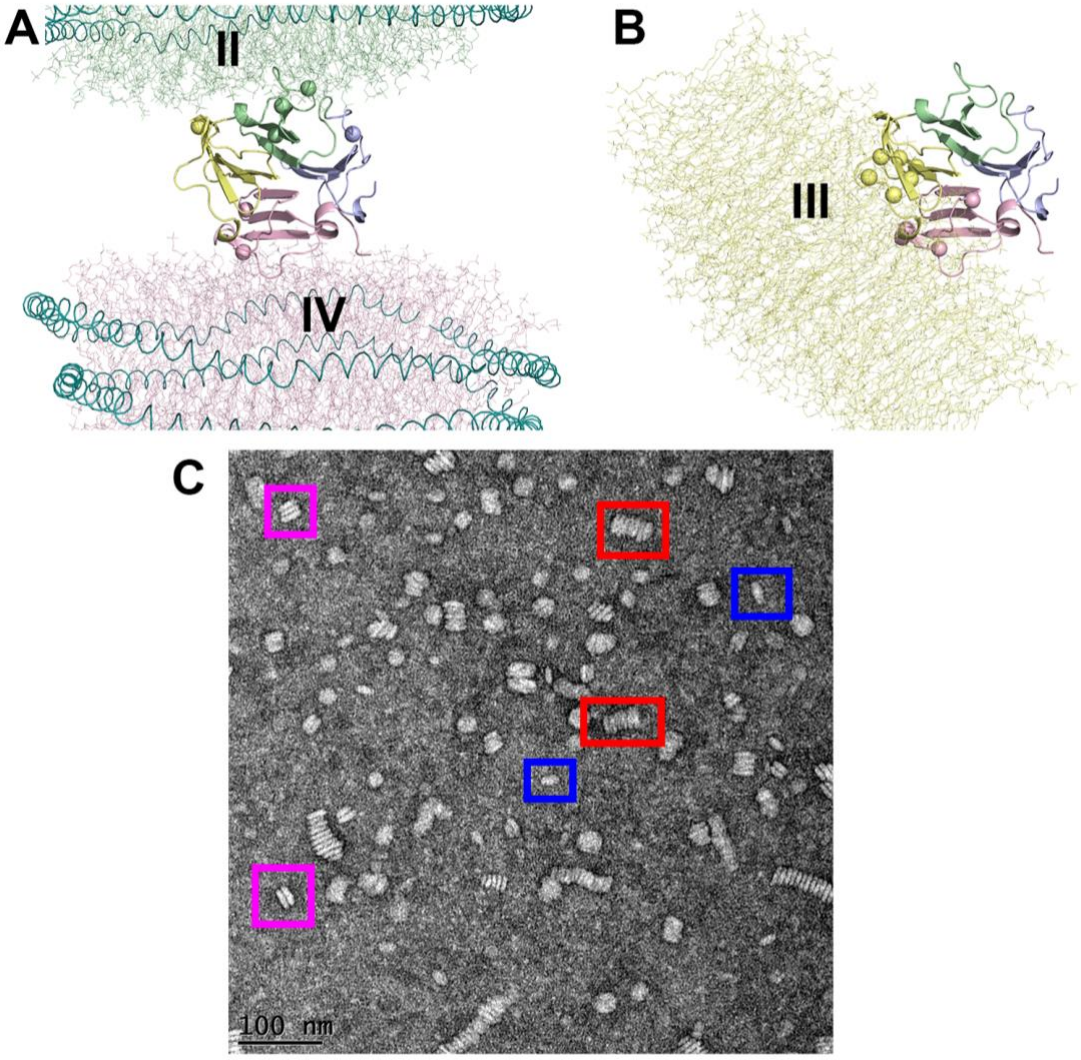

Figure II.9 (S3) Site-directed fluor labeling confirms the proximity to DMPC vesicles of blades II and IV and disputes the proximity of blades I and III

The polarity-sensitive fluorophore IANBD was conjugated to a single cysteine substitution at each of six sites on the HPX domain of MT1-MMP.

(A) The fluorescence emission of IANBD in the presence of SUVs is normalized by that in the absence. Increases of fluorescence emission of 1.3-fold or greater are considered evidence of the exposed NBD groups dipping into a hydrophobic phase such as the acyl chains of a lipid bilayer.

(B) The sites of single cysteine substitutions are marked by spheres on the crystal structure (PDB: 3C7X).

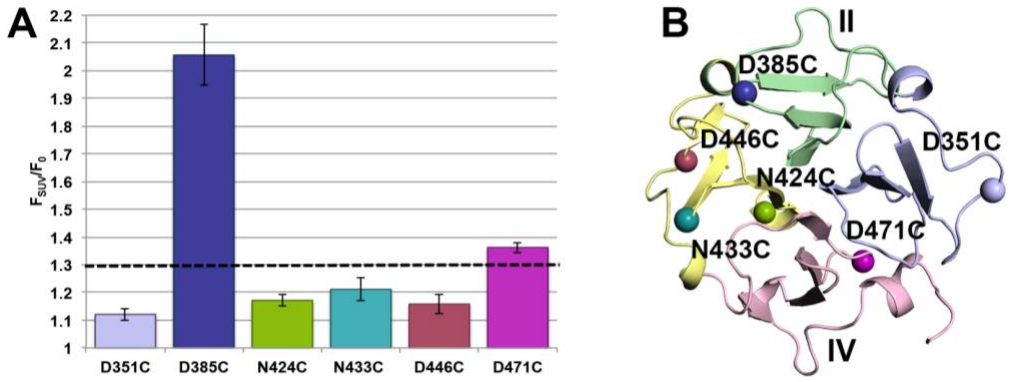

Figure II.10 (S4) Evolutionary Trace Analysis of MMP HPX Domains Reveals that MT MMPs with Transmembrane Helices Conserve the PGyP Sequence Motif in Blades II and IV.

This includes the EPGYPK loops of MT1-MMP that insert into Nanodisc bilayers.
(A) The phylogenetic tree of aligned sequences from MMPs spanning 10 species of vertebrates.
(B) "Consensus sequences" conserved within subfamilies of MMPs are listed. The sequences are divided into subfamilies at the sequence identity cutoff named Trace level 12 which is pointed out by the arrow in panel A to the 12th vertical line from the left.
(C) Coloration of the conservation on the HPX structure from MT1-MMP indicates the second proline in the EPGY**P**K loop of blade II (pink) to be conserved over almost all MMPs.

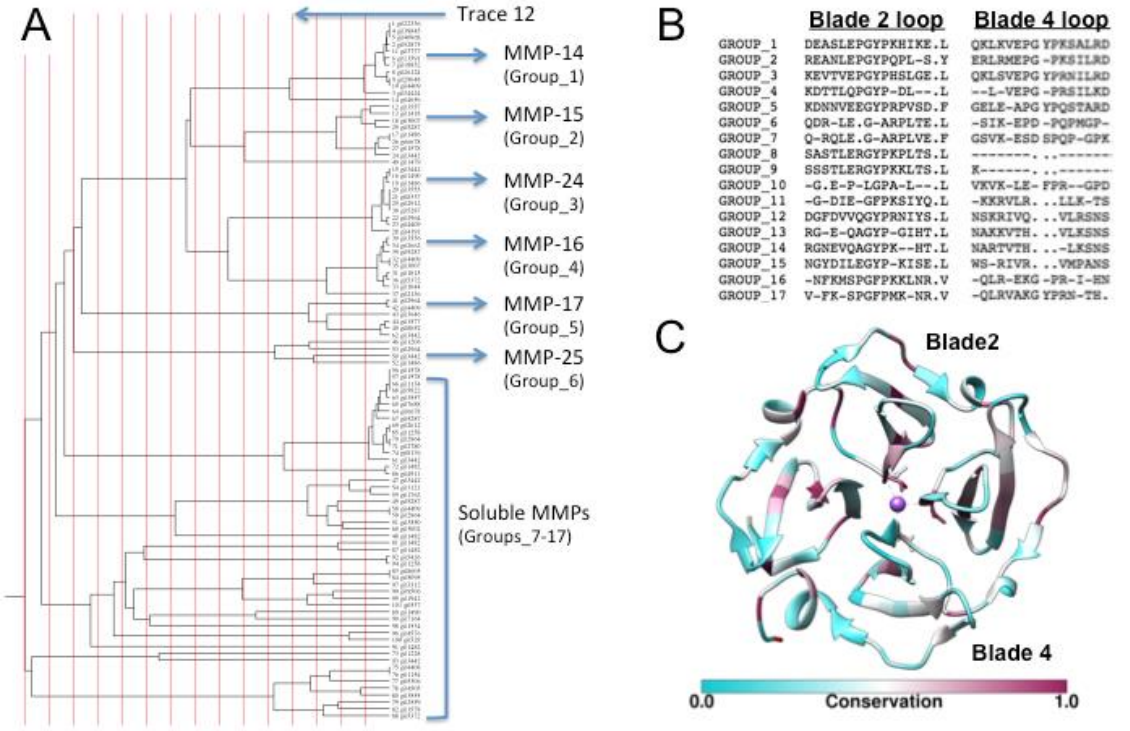

Figure II.11 (S5) Interplay between Vesicle and Collagen Triple-Helical Peptide Interactions with sMT1-MMP

(A) Additions of SUVs enhance hydrolysis of the fTHP-9 substrate. The amount of DMPC monomers present is given in the legend.
(B) Excess THP competes with SUVs for binding sMT1-MMP. Trp fluorescence emission is plotted on the ordinate and all measurements are normalized to free sMT1-MMP emission. The mole ratio of triple-helical peptide, α1(I)772–786 THP, to sMT1-MMP is indicated. Higher emission at 315 nm indicates less proximity to the pyrene quencher placed in the SUVs. The SUVs present throughout were composed of DMPC monomers at 250 μM with the addition of Pyrene-PE at 5 μM to quench the Trp fluorescence emission.

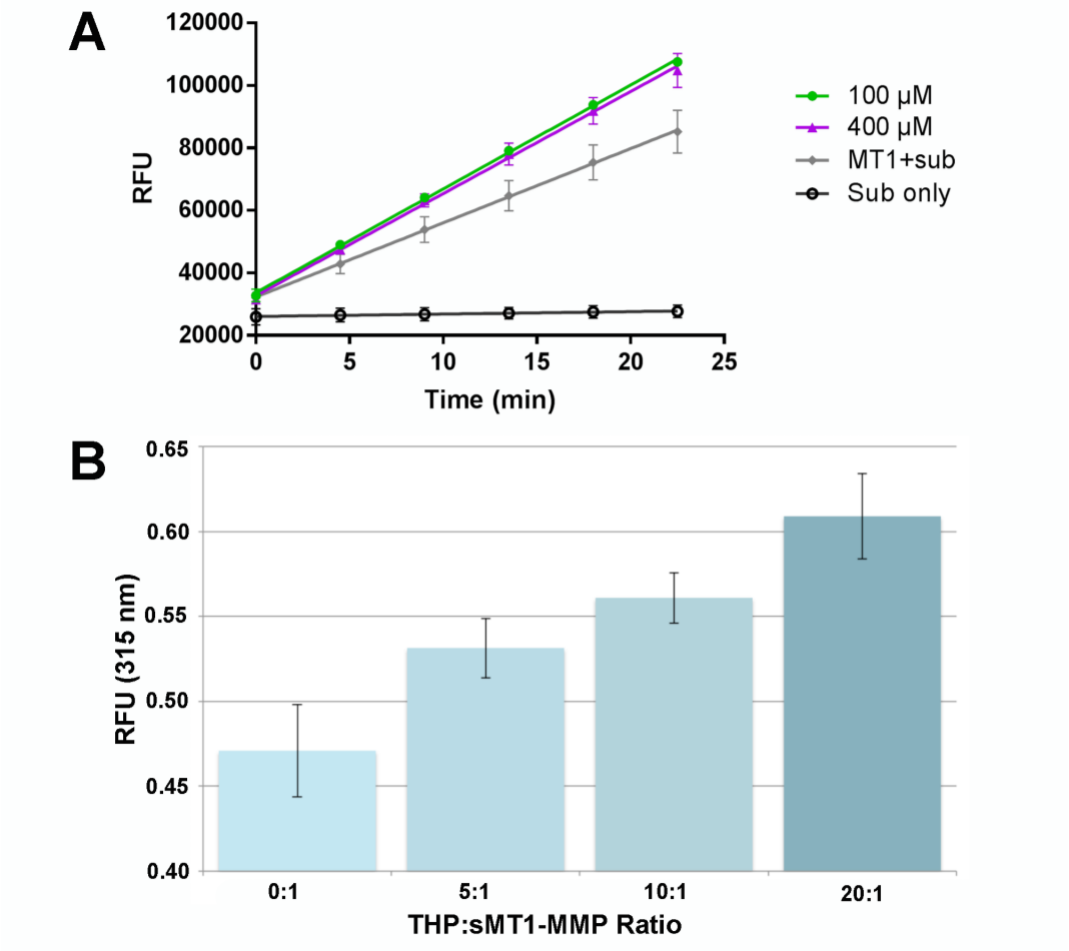

Figure II.12 (S6) Restrained MD Attempts to Satisfy the PRE-Based Distance Restraints of Nanodiscs to Both Blades II and IV of the symmetric (V-shaped) Dimer Distort Both EPGYPK Membrane-Binding Loops.

(A) The lowest energy structure generated by 3 ns of minimization and equilibration with the PRE NMR-based distance restraints is plotted. Residues mutated in one study (25) are highlighted with orange dots. Epitopes targeted by peptide inhibitors in another study are colored bright green (32). The path of collagen triple-helix binding to the HPX domain alone (29) is indicated by the triple-helix plotted with red ribbon.
(B) The distortion of blade II by the restrained MD is shown by the overlay of the structural model from (A; blade II in light green) with the crystallographic starting coordinates (PDB: 3C7X) in magenta.
(C) The distortion of blade IV is shown by the overlay of the outcome of the same restrained MD simulation (blade IV in light pink) with the crystal structure (magenta).

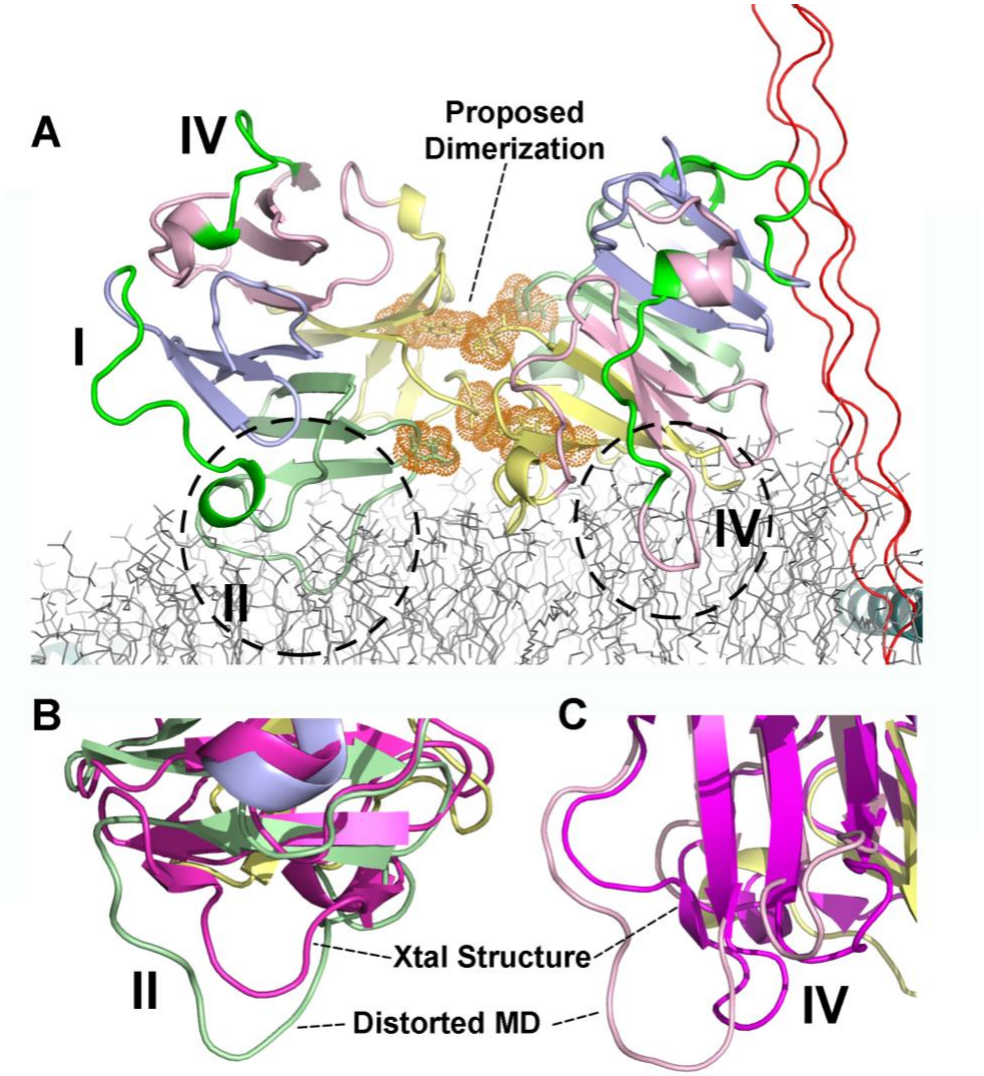
A
IV
Proposed
Dimerization
I
II
IV
B
C
Xtal Structure
Distorted MD
II
IV

Table II-2 (S1) Polar Contacts of HPX Domain with Lipid Head Groups, Conservatively Listing Minimum Frequencies in Each Ensemble

Blade 2 interface		***H-bonds to DMPC***	***Salt bridge to DMPC***
ARG 362	HE		O12 (214) 7%
	HH1		O32^(204) 20%
	HH2		O12 (214) 33%
SER 394	NH	O13 (214) 40%	
	HG	O12 (218) 47%	
LYS 401	HZ1		O13 (213) 53%
	HZ1		O13 (215) 13%
ARG 443	HH2		O14 (215) 80%
Blade 4 interface			
LYS454	HZ1		O11/13/14 (195) 33%
LYS 482	HZ1		O14 (212) 47%
	HZ1		O14 (217) 80%
LYS 490	HZ1		O13/14 (201) 27%
	HZ2		O13/22^ (213) 66%
GLY 496	NH	O14 (215) 60%	
LYS 499	NZ1		O11/13 (216) 54%
ARG 503	HH1		O12/13 (218) 80%
SER 510	HG	O14 (214) 60%	

¢ Phosphate oxygen, except where noted. The number of the lipid molecule is listed in parentheses.

^Ester carbonyl oxygen

II.10 REFERENCES

1. Sato, H., Takino, T., Okada, Y., Cao, J., Shinagawa, A., Yamamoto, E., and Seiki, M. (1994) A matrix metalloproteinase expressed on the surface of invasive tumour cells. *Nature* **370**, 61-65

2. Sabeh, F., Shimizu-Hirota, R., and Weiss, S. J. (2009) Protease-dependent versus -independent cancer cell invasion programs: three-dimensional amoeboid movement revisited. *The Journal of Cell Biology* **185**, 11-19

3. Itoh, Y. (2015) Membrane-type matrix metalloproteinases: Their functions and regulations. *Matrix Biol* **44-46**, 207-223

4. Chun, T. H., Sabeh, F., Ota, I., Murphy, H., McDonagh, K. T., Holmbeck, K., Birkedal-Hansen, H., Allen, E. D., and Weiss, S. J. (2004) MT1-MMP-dependent neovessel formation within the confines of the three-dimensional extracellular matrix. *J Cell Biol* **167**, 757-767

5. Sabeh, F., Ota, I., Holmbeck, K., Birkedal-Hansen, H., Soloway, P., Balbin, M., Lopez-Otin, C., Shapiro, S., Inada, M., Krane, S., Allen, E., Chung, D., and Weiss, S. J. (2004) Tumor cell traffic through the extracellular matrix is controlled by the membrane-anchored collagenase MT1-MMP. *J Cell Biol* **167**, 769-781

6. Davis, G. E., and Saunders, W. B. (2006) Molecular balance of capillary tube formation versus regression in wound repair: role of matrix metalloproteinases and their inhibitors. *J Investig Dermatol Symp Proc* **11**, 44-56

7. Fisher, K. E., Sacharidou, A., Stratman, A. N., Mayo, A. M., Fisher, S. B., Mahan, R. D., Davis, M. J., and Davis, G. E. (2009) MT1-MMP- and Cdc42-dependent signaling co-regulate cell invasion and tunnel formation in 3D collagen matrices. *J Cell Sci* **122**, 4558-4569

8. Wolf, K., Wu, Y. I., Liu, Y., Geiger, J., Tam, E., Overall, C., Stack, M. S., and Friedl, P. (2007) Multi-step pericellular proteolysis controls the transition from individual to collective cancer cell invasion. *Nat Cell Biol* **9**, 893-904

9. Friedl, P., and Wolf, K. (2008) Tube travel: the role of proteases in individual and collective cancer cell invasion. *Cancer Res* **68**, 7247-7249

10. Koshikawa, N., Giannelli, G., Cirulli, V., Miyazaki, K., and Quaranta, V. (2000) Role of cell surface metalloprotease MT1-MMP in epithelial cell migration over laminin-5. *J Cell Biol* **148**, 615-624

11. Gilles, C., Polette, M., Coraux, C., Tournier, J. M., Meneguzzi, G., Munaut, C., Volders, L., Rousselle, P., Birembaut, P., and Foidart, J. M. (2001) Contribution of MT1-MMP and of human laminin-5 γ2 chain degradation to mammary epithelial cell migration. *Journal of Cell Science* **114**, 2967-2976

12. Koshikawa, N., Mizushima, H., Minegishi, T., Iwamoto, R., Mekada, E., and Seiki, M. (2010) Membrane type 1-matrix metalloproteinase cleaves off the NH 2-terminal portion of heparin-binding epidermal growth factor and converts it into a heparin-independent growth factor. *Cancer Research* **70**, 6093-6103

13. Kajita, M., Itoh, Y., Chiba, T., Mori, H., Okada, A., Kinoh, H., and Seiki, M. (2001) Membrane-type 1 matrix metalloproteinase cleaves CD44 and promotes cell migration. *J Cell Biol* **153**, 893-904

14. Endo, K., Takino, T., Miyamori, H., Kinsen, H., Yoshizaki, T., Furukawa, M., and Sato, H. (2003) Cleavage of syndecan-1 by membrane type matrix metalloproteinase-1 stimulates cell migration. *J Biol Chem* **278**, 40764-40770

15. Deryugina, E. I., Ratnikov, B. I., Postnova, T. I., Rozanov, D. V., and Strongin, A. Y. (2002) Processing of integrin alpha(v) subunit by membrane type 1 matrix metalloproteinase stimulates migration of breast carcinoma cells on vitronectin and enhances tyrosine phosphorylation of focal adhesion kinase. *J Biol Chem* **277**, 9749-9756

16. Sithu, S. D., English, W. R., Olson, P., Krubasik, D., Baker, A. H., Murphy, G., and D'Souza, S. E. (2007) Membrane-type 1-matrix metalloproteinase regulates intracellular adhesion molecule-1 (ICAM-1)-mediated monocyte transmigration. *J Biol Chem* **282**, 25010-25019

17. Hakulinen, J., Sankkila, L., Sugiyama, N., Lehti, K., and Keski-Oja, J. (2008) Secretion of active membrane type 1 matrix metalloproteinase (MMP-14) into extracellular space in microvesicular exosomes. *J Cell Biochem* **105**, 1211-1218

18. Mori, H., Tomari, T., Koshikawa, N., Kajita, M., Itoh, Y., Sato, H., Tojo, H., Yana, I., and Seiki, M. (2002) CD44 directs membrane-type 1 matrix metalloproteinase

to lamellipodia by associating with its hemopexin-like domain. *Embo J* **21**, 3949-3959

19. Wang, Z., Zhang, F., He, J., Wu, P., Tay, L. W. R., Cai, M., Nian, W., Weng, Y., Qin, L., Chang, J. T., McIntire, L. B., Di Paolo, G., Xu, J., Peng, J., and Du, G. (2017) Binding of PLD2-Generated Phosphatidic Acid to KIF5B Promotes MT1-MMP Surface Trafficking and Lung Metastasis of Mouse Breast Cancer Cells. *Dev. Cell* **43**, 186-197.e187

20. Albrechtsen, R., Stautz D, Sanjay A, Kveiborg M , Wewer, U. M. (2015) Extracellular engagement of ADAM12 induces clusters of invadopodia with localized ectodomain shedding activity.

21. Yamaguchi, H., Takeo, Y., Yoshida, S., Kouchi, Z., Nakamura, Y., and Fukami, K. (2009) Lipid Rafts and Caveolin-1 Are Required for Invadopodia Formation and Extracellular Matrix Degradation by Human Breast Cancer Cells. *Cancer Research* **69**, 8594-8602

22. Shimoda, M., and Khokha, R. (2017) Metalloproteinases in extracellular vesicles. *Biochimica et Biophysica Acta (BBA) - Molecular Cell Research* **1864**, 1989-2000

23. Hoshino, D., Kirkbride, K. C., Costello, K., Clark, E. S., Sinha, S., Grega-Larson, N., Tyska, M. J., and Weaver, A. M. (2013) Exosome secretion is enhanced by invadopodia and drives invasive behavior. *Cell Rep* **5**, 1159-1168

24. Bode, W. (1995) A helping hand for collagenases: the haemopexin-like domain. *Structure* **3**, 527-530

25. Tochowicz, A., Goettig, P., Evans, R., Visse, R., Shitomi, Y., Palmisano, R., Ito, N., Richter, K., Maskos, K., Franke, D., Svergun, D., Nagase, H., Bode, W., and Itoh, Y. (2011) The dimer interface of the membrane type 1 matrix metalloproteinase hemopexin domain: crystal structure and biological functions. *J Biol Chem* **286**, 7587-7600

26. Cerofolini, L., Amar, S., Lauer, J. L., Martelli, T., Fragai, M., Luchinat, C., and Fields, G. B. (2016) Bilayer Membrane Modulation of Membrane Type 1 Matrix Metalloproteinase (MT1-MMP) Structure and Proteolytic Activity. *Sci Rep* **6**, 29511

27. Van Doren, S. R., Marcink, T. C., Koppisetti, R. K., Jurkevich, A., and Fulcher, Y. G. (2017) Peripheral membrane associations of matrix metalloproteinases. *Biochim Biophys Acta*

28. Collier, I. E., Legant, W., Marmer, B., Lubman, O., Saffarian, S., Wakatsuki, T., Elson, E., and Goldberg, G. I. (2011) Diffusion of MMPs on the surface of collagen fibrils: the mobile cell surface-collagen substratum interface. *PLoS One* **6**, e24029

29. Zhao, Y., Marcink, T. C., Sanganna Gari, R. R., Marsh, B. P., King, G. M., Stawikowska, R., Fields, G. B., and Van Doren, S. R. (2015) Transient collagen triple helix binding to a key metalloproteinase in invasion and development. *Structure* **23**, 257-269

30. Tam, E. M., Moore, T. R., Butler, G. S., and Overall, C. M. (2004) Characterization of the distinct collagen binding, helicase and cleavage mechanisms of matrix metalloproteinase 2 and 14 (gelatinase A and MT1-MMP): the differential roles of the MMP hemopexin c domains and the MMP-2 fibronectin type II modules in collagen triple helicase activities. *J Biol Chem* **279**, 43336-43344

31. Li, X. Y., Ota, I., Yana, I., Sabeh, F., and Weiss, S. J. (2008) Molecular dissection of the structural machinery underlying the tissue-invasive activity of membrane type-1 matrix metalloproteinase. *Mol Biol Cell* **19**, 3221-3233

32. Zarrabi, K., Dufour, A., Li, J., Kuscu, C., Pulkoski-Gross, A., Zhi, J., Hu, Y., Sampson, N. S., Zucker, S., and Cao, J. (2011) Inhibition of matrix metalloproteinase 14 (MMP-14)-mediated cancer cell migration. *J Biol Chem* **286**, 33167-33177

33. Amar, S., Smith, L., and Fields, G. B. (2017) Matrix metalloproteinase collagenolysis in health and disease. *Biochim Biophys Acta* **1864**, 1940-1951

34. Itoh, Y., Takamura, A., Ito, N., Maru, Y., Sato, H., Suenaga, N., Aoki, T., and Seiki, M. (2001) Homophilic complex formation of MT1-MMP facilitates proMMP-2 activation on the cell surface and promotes tumor cell invasion. *EMBO J* **20**, 4782-4793

35. Itoh, Y., Palmisano, R., Anilkumar, N., Nagase, H., Miyawaki, A., and Seiki, M. (2011) Dimerization of MT1-MMP during cellular invasion detected by fluorescence resonance energy transfer. *Biochem J* **440**, 319-326

36. Lehti, K., Lohi, J., Juntunen, M. M., Pei, D., and Keski-Oja, J. (2002) Oligomerization through hemopexin and cytoplasmic domains regulates the activity and turnover of membrane-type 1 matrix metalloproteinase. *J Biol Chem* **277**, 8440-8448

37. Itoh, Y., Ito, N., Nagase, H., Evans, R. D., Bird, S. A., and Seiki, M. (2006) Cell surface collagenolysis requires homodimerization of the membrane-bound collagenase MT1-MMP. *Mol Biol Cell* **17**, 5390-5399

38. Itoh, Y., Ito, N., Nagase, H., and Seiki, M. (2008) The second dimer interface of MT1-MMP, the transmembrane domain, is essential for ProMMP-2 activation on the cell surface. *J Biol Chem* **283**, 13053-13062

39. von Nandelstadh, P., Gucciardo, E., Lohi, J., Li, R., Sugiyama, N., Carpen, O., and Lehti, K. (2014) Actin-associated protein palladin promotes tumor cell invasion by linking extracellular matrix degradation to cell cytoskeleton. *Mol Biol Cell* **25**, 2556-2570

40. Basu, B., Correa de Sampaio, P., Mohammed, H., Fogarasi, M., Corrie, P., Watkins, N. A., Smethurst, P. A., English, W. R., Ouwehand, W. H., and Murphy, G. (2012) Inhibition of MT1-MMP activity using functional antibody fragments selected against its hemopexin domain. *Int J Biochem Cell Biol* **44**, 393-403

41. Botkjaer, K. A., Kwok, H. F., Terp, M. G., Karatt-Vellatt, A., Santamaria, S., McCafferty, J., Andreasen, P. A., Itoh, Y., Ditzel, H. J., and Murphy, G. (2016) *Development of a specific affinity-matured exosite inhibitor to MT1-MMP that efficiently inhibits tumor cell invasion in vitro and metastasis in vivo*,

42. Denisov, I. G., and Sligar, S. G. (2016) Nanodiscs for structural and functional studies of membrane proteins. *Nat Struct Mol Biol* **23**, 481-486

43. Denisov, I. G., and Sligar, S. G. (2017) Nanodiscs in Membrane Biochemistry and Biophysics. *Chem Rev* **117**, 4669-4713

44. Mazhab-Jafari, M. T., Marshall, C. B., Smith, M. J., Gasmi-Seabrook, G. M., Stathopulos, P. B., Inagaki, F., Kay, L. E., Neel, B. G., and Ikura, M. (2015) Oncogenic and RASopathy-associated K-RAS mutations relieve membrane-dependent occlusion of the effector-binding site. *Proc Natl Acad Sci U S A* **112**, 6625-6630

45. Mazhab-Jafari, M. T., Marshall, C. B., Stathopulos, P. B., Kobashigawa, Y., Stambolic, V., Kay, L. E., Inagaki, F., and Ikura, M. (2013) Membrane-dependent modulation of the mTOR activator Rheb: NMR observations of a GTPase tethered to a lipid-bilayer nanodisc. *J Am Chem Soc* **135**, 3367-3370

46. Kutateladze, T. G., Capelluto, D. G., Ferguson, C. G., Cheever, M. L., Kutateladze, A. G., Prestwich, G. D., and Overduin, M. (2004) Multivalent mechanism of membrane insertion by the FYVE domain. *J Biol Chem* **279**, 3050-3057

47. Koppisetti, R. K., Fulcher, Y. G., Jurkevich, A., Prior, S. H., Xu, J., Lenoir, M., Overduin, M., and Van Doren, S. R. (2014) Ambidextrous binding of cell and membrane bilayers by soluble matrix metalloproteinase-12. *Nat Commun* **5**, 5552

48. Prior, S. H., Fulcher, Y. G., Koppisetti, R. K., Jurkevich, A., and Van Doren, S. R. (2015) Charge-Triggered Membrane Insertion of Matrix Metalloproteinase-7, Supporter of Innate Immunity and Tumors. *Structure* **23**, 2099-2110

49. Marcink, T. C., Koppisetti, R. K., Fulcher, Y. G., and Van Doren, S. R. (2017) Mapping Lipid Bilayer Recognition Sites of Metalloproteinases and Other Prospective Peripheral Membrane Proteins. in *Matrix Metalloproteases: Methods and Protocols* (Galea, C. A. ed.), Springer New York, New York, NY. pp 61-86

50. Lenoir, M., Coskun, U., Grzybek, M., Cao, X., Buschhorn, S. B., James, J., Simons, K., and Overduin, M. (2010) Structural basis of wedging the Golgi membrane by FAPP pleckstrin homology domains. *EMBO Rep* **11**, 279-284

51. Hagn, F., Etzkorn, M., Raschle, T., and Wagner, G. (2013) Optimized phospholipid bilayer nanodiscs facilitate high-resolution structure determination of membrane proteins. *J Am Chem Soc* **135**, 1919-1925

52. Dominguez, C., Boelens, R., and Bonvin, A. M. (2003) HADDOCK: a protein-protein docking approach based on biochemical or biophysical information. *J Am Chem Soc* **125**, 1731-1737

53. Huang, J., and MacKerell, A. D., Jr. (2013) CHARMM36 all-atom additive protein force field: validation based on comparison to NMR data.

54. Ganguly, B., Banerjee, J., Elegbede, A. I., Klocke, D. J., Mallik, S., and Srivastava, D. K. (2007) Intrinsic selectivity in binding of matrix metalloproteinase-7 to differently charged lipid membranes. *FEBS Lett* **581**, 5723-5726

55. Tatulian, S. A. (2017) Chapter Nine - Interfacial Enzymes: Membrane Binding, Orientation, Membrane Insertion, and Activity. in *Methods Enzymol.* (Michael, H. G. ed.), Academic Press. pp 197-230

56. Schulz, T. A., Choi, M. G., Raychaudhuri, S., Mears, J. A., Ghirlando, R., Hinshaw, J. E., and Prinz, W. A. (2009) Lipid-regulated sterol transfer between closely apposed membranes by oxysterol-binding protein homologues. *J Cell Biol* **187**, 889-903

57. Lichtarge, O., Bourne, H. R., and Cohen, F. E. (1996) An evolutionary trace method defines binding surfaces common to protein families. *J Mol Biol* **257**, 342-358

58. Yu, Z., Visse, R., Inouye, M., Nagase, H., and Brodsky, B. (2012) Defining requirements for collagenase cleavage in collagen type III using a bacterial collagen system. *J Biol Chem* **287**, 22988-22997

59. Sabeh, F., Li, X. Y., Saunders, T. L., Rowe, R. G., and Weiss, S. J. (2009) Secreted versus membrane-anchored collagenases: relative roles in fibroblast-dependent collagenolysis and invasion. *J Biol Chem* **284**, 23001-23011

60. Turunen, S. P., Tatti-Bugaeva, O., and Lehti, K. (2017) Membrane-type matrix metalloproteases as diverse effectors of cancer progression. *Biochimica et Biophysica Acta (BBA) - Molecular Cell Research* **1864**, 1974-1988

61. Deryugina, E. I., and Quigley, J. P. (2011) The Role of Matrix Metalloproteinases in Cellular Invasion and Metastasis. in *Extracellular Matrix Degradation* (Parks, W. C., and Mecham, R. P. eds.), Springer-Verlag, Berlin. pp 145-191

62. Rouck, J. E., Krapf, J. E., Roy, J., Huff, H. C., and Das, A. (2017) Recent advances in nanodisc technology for membrane protein studies (2012-2017). *FEBS Lett* **591**, 2057-2088

63. Arumugam, S., Hemme, C. L., Yoshida, N., Suzuki, K., Nagase, H., Berjanskii, M., Wu, B., and Van Doren, S. R. (1998) TIMP-1 contact sites and perturbations of

stromelysin 1 mapped by NMR and a paramagnetic surface probe. *Biochemistry* **37**, 9650-9657.

64. Arumugam, S., and Van Doren, S. R. (2003) Global orientation of bound MMP-3 and N-TIMP-1 in solution via residual dipolar couplings. *Biochemistry* **42**, 7950-7958

65. Takeda, M., Terasawa, H., Sakakura, M., Yamaguchi, Y., Kajiwara, M., Kawashima, H., Miyasaka, M., and Shimada, I. (2003) Hyaluronan recognition mode of CD44 revealed by cross-saturation and chemical shift perturbation experiments. *J Biol Chem* **278**, 43550-43555

66. Clore, G. M., Tang, C., and Iwahara, J. (2007) Elucidating transient macromolecular interactions using paramagnetic relaxation enhancement. *Curr Opin Struct Biol* **17**, 603-616

67. Clore, G. M. (2015) Chapter Seventeen - Practical Aspects of Paramagnetic Relaxation Enhancement in Biological Macromolecules. in *Methods Enzymol.* (Peter, Z. Q., and Kurt, W. eds.), Academic Press. pp 485-497

68. Prior, S. H., Byrne, T. S., Tokmina-Roszyk, D., Fields, G. B., and Van Doren, S. R. (2016) Path to Collagenolysis: Collagen V Triple-Helix Model Bound Productively and in Encounters by Matrix Metalloproteinase-12. *J Biol Chem*

69. Houghton, A. M., Hartzell, W. O., Robbins, C. S., Gomis-Ruth, F. X., and Shapiro, S. D. (2009) Macrophage elastase kills bacteria within murine macrophages. *Nature* **460**, 637-641

70. Itoh, Y., and Seiki, M. (2006) MT1-MMP: a potent modifier of pericellular microenvironment. *J Cell Physiol* **206**, 1-8

71. Tzeng, S. R., Pai, M. T., and Kalodimos, C. G. (2012) NMR studies of large protein systems. *Methods Mol Biol* **831**, 133-140

72. Denisov, I. G., Grinkova, Y. V., Lazarides, A. A., and Sligar, S. G. (2004) Directed self-assembly of monodisperse phospholipid bilayer Nanodiscs with controlled size. *J Am Chem Soc* **126**, 3477-3487

73. Bayburt, T. H., Denisov, I. G., Grinkova, Y. V., and Sligar, S. G. Nanodisc Technology: Protocols for Preparation of Nanodiscs. http://sligarlab.life.uiuc.edu/nanodisc/protocols.html. University of Illinois, Urbana-Champaign, Illinois

74. Schuler, M. A., Denisov, I. G., and Sligar, S. G. (2013) Nanodiscs as a new tool to examine lipid-protein interactions. *Methods Mol Biol* **974**, 415-433

75. de Vries, S. J., van Dijk, M., and Bonvin, A. M. (2010) The HADDOCK web server for data-driven biomolecular docking. *Nat Protoc* **5**, 883-897

76. Liu, Y., and Prestegard, J. H. (2008) Direct measurement of dipole-dipole/CSA cross-correlated relaxation by a constant-time experiment. *J Magn Reson* **193**, 23-31

77. Lee, D., Hilty, C., Wider, G., and Wuthrich, K. (2006) Effective rotational correlation times of proteins from NMR relaxation interference. *J Magn Reson* **178**, 72-76

78. Jo, S., Kim, T., Iyer, V., and Im, W. (2008) CHARMM-GUI: a web-based graphical user interface for CHARMM.

79. Phillips, J. C., Braun, R., Wang, W., Gumbart, J., Tajkhorshid, E., Villa, E., Chipot, C., Skeel, R. D., Kale, L., and Schulten, K. (2005) Scalable molecular dynamics with NAMD. *J Comput Chem* **26**, 1781-1802

80. An, B., Abbonante, V., Yigit, S., Balduini, A., Kaplan, D. L., and Brodsky, B. (2014) Definition of the Native and Denatured Type II Collagen Binding Site for Fibronectin Using a Recombinant Collagen System. *Journal of Biological Chemistry* **289**, 4941-4951

81. Minond, D., Lauer-Fields, J. L., Cudic, M., Overall, C. M., Pei, D., Brew, K., Visse, R., Nagase, H., and Fields, G. B. (2006) The roles of substrate thermal stability and P2 and P1' subsite identity on matrix metalloproteinase triple-helical peptidase activity and collagen specificity. *J Biol Chem* **281**, 38302-38313

82. Minond, D., Lauer-Fields, J. L., Nagase, H., and Fields, G. B. (2004) Matrix metalloproteinase triple-helical peptidase activities are differentially regulated by substrate stability. *Biochemistry* **43**, 11474-11481

83. Palmier, M. O., and Van Doren, S. R. (2007) Rapid determination of enzyme kinetics from fluorescence: overcoming the inner filter effect. *Anal Biochem* **371**, 43-51

84. Lauer-Fields, J. L., Minond, D., Chase, P. S., Baillargeon, P. E., Saldanha, S. A., Stawikowska, R., Hodder, P., and Fields, G. B. (2008) High throughput screening of potentially selective MMP-13 exosite inhibitors utilizing a triple-helical FRET substrate. *Bioorg Med Chem*

85. Lauer-Fields, J. L., Chalmers, M. J., Busby, S. A., Minond, D., Griffin, P. R., and Fields, G. B. (2009) Identification of specific hemopexin-like domain residues that facilitate matrix metalloproteinase collagenolytic activity. *J Biol Chem* **284**, 24017-24024

III. Mapping Lipid Bilayer Recognition Sites of Metalloproteinases and other Prospective Peripheral Membrane Proteins

Reprinted by permission from Tara Marcink and Steven Van Doren: Springer Nature, Springer eBook

Marcink T.C., Koppisetti R.K., Fulcher Y.G., Van Doren S.R. (2017) Mapping Lipid Bilayer Recognition Sites of Metalloproteinases and Other Prospective Peripheral Membrane Proteins. In: Galea C. (eds) Matrix Metalloproteases. Methods in Molecular Biology, vol 1579. Humana Press, New York, NY

III.1 ABSTRACT

Peripheral binding of proteins to lipid bilayers is critical not only in intracellular signaling but also in metalloproteinase shedding of signaling proteins from cell surfaces. Assessment of how proteins recognize fluid bilayers peripherally using crystallography or structure-based predictions has been important but incomplete. Assay of dynamic protein-bilayer interactions in solution has become feasible and reliable using paramagnetic NMR and site-directed fluor labeling. Details of preparations and assay protocols for these spectroscopic measurements of bilayer proximity or contact, respectively, are described.

III.2 INTRODUCTION

Protein-mediated membrane-proximal events are critical in cell biology. The best characterized peripheral membrane interactions involve intracellular signaling proteins, and include many studies of proteins that bind phosphoinositides or head groups of phospholipids (1). Fewer studies have examined proteins that bind peripherally to the cell surface and the extracellular leaflet of plasma membranes. The matrix metalloproteinases (MMPs) have important proteolytic targets on the cell surface such as receptors, growth factors, growth factor binding proteins, and cell adhesion molecules (2) while the ectodomains of some of these proteins may be shed from the cell surface by MMPs (2,3). Related ADAM proteases (a disintegrin and metalloproteinase) are prominent as sheddases (3-5) while soluble MMP-2, -7, -8, -9, and -12 have been observed in compartments at or near cell

surfaces (6-12) and may also be involved in cleavage of these cell surface proteins.

Paramagnetic NMR and fluorescence studies have revealed the dual modes of peripheral binding of MMP-12 and -7 to model membranes and cellular membranes (13,14). Comparison of four methods for mapping the interfaces of these proteins with membranes (and interfaces of other proteins under study), suggests the following relative reliability and priority of the mapping methods: paramagnetic NMR (section 3.6) > site-directed fluor labeling (section 3.8) > bilayer-induced shifts or broadening of NMR peaks (section 3.6) ≥ predictions from structural coordinates (section 3.1). The approaches developed for studying bilayer interactions for soluble MMP-7 and -12 (13,14) should be applicable for other soluble MMPs and potential peripheral membrane-binding proteins. The methodology we propose for studying peripheral membrane interactions involves the following steps.

1) Anticipate potential sites for peripheral binding to membranes using recently reported predictive methods that use high-resolution structural coordinates for the protein of interest.
2) Isotopically-label the protein and assign NMR spectral peaks.
3) Prepare spin-labeled membrane bilayer mimics.
4) Localize and quantify paramagnetic NMR line broadening resulting from proximity to the spin-labeled lipid.

5) Use site-directed fluor labeling (SDFL) to verify the NMR-mapped binding sites for recognition of (A) liposomes and (B) cells, as well as (C) effects of lipid composition.

The cornerstone of this strategy for accurately determining membrane binding sites and orientation is to measure strongly distance-dependent NMR line broadening emanating from mobile electron spin-labeled phospholipids placed in the membrane (13-16). Our experience in mapping protein-protein and other protein-macromolecular interfaces is that paramagnetic NMR line broadening is superior in accuracy and interpretability to more conventional mapping of shifted NMR peaks onto the structure of the protein (17-23). Paramagnetic relaxation enhancements (PREs) provide insightful assessment of dynamic, transient and light occupation of binding modes (24-28), including with bilayer-like partners (13,14). SDFL can be used to confirm modes of binding determined by NMR methods (13,14). Alternatively, other investigators have utilized site-directed mutagenesis to confirm these NMR-derived phospholipid binding interfaces (29).

Two types of disk-like mimics of lipid bilayers are promising for NMR studies in solution: (a) a class of small bicelles and (b) nanodiscs. Bilayered micelles or bicelles form disks containing an interior long-chain phospholipid bilayer circumscribed by an annulus of short-chain phospholipids (30). Bicelles are well-suited to solution NMR studies of membrane-associated proteins (31-34). The bicelles are discoidal, tumble rapidly and isotropically, and have a low critical micelle concentration (CMC) (33).

Nanodiscs are disks of lipid bilayers encircled by two belts of molecular scaffolding proteins, which define their size and planarity (35). There are several reasons why nanodiscs are well suited for biophysical studies of membrane proteins. These include: (i) a diameter near 10 nm that is large enough to accommodate two interacting proteins, (ii) homogeneity, (iii) long-term stability, and (iv) high fluidity at the high concentrations needed for NMR experiments (36). A marked disadvantage for solution NMR of proteins embedded in nanodiscs is their high molecular weight, resulting in slow tumbling, rapid decay of NMR signals, and spectra with broad peaks (37-40). This led to efforts to decrease their size by engineering shorter molecular scaffolding proteins which has in turn resulted in enhanced NMR spectra (40). The peripheral binding of proteins to nanodiscs is transient or dynamic so their NMR spectra are usually less affected by slow tumbling associated with embedded membrane proteins. The solubility limit of nanodiscs is ~500 μM which constrains mixtures and titrations with proteins binding them peripherally to concentrations that are comparatively low for NMR studies. To summarize, se nanodiscs benefit NMR in solution with enough space and a stabilizing environment for a membrane protein assembly. However, these advantages come at the cost of weakening the NMR spectra by slowing the tumbling.

III.3 MATERIALS

III.3.1 Protein expression and purification

1. Beckman ultracentrifuge, and an ultracentrifuge rotor such as a Ti 70
2. Bath sonicator (Laboratory Supplies Co., Hicksville, NY)
3. Sorvall or other centrifuge
4. Cell homogenizer such as a motor-driven Potter-Elvehjem tissue grinder
5. Bacterial cell disruptor such as a French press
6. Low to medium-pressure chromatography system
7. Column for gel permeation chromatography such as Superdex 200 10/300 GL
8. Ni-NTA column.
9. Trace minerals (41) (5000X stock)
10. MEM vitamin solution (100X stock; HyClone)
11. Minimal growth medium: 50 mM Na_2HPO_4, 50 mM KH_2PO_4, 5 mM Na_2SO_4, 2 mM $MgSO_4$, 50 mM NH_4HCl, 0.5% (w/v) glucose, and 0.2x trace metals. **(*see* Note 1)**
12. Isopropyl β-D-1-thiogalactopyranoside (IPTG, Sigma-Aldrich).
13. Lysis Buffer: 20 mM Tris·HCl, 10 mM EDTA, pH 7.5.
14. 1,2-dimyristoyl-*sn*-glycero-3-phosphocholine (DMPC) (Avanti Polar Lipids)
15. 1,2-diheptanoyl-*sn*-glycero-3-phosphocholine (D7PC) (Avanti Polar Lipids).
16. Dipalmitoylphosphatidylcholine (DPPC) variants with doxyl spin-label at 5, 10, or 14 position in one acyl chain (i.e. 1-palmitoyl-2-stearoyl-(X-doxyl)-*sn*-

glycero-3-phosphocholine, where X is 5, 10, or 14). (Sigma-Aldrich) Store lipids at 20 ^{o}C in a tightly sealed container.

17. Chloroform (ACS-grade) (Sigma-Aldrich).
18. Sodium cholate (Sigma-Aldrich).
19. Bio-Beads SM2 (BioRad).
20. NMR buffer for MMPs: 20 mM imidazole (pH 6.6), 10 mM $CaCl_2$, 20 µM $ZnCl_2$, 0.02% NaN_3, and 5% $^{2}H_2O$.
21. Molecular scaffolding protein MSP1D1 (Sigma-Aldrich). See ref (42) and section 3.5.1.
22. MSP buffer: 20 mM Tris-HCl (pH 7.4), 0.1 M NaCl, 0.5 mM EDTA, 0.01% NaN_3.
23. TEV protease (Sigma-Aldrich).
24. Tris buffer: 20 mM Tris-HCl (pH 7.2)
25. TNC buffer: 20 mM Tris-HCl (pH 7.4), 150 mM NaCl, 10 mM $CaCl_2$

III.3.2 Fluorescence spectroscopy

1. Freshly prepared 10 mM N,N′-dimethyl-N-(iodoacetyl)-N′-(7-nitrobenz-2-oxa-1,3-diazol-4-yl) ethylenediamine (IANBD) (ThermoFisher),
2. Dimethylsulfoxide (DMSO; Sigma-Aldrich),
3. G-25 desalting resin (Sigma-Aldrich).
4. Dulbecco's modified Eagle's medium (DMEM) with 10% fetal bovine serum, supplemented with L-glutamine and Non-Essential Amino Acid (NEAA).
5. Cell lines (ATCC)

6. Biotek Synergy MX plate reader **(*see* Note 2)**
7. Zeiss LSM 510 Meta confocal microscope for imaging live cells (13,14)

III.3.3 NMR spectroscopy

1. NMR spectrometer operating at a ^{1}H frequency of 600 MHz or higher. **(*see* Note 3)**
2. 5 mm NMR tubes (Norell) **(*see* Note 4)**

III.4 METHODS

III.4.1 Navigating Servers for predicting Protein Binding Peripherally to Membranes

Two excellent servers are available to predict the atomic structural coordinates of proteins that peripherally bind to membranes: Membrane Optimal Docking Area (MODA) (43) and Positioning of Proteins in Membranes (PPM) (44). MODA is designed for predicting membrane binding sites of peripheral membrane proteins (43). PPM is designed for predicting the positioning of both peripheral and integral membrane proteins with respect to bilayers (44). PPM was preceded by the well-developed OPM database of predictions of positions and orientations of proteins in and on membranes (44-47). The predictions may be used to determine whether it is worthwhile undertaking experimental testing of membrane interactions. For example, a comparison of a PPM prediction for the catalytic

domain of MMP-12 with results of experimental docking studies using paramagnetic NMR (13) is shown in **Figure 1**. The PPM prediction failed to predict the α-interface **(Figure 1A)**. However, it did predict one of the three experimentally determined loops (the II-III loop) of the β-interface (13). This prediction bears resemblance to the measured orientation, but approaches the bilayer at a different angle **(Figure 1B)**. While MODA predicted residues for the other two experimentally defined loops (III-IV and IV-V loops) within the β-interface (13).

III.4.2 MODA and PPM predictions:

1. First obtain the PDB file containing the structural coordinates for the protein of interest from the Protein Data Bank (www.rcsb.org).
2. MODA predictions (http://molsoft.com/~eugene/moda/modamain.cgi)
    a. Enter the PDB accession code or upload the PDB coordinate file. If the PDB file contains multiple chains, indicate which chain should be used for the prediction, e.g., A, B, C. Select “Predict” and wait for the results. **(*see* Note 5)**
    b. After the server identifies potential sites of membrane binding, it outputs a tabulated list of MODA scores for each of the amino acid residues in the sequence. The plain MODA score is scaled down by curvIndex to the more conservative curvMODA score.
    c. If the curvMODA score for a residue is above 40 (48) and it has one or more neighbors (in sequence or space) with a high curvMODA score, that patch of residues is likely to interact with membrane

bilayers. Residues with curvMODA score between 20 and 40 that cluster with other high-scoring residues possibly also interact with lipid bilayers.

d. Download the spreadsheet readable text file in .CSV format. One should either manually mark high scoring residues on the protein structure with a molecular graphics software such as Pymol. Alternately, residues predicted to interact with membranes can be semi-automatically denoted by opening the ICB file in the program MolSoft.

3. PPM predictions (http://opm.phar.umich.edu/server.php),

e. Upload the PDB file of interest.

f. Specify the topology of the protein (N-terminus being in or out of the membrane) and whether you wish to include non-standard residues or atoms in the prediction. Submit and wait for the results to appear on a fresh webpage.

g. The calculated predictions include the depth that the protein penetrates into the membrane, the water-to-membrane transfer free energy (ΔG_{trans} in kcal/mol), and the tilt angle (°) of the protein in the membrane.

h. To display the predicted model of the protein-membrane interaction select the “jmol” link under the heading “Image of the protein in membrane”. This model is best viewed using a web browser that supports Java applets, such as Firefox.

i. Download the PDB file generated for the predicted model to examine the hypothetical protein-membrane interface in a molecular graphics software package like PyMol or Chimera. The projected location of the membrane bilayer in the predicted protein-membrane model is defined by a grid of dummy atoms.

III.4.3 Preparation of *E. coli* inclusion bodies harboring recombinant isotopically labeled MMP (or other eukaryotic protein) for NMR studies

1. Prepare at least 100 ml of unlabeled PG medium (41) and at least 250 ml of PG medium using 99% D_2O in lieu of H_2O, as well as $^{15}NH_4Cl$ (Sigma-Isotec or Cambridge Isotope Laboratories) as the sole nitrogen source. **(*see* Note 6)**.
2. Transform competent *E.coli* BL21(DE3) Gold cells with the expression plasmid and plate 20 to 50 µl of the mixture onto a PG medium agar plate containing an appropriate antibiotic.
3. After incubating at 37 ºC overnight, pick a few colonies from the plate and add to 1 ml of PG medium containing the antibiotic and incubate for 8 h at 37 ºC on a shaker operating at 250 rpm.
4. Transfer the entire 1 ml of culture into 50 ml of PG medium containing antibiotics in a 250 ml flask. Incubate overnight at 37 ºC in the shaker at 250 rpm.

5. Subculture 1 to 2% of the overnight culture into 250 ml of labeled PG medium containing antibiotic in a 2-liter shake flask.
6. When A_{600} reaches 0.4 to 0.8, add 0.5 mM IPTG to induce protein expression and incubated overnight at 37 ºC in a shaking incubator at 250 rpm.
7. Collect the bacterial cell pellet by centrifugation and store at -20 ºC until needed.
8. Resuspend the cell pellet with lysis buffer and homogenize the suspension with a motor-driven Potter-Elvehjem tissue grinder.
9. Rupture the cell suspension, preferably by two slow passes through a French pressure cell, until the milky suspension darkens due to breakage of the cells.
10. Centrifuge at 20,000 x g for 40 min at 4 ºC. Discard the supernatant as the MMP construct should be in the pellet in inclusion bodies. This pellet may optionally be washed by resuspension in lysis buffer containing 0.01% Triton X-100 and centrifuging again.
11. The inclusion bodies are dissolved in concentrated urea or guanidinium·HCl, centrifuged to remove insoluble debris, refolded, chromatographically purified, and concentrated in a centrifugal filter unit (Millipore). Optimal procedures for the purification and refolding of the protein are specific to the construct and have been described for MMP-1 (49,50), MMP-3 (51), MMP-7 (52), MMP-12 (21,53,54), MMP-13 (55), and MMP-14 (56,57).

III.4.4 Assignment of NMR spectral peaks

1. Initially check to determine whether the assignments for the backbone amide NMR peaks are not available in the literature or in the BioMagResBank database (http://www.bmrb.wisc.edu/).
2. If *de novo* NMR peak assignments are required, prepare the $^{15}N/^{13}C$ labeled protein at a concentration of at least 150 µM using the procedure outlined in section 3.2 **(*see* Notes 7 and 8)**.
3. Acquire standard NMR spectra for spectral peak assignments (including HNCA, HN(CO)CA, CBCA(CO)NH and HNCACB triple resonance spectra) **(*see* Note 9)**.
4. Semi-automated assignments for a majority of the backbone resonance peaks can be readily determined by non-specialists using the program PINE, a downloadable, integrated software environment which comes with a set of explanatory tutorials (58). The software relies heavily upon NMR spectral analysis software NMRFAM-Sparky for visualizing the spectra (59) and PONDEROSA for automation of peak assignments (60,61).
5. Assignments of methyl peaks for hydrophobic side chains are optional, but are desirable in order to provide additional distance constraints between protein residues and atoms within the lipid bilayer. This typically involves selective “ILV” labeling of isoleucine, leucine, and valine residues in a perdeuterated medium supplemented with α-ketoacids containing $^{1}H/^{13}C$-labeled methyl group(s) and optional deuteration (62) **(*see* Note 10)**.

6. Methyl peaks can be assigned for smaller proteins using HMCM[CG]CBCA (HMCACB) (63) and CC(CO)NH or HNCACB triple resonance spectra, supplemented with NOESY-derived NOEs to the backbone (64) and methyl-amides (56). This strategy works well for single domain proteins. To extend assignments of methyl peaks to multiple domain protein constructs such as MMPs, the assignments of methyl peaks from the single domains can simply be combined and then revised using NOEs among methyl groups in the large construct (64,65). Software designed to aid in the determination of methyl peak assignments that utilizes additional experimental data such as structural coordinates, methyl-methyl NOEs, and PREs is also available (66).

III.4.5 Preparation of small bicelles for NMR studies

Bilayered micelles or bicelles that are small, discoidal, and isotropic in tumbling are preferred for solution NMR (30,32,33,67). These are composed of two to three equivalents of detergent-like short chain lipids per equivalent of long chain phospholipid, which are designated q = 0.5 to q = 0.33 (ratio of long to short chains), respectively. Short chain lipids are amendable to forming curved surfaces, in this case, the rims of the bicelle disks (30) **(Figure 2B)**. Long chain phospholipids, such as DMPC, form the planar bilayers in the interior of the disks **(Figure 2B)**. Dihexanoylphosphatidylcholine (D6PC) with its 6-carbon acyl chains has dominated biophysical studies (30) but suffers the limitation of not aggregating into micelles or bicelles until reaching a critical micelle concentration (CMC) as

high 14 mM in monomers (33). D7PC with its 7-carbon acyl chains has the much lower and more favorable CMC of 1.2 mM allowing D7PC-DMPC bicelles ($q \leq 0.5$) to form at much lower lipid concentrations with only 1.2 mM monomers in solution (33). Preparation of bicelles incorporating the latter and using our recommended formulation is outlined below.

1. Weigh 20 mg of the powder form of D7PC into a clean 5 ml glass tube and dissolve in 1.5 ml of chloroform.
2. Blow a gentle stream of argon or nitrogen gas into the glass tube for 30 to 45 min to evaporate the chloroform. Disturbance of the liquid by the nitrogen (or argon) stream should be slight and barely visible, with no splashing of liquid. Upon drying, a solid lipid film will form at the bottom of the glass tube. Dried lipids should be white in appearance. If the film appears glassy, it means that some residual chloroform remains in the lipid film.
3. Cover the glass tube with a piece of parafilm and pierce this several times. Place the covered tube in a jar containing desiccant or under vacuum for drying overnight.
4. To the dried D7PC, add 35 µl of NMR buffer. Cover with parafilm and hydrate at 42 ºC for 1 h. Frequently and gently centrifuge using either a hand-cranked centrifuge or a microfuge on its slowest setting in order to collect the micelles from the sides of the tube.
5. Dissolve 20 mg of DMPC in 2 ml of Tris buffer. Hydrate at 42 ºC for 2 h. Vortex occasionally to ensure an even suspension.

6. Place the glass tube in a bath sonicator. Adjust the glass tube so that the water barely covers the liposome dispersion.
7. Sonicate for 10 min. **(*see* Note 11)** The solution will turn from milky white to translucent. **(*see* Note 12)** Incubate at 42 ºC for 1 h.
8. Ultracentrifuge the DMPC liposomes in a Ti 70 rotor for 1 h at ~64,000 x g and 20 ºC. Decant the supernatant which contains the small unilamellar vesicles (SUVs), freeze and store at -80 ºC for later use in fluorescence assays. The nearly white flocculent material at the bottom of the centrifuge tube contains large unilamellar vesicles (LUVs) and medium-sized unilamellar vesicles (MUVs) which will be used for preparing bicelles in the next step.
9. Resuspend the DMPC liposomes (LUVs and MUVs) with the solution containing the D7PC micelles. Incubate at 42 ºC until an even suspension is achieved. Be careful to minimize frothing.
10. Plunge the suspension into liquid nitrogen and freeze. Thaw at 42 ºC.
11. Transfer to a 500 µl microfuge tube and bring the volume up to 100 µl with NMR buffer. Freeze in liquid nitrogen again and thaw at 42 ºC.
12. Transfer 25 µl aliquots to a fresh tube and freeze in liquid nitrogen. Store at -80 ºC until needed.

III.4.6 Preparation of nanodiscs for NMR or fluorescence assays

This is a synopsis of the previously reported protocol for preparing nanodiscs (42,68,69). This protocol uses the MSP1D1 variant of the molecular scaffolding

protein to encircle a DMPC phospholipid disc. Other lipids and MSP variants may also be assembled into nanodiscs.

1. MSP1D1 (42) may be purchased from Sigma-Aldrich or the His-tagged protein can be expressed from a plasmid (Addgene) and purified by affinity chromatography on Ni-NTA agarose in a buffer containing sodium cholate (68).
2. Pool fractions containing the His-tagged MSP1D1 and dialysis against MSP buffer
3. Treat with TEV protease to release the His-tag. Remove the peptide containing the His tag by capturing it on the Ni-NTA column. Measure the concentration of the cleaved protein using an molar extinction coefficient (ε_{280}) of 18,200 $M^{-1}cm^{-1}$ (69).
4. Dissolve sodium cholate in MSP1D1 or NMR buffer to make a solution that is 20 to 40 mM in sodium cholate monomers. **(*see* Note 13)**. Add this solution to 40 mg of dry DMPC at a molar ratio of two detergent molecules per phospholipid molecule. Vortex and heat in a water bath at 60 ^{o}C for 1 hour. Then sonicate in a bath sonicator until clear.
5. Add the MSP1D1 to the cholate-solublized DMPC solution to achieve a final ratio of 1:80, while keeping the concentration of sodium cholate above 20 mM. Then mix. **(*see* Note 14)**
6. Incubate with 0.5 to 0.8 g of damp BioBeads SM2 per ml of sample for 2 to 3 hours to remove the detergent micelles.

7. Wash the BioBeads with an excess of MSP or NMR buffer in order to release more nanodiscs.
8. If turbidity or precipitation is present, pellet the particles by briefly spinning in a microcentrifuge. Inject the clarified solution of nanodiscs onto a gel filtration column such as Superdex 200 10/300 GL and run with a flow rate of ~0.5 ml/min. Collect 1 ml fractions. The elution profile for a preparation of nanodiscs composed of DMPC and MSP1D1 superimposed with that for several molecular weight standards is shown in Figure 3.

III.4.7 NMR to measure proximity to mimics of membrane bilayers

The main idea here is to estimate distances from protein amide and methyl groups to doxyl spin labelled DPPC, with around one or two such DPPC added per leaflet of the bilayer mimetic. PRE (paramagnetic relaxation enhancement) measurements from the unpaired electron of the doxyl group to the amide or methyl proton of the protein depends strongly ($\alpha\ r^{-6}$) on the distance r between them and less strongly on the time constant τ_c of their rotational diffusion. The PREs are measured from the increased paramagnetic relaxation rate enhancement Γ_2 resulting from the addition of an unpaired electron.

1. Prepare a ^{15}N-^{2}H labeled protein sample according to **section 3.1.1** and concentrate to between 200 and 600 µM in NMR buffer in a volume of at least 400 µl, typically using a centrifugal membrane concentrator (Millipore or Vivaspin).

2. Titrate the protein sample with the bicelles, nanodiscs, or liposomes. Record ^{1}H-^{15}N TROSY NMR spectra of the protein amide spectral region at each lipid concentration in the titration. If protein methyl groups are specifically labeled, also collect ^{13}C HMQC spectra of the methyl spectral region at each concentration. Titrate the membrane mimic to at least half of the molar equivalents of the discoidal bilayer assembly per equivalent of protein, in order to provide at least one discoidal leaflet as a potential binding site for every protein molecule (expecting instances of two protein molecules per disc).
3. Continue the titration to a ratio of 1:1 and beyond, in order to maximize the number of assemblies harboring one protein bound per disc-like bilayer. **(*see* Note 15 and 16).**
4. Estimate the rotational correlation time τ_c to confirm bilayer-protein association and calibrate distance estimates. ^{15}N NMR relaxation indicative of τ_c is measured, preferably at each concentration point in the titration of **section 3.4.1**. **(*see* Note 17)** Acquire a 1D relaxation series with at least five increments of constant-time relaxation using an appropriate pulse sequence for measuring ^{15}N NMR transverse dipole-dipole/CSA cross-correlated relaxation (70) . Set the longest relaxation period to attenuate peak heights to around 35 to 50% of the initial intensity.
5. Integrate the 1D spectral envelope at each relaxation time, while omitting the central region from 7.6 to 8.4 ppm which is enriched in signal from unstructured loops. An exponential relaxation rate constant is fitted to these

integrals. This constant is known as the transverse cross-correlated relaxation rate, or η_{xy}.

6. Use η_{xy} to estimate τ_c. The relationship between η_{xy} and τ_c is given by the following equations of ref (71):

$$\eta_{xy} = p\delta_N(4J(0) + 3J(\omega_N))(3cos^2\theta - 1) \quad \text{equation 1}$$

where p is the dipole-dipole coupling between the ^{1}H and ^{15}N of the amide group

$$p = \mu_0\gamma_H\gamma_N h/(16\pi^2\sqrt{2}r_{HN}^3) \quad \text{equation 2}$$

δ_N is the chemical shift anisotropy of the ^{15}N nucleus defined as

$$\delta_N = \gamma_N B_0 \Delta\delta_N/(3\sqrt{2}) \quad \text{equation 3}$$

where γ_H are γ_N are the respective ^{1}H and ^{15}N gyromagnetic ratios, h is Planck's constant, r_{HN} is the distance between amide ^{1}H and ^{15}N nuclei, $\Delta\delta_N$ is the difference between the two main components of the ^{15}N chemical shift tensor, and $J(\omega)$ is the spectral density function that depends on frequency ω

$$J(\omega) = 0.4\tau_C/[1 + (\omega\tau_C)^2] \quad \text{equation 4}$$

These equations, the constants, and the ^{15}N resonance frequency of an 800 MHz spectrometer define the relationship of η_{xy} and τ_c as:

$$\eta_{xy} = 9.075e8 * 0.4*\tau_c*(4 + 3/(1+ \tau_c * 5.0948e8)^2)) \quad \text{equation 5}$$

Using Eq. 5, η_{xy} is plotted versus τ_c and is almost linear. At the measured η_{xy} rate, the τ_c value corresponding to this point on the line is read from this plot. This estimate of τ_c represents the hydrodynamics. It can be monitored throughout the titration. An increase in τ_c during the titration indicates the binding of protein to the membrane and slower tumbling of the protein due to its association with the membrane.

7. Measure the ^{1}H NMR transverse (R_2) relaxation rate constants of the diamagnetic state of the lipid-protein mixture. (These exponential rate constants will be used as the reference values to which the distance-dependent Γ_2 values increase relaxation). Use an NMR pulse sequence modified to include a PROJECT-CPMG train that suppresses proton-proton J-couplings (72). For amide ^{1}H relaxation, either a ^{15}N TROSY sequence with a prepended PROJECT-CPMG train or an ^{15}N HSQC with the PROJECT-CPMG train appended are recommended (13,14,56). For methyl ^{1}H relaxation, use a ^{13}C HMQC incorporating PROJECT-CPMG (13,56). Set the ^{1}H transmitter frequency offset to the water resonance peak near 4.7 ppm. Determine and set the ^{1}H 90º pulse length at high power. Attenuate the ^{1}H power level for the PROJECT-CPMG train by 3 dB and set its constituent 90º pulse widths $\sqrt{2}$-fold longer than the high power pulse width. Acquire trial 1D spectra as a series of 4 ms steps for the length of the CPMG train in order to monitor the degree of exponential reduction in overall peak height. Use this spectral series to determine the CPMG periods (multiples of 4 ms) to use for acquiring a series of 2D spectra. For relaxation of amide

peaks, try CPMG periods from 0 to 32 ms. For methyl relaxation, try CPMG periods out to 40 or 48 ms. Choose a maximum CPMG period in which the spectrum has decayed to 35 to 50% of the intensity with a CPMG period of 0 ms.

8. Copy the optimized parameters into a number of 2D experiments with increasing the value of the CPMG period by a multiple of 4 msec for each successive experiment. Increase the number of transients acquired to achieve a S/N ≥ 20 for the spectrum with the longest CPMG period. Measure the ^{1}H NMR transverse relaxation with a series of five or six relaxation delays (13,14,56).
9. To prepare the paramagnetic lipid DPPC (modified with the doxyl spin label at the 5, 10, or 14-position) dissolve 1 mg of doxyl-substituted DPPC in 250 µl of methanol to make a stock solution of 4.6 mM. Store at 4 ºC.
10. Estimate the volume of this solution needed to incorporate an average of one (possibly two) doxyl-DPPC molecules per leaflet of the bicelles or nanodiscs. Transfer this volume of solution to a fresh tube and evaporate using a gentle stream of nitrogen or argon gas. Add the sample of labeled protein with bicelles or nanodiscs to the dried doxyl-DPPC and incubate for 10 to 15 min. to incorporate the spin label in the bilayers. **(*see* Note 18)**. The incorporation of the doxyl-DPPC introduces its unpaired electron to the membrane bilayer. This broadens the ^{1}H NMR peaks of nearby hydrogen atoms. The breadth of the NMR peak is measured in the time domain as relaxation rate constant R_2, which decays exponentially with the length of

the CPMG time period used in the NMR pulse sequence. The acceleration of the ^{1}H R_2 relaxation by the unpaired electron in the vicinity is Γ_2, the distance-dependent PRE needed. Γ_2 values may be measureable on protons on the protein as far as 25 Å from the doxyl group.

11. Repeat the series of CPMG experiments for the paramagnetic doxyl-DPPC incorporated membrane. Use the same buffer, temperature and membrane mimic to protein ratio as used for the diamagnetic sample. **(*see* Notes 19 and 20)**. Fit an exponential decay function and rate constant of decay to each resolved and confidently assigned peak. The exponential decay rate in the paramagnetic sample minus the exponential decay rate of the diamagnetic sample is equal to Γ_2, the rate constant of the paramagnetic relaxation for a given NMR resonance peak.
12. These experiments should be repeated using other DPPC analogues, where the doxyl label is incorporated at different positions along the acyl chain, in order to sample varying depths and magnitudes of PREs **(Fig. 4)**. This provides additional information about the depth (or lack of) penetration of the protein into the membrane. These experiments provide additional distance constraints that can be used for structural modeling of the peripheral membrane binding.
13. Estimate the distance *r* from the mobile doxyl spin label to each amide or methyl resonance peak using the expression:

$$r = 4K\tau_c/\Gamma_2 \quad \text{equation 6}$$

Here K = 1.23x10^{-44} m^6s^{-2} and τ_c is the rotational correlation time. These estimates can then be used as distance constraints in rigid body structural calculations using a docking program, such as HADDOCK (13,29), to define areas of interaction between the protein and the membrane mimic, and in subsequent restrained molecular dynamics calculations. Computational details of the docking calculations are complex and beyond this chapter's scope, but have been introduced previously (13,14).

III.4.8 Preparation of liposomes for fluorescence assays

Fluorescence assays are recommended to confirm modes of bilayer binding determined by the paramagnetic NMR measurements described in section 3.6 (13,14). These fluorescence assays can be undertaken using classic liposomes. Small unilamellar vesicles (SUVs) are recommended over larger vesicles in order to decrease light scattering that adds unwanted background to the detected fluorescence signal. Overall, the protocol outlined below involves preparing a stock suspension of SUVs of DMPC that is 10 mM in lipid monomers. SUVs may be also prepared from other lipids.

1. Dissolve 3.4 mg of DMPC (MW 677.94) in 500 µl of assay buffer. **(*see* Note 21)**.
2. Hydrate the lipids by placing the solution in a 42 ºC water bath for 2 h. Vortex every 30 min in order to suspend them.

3. Sonicate the suspension until it is clear. This should take 10 to 15 min. If it does not become clear or if the concentration of lipid is low, use freeze-thaw cycles in a plastic tube with liquid nitrogen as described for preparing bicelles in section 3.4. That is, incubate the plastic tube for 3 min in liquid nitrogen followed by 6 min in a 42 ºC water bath. Remove MUVs by spinning for 1 to 2 min in a microcentrifuge at 10,000 rpm. The SUVs can be stored in the 42 ºC water bath. It is best to use them within one to two days of preparation, but they may be useable for up to a week. SUVs stored at 4 ºC will form MUVs or aggregates. **(*see* Note 22 and 23)**

III.4.9 Site-Directed Fluor Labeling (SDFL) to Interrogate Binding to Liposomes

Preparation of fluorescently-labeled protein

A fluorophore that exhibits enhanced fluorescence upon insertion into lipid bilayers has proven useful to experimentally determine the site and orientation of interaction of peripheral proteins with membrane bilayers of both liposomes and cells (13,14,73,74) **(Figure 5)**. We recommend using site-directed fluor labeling (SDFL) to confirm peripheral membrane binding sites determined by paramagnetic NMR. Alternately, SDFL can be utilized as the primary method for mapping the membrane-protein binding interface when it is not feasible to use paramagnetic NMR. The general approach for using SDFL to define the

interaction of peripheral binding protein with membrane bilayers is outlined below:

1. To confirm membrane-binding sites identified by paramagnetic NMR, a number of single cysteine residue protein mutants need to be prepared containing cysteine residues located at positions corresponding to the interfacial binding site and one or more distant locations to serve as negative control(s) **(Figures 5)**. **(*see* Notes 24 and 25)** The substituted cysteine residues should be placed at a surface-accessible site, typically in a loop, inside or outside the proposed interface **(*see* Note 26)**
2. Reduce the single reactive Cys residue of the mutated protein (typically ≥ 1 μM) with at least a 10-fold molar excess of thiol reductant , e.g. 1 mM β-mercaptoethanol (BME). **(*see* Note 27)**
3. Dialyze against TNC buffer to remove excess reductant. **(*see* Note 28)**
4. To a solution containing 1 μM protein add a 10-fold molar excess of IANBD. **(*see* Note 29 and Figure 6)**
5. Let the conjugation reaction proceed for 2 h at room temperature or overnight at 4 ºC. Perform this in an anaerobic chamber under argon.
6. Add excess BME or glutathione to consume excess thiol-reactive IANBD.
7. Concentrate the reaction mixture before loading onto a G-25 desalting column equilibrated in 10 column volumes of Tris buffer containing between 5 and 10 mM $CaCl_2$.

8. Collect the eluted conjugated protein and determine the extent of the conjugation reaction as follows. Determine the protein concentration using a protein assay such as a Bradford assay or absorbance at 280 nm. Determine the concentration of IANBD groups by measuring the maximum absorbance between 472 and 480 nm and using an extinction coefficient of 23700 $M^{-1}cm^{-1}$ (75). The ratio of the concentration of protein to that of the fluorphore (IANBD) equals the apparent percentage labeling, which typically appears to be ~85 to 105%. The excess over 100% could suggest incomplete removal of free IANBD.

Fluorescent binding-assay

1. In a 96-well plate prepare a series of 200 µl solutions (in quadruplicate) containing 10 to 100 nM fluorophore-conjugated protein. Measure fluorescence at 541 nm using an excitation wavelength of 478 nm to establish sensitivity and fluorescence linearity; **(*see* Note 30)**.
2. x Each 200 µl solution should containi 250 to 300 µM liposome monomers, typically prepared by diluting 5 to 6 µl from a 10 mM stock solution. Measure fluorescence intensity every 10 to 30 min for two to three hours in order to allow the protein time to equilibrate in inserting into liposomes, before photobleaching takes a toll on emission from the IANBD. Normalize the fluorescence intensity in the presence of the liposomes (F_{SUV}) values by dividing it by the fluorescence in the absence of membranes (F_0),i.e. F_0/F_{SUV}.

Bilayer insertion of the NBD moiety is accompanied by an increase in fluorescence intensity with $F_{SUV}/F_0 \geq 1.5$ (13,73). **(*see* Note 31)**

Confocal imaging of binding to live cells

1. The IANBD-tagged protein may also be used to investigate interactions with cell membranes and their compartments. We have used human HeLa cells or Raw264.7 murine macrophages grown in suspension (13,14), (Macrophages secrete several MMPs). Like the assays with liposomes, the degree of association with cell membranes is quantified using the plate reader measurements of the fluorescence emission with cells present (F_{cells}) divided by the emission in their absence, i.e. F_{cells}/F_0. Use of three to 5 million cells per well has been effective in our experiments (13).
2. The mammalian cell line is seeded on sterile MatTek glass bottom culture dishes and grown overnight at 37 ºC in a 5% CO_2 incubator until reaching about 60 to 80% confluency.
3. The cells are washed three times with DMEM without phenol red and incubated with media containing a fluorescent staining reagents specific for the membrane compartment of interest and nuclei for 10 min at 37 ºC in a 5% CO_2 incubator.
4. The cells are then washed three times with 20 mM Tris, pH 7.2, 5 mM $CaCl_2$, 0.1 mM ZnCl.
5. The culture dish is then placed on the stage of a confocal microscope (in our case a Leica TCP SP8 MP equipped with 405 nm and tunable white

light lasers). The excitation / emission bandpass wavelengths used to detect IANBD, Hoechst 33342, and Alexa Fluor 594 WGA are set to 472/485-525, 405/415-470, and 594/610-680 nm, respectively.

6. Confocal fluorescence images are taken immediately (control images). IANBD-labeled protein is then added to the dish and images are collected every 90s for 15 to 30 min.

III.5 NOTES

1. This minimal growth medium for high-level expression in *E. coli* is Studier's non-inducing PG medium (P-0.5G) (41), with the addition of vitamins and use of an alternative choice of ammonium salts.
2. The authors used a Biotek Synergy MX plate reader, an instrument with the advantage of monochromator selection of excitation and detections wavelengths 478 and 541 nm, respectively. With a number of other plate readers, an appropriate set of filters are used instead on the excitation and emission channels.
3. A cryogenic probe is highly recommended for the sensitivity needed given the dilution and line broadening accompanying association with a slowly tumbling bilayer disc, and the quantitative nature of measurements of paramagnetic NMR relaxation. The authors have used a Bruker Avance III 800 MHz NMR spectrometer with TCI cryoprobe for proteins of 20 kDa and greater, and a Bruker Avance HD 600 MHz system with TCI/F cryoprobe for proteins < 20 kDa

4. Five millimeter NMR tubes are recommended for sufficient sample volume to accommodate the dilution of the protein sample upon mixing with a discoidal membrane mimic.
5. The option to incorporate electrostatics appears to be inconsequential. The option of clustering spreads the scores across more residues, without filling in the omissions of binding modes that we have observed anecdotally; we do not recommend clustering.
6. To prepare double-labelled protein for assignment of NMR chemical shift peaks also substitute 0.3% (w/v) $^{13}C_6$-glucose as the sole carbon source. In some circumstances (e.g. severe spectral overlap) it is possible to selectively label specific amino acids by α-keto acids or other precursors (62)
7. Some assignment projects may be especially challenging due to line broadening caused by the slow tumbling of the membrane-associated protein, low protein concentration, or overlapped peaks. In these cases, combinatorial or selective labeling strategies for partial assignment of specific amino acid residues or protein segments can be worthwhile (76-78). If insect cells are required for high-level expression and proper folding, media for insects can now be labeled affordably by supplementing with $^{15}N/^{13}C/^{2}H$-labeled yeast extracts (79).
8. Proteins exceeding 20 kDa in mass should be fractionally deuterated to at least 60% (preferably 99%) by inclusion of D_2O in the growth medium (79) in order to achieve narrower linewidths and increased sensitivity (80).

9. For proteins greater than 20 kDa, TROSY versions of these and other triple resonance spectra are recommended (81,82). For proteins less than 20 kDa with sharper line widths, rapid acquisition BEST versions of triple resonance spectra are recommended (83,84).
10. Selective labeling of the methyl groups of alanine, methionine, and threonine is also feasible (62,85).
11. While using the bath sonicator, monitor the temperature of the water to ensure that it does not rise above about 40 ^{o}C. Turning the sonicator off for a while will allow it to cool toward room temperature.
12. A translucent, blue tinted solution is a clear sign of the formation of liposomes. If the suspension has not clarified, then liposomes have not yet formed adequately. Continue sonicating for a further 5 to 10 min.
13. This forms detergent micelles since the CMC of sodium cholate is 3 mM (86).
14. The optimal molar ratio of MSP1D1 to DMPC is 1:80.
15. The 1:1 assemblies should tumble faster and have sharper NMR peaks than 2:1 assemblies.
16. Note residues with NMR peaks broadened or shifted by addition of the membrane mimics. Such spectral perturbations suggest that the protein is binding to the membrane mimic and the general location of binding or conformational perturbations linked to binding.
17. This is performed before doping the bilayers with doxyl-substituted DPPC, which is paramagnetic.

18. We have had success with D7PC/DMPC (q = 0.5) bicelles at 300 μM discoidal aggregates, corresponding to 100 mM in total lipid monomers. These conditions require addition of the doxyl-DPPC to 600 μM for an average of one per leaflet.
19. The R_2 ^{1}H NMR relaxation rate constants fitted to the series should be insensitive to experimental choices of length of signal averaging, spectral window, and exact concentrations.
20. The R_2 values do depend on the hydrodynamics, which are sensitive to temperature and degree of molecular association, which should be kept uniform for making comparisons. Using similar protein and lipid concentrations for the diamagnetic (control) and paramagnetic experiments ensures similar degrees of molecular association are obtained in both experiments.
21. Minimize exposure to air while weighing the dry lipids. Weigh out a 10% excess of DMPC in order to obtain with desired concentration of SUVs since ~10% of the DMPC will form MUVs which will subsequently be removed by microcentrifugation.
22. Lipids dissolved in chloroform can be used to prepare the SUVs, provided an additional day is allowed to evaporate the chloroform and dry the lipids overnight under vacuum.
23. The aggregates could be sonicated to recover SUVs, but it is not recommended.

24. If one or more such cysteine already exists in the protein at an experimentally undesirable location, it should first be removed by site-directed mutagenesis.
25. If mapping by NMR (preferably paramagnetic NMR) is not available, the interfaces predicted by MODA and PPM should be regarded as the hypotheses to test, realizing that these algorithms have each missed one of the dual membrane-binding sites that we located experimentally (13,14) **(Figure 1A)**.
26. Since basic and hydrophobic residues are frequently found within peripheral membrane interfaces, care should be taken not to substitute Arg, Lys, Phe, Tyr, Leu, and Ile residues within this region as this could disrupt binding at the protein-membrane interface.
27. We recommend performing these steps in an anaerobic or semi-anaerobic environment in order to prevent oxidation of thiols to disulfides. All buffers should be deoxygenated, e.g. by bubbling through argon and reactions should be carried out under an inert atmosphere of argon.
28. Constructs containing an MMP catalytic domain require 5 to 10 mM $CaCl_2$ to stabilize the catalytic domain.
29. Use a fresh 10 mM stock solution of IANBD.
30. Linearity of fluorescence deteriorates as the sum of the absorbance at the excitation and emission wavelengths exceeds 0.08 (87).
31. Examination of other lipids that are found in cell membranes is also recommended in order to get a explore biological specificity. These may

include anionic lipids like phosphatidylserine (88), signaling lipids potentially relevant to your target protein (e.g. phosphoinositides) (1), unsaturated lipids, sterols, sphingholipids, glycolipids, etc.

32. Our studies have been utilyzing the Image-It™ kit (Life Technologies) containing the Alexa Fluor 594 conjugate of wheat germ agglutinin (WGA) at 5 µg/ml to dye the glycosylation red on the outer face of the plasma membranes and 2 µM of Hoechst 33342 to label chromatin and nuclei blue.

III.6 ACKNOWLEDGMENT

This work was supported primarily by NIH grant GM057289, but also by NIH grant CA098799.

III.7 FIGURES

Figure III.1 Comparison of the PPM predicted and experimentally determined mode of bilayer binding by MMP-12.

The protein backbone shown is used both to illustrate the experimental dockings and the predicted docking. The lipid chains plotted are from the experimental docking. The blue grid indicates the predicted location of bilayer head groups where the bilayer contacts the II-III loop of MMP-12. . **(A)** The experimental structural model bound to the membrane via the α-interface (PDB: 2MLR, with lipid chains) is superposed with predicted interfaced marked by the blue grid. Molecules comprising the bilayer are shown and phosphorous atoms of the DMPC head groups are illustrated as orange spheres. The protein chain is rainbow colored from blue at the N-terminus to red at the C-terminus. **(B)** The experimental structural model bound to the membrane via the β-interface (PDB: 2MLS, with lipid chains) which includes not only the II-III loop but also the III-IV and IV-V loops, resulting in a different tilt angle than predicted by PPM (blue grid).

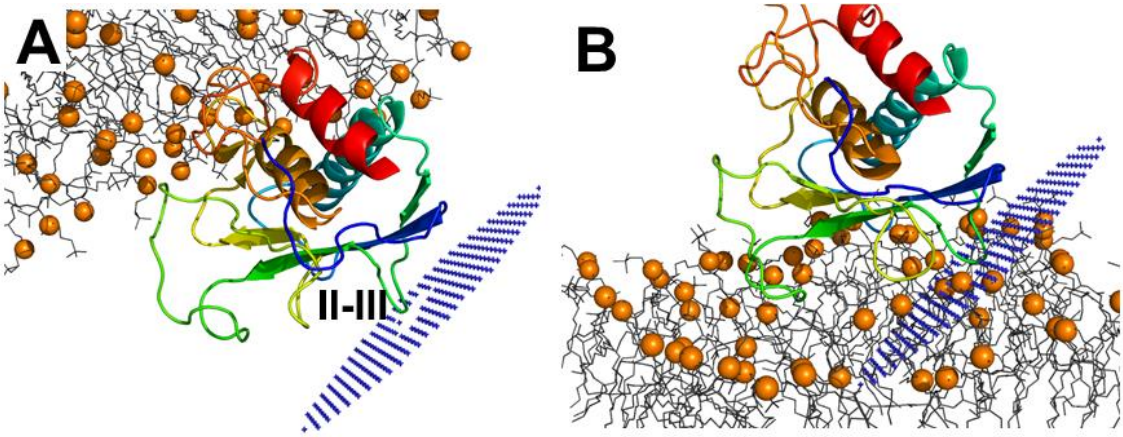

Figure III.2 Phosphatidylcholine molecules with 7- and 14-carbon acyl chains **(A)** form the annulus and center, respectively, of disk-like bicelles **(B)**.

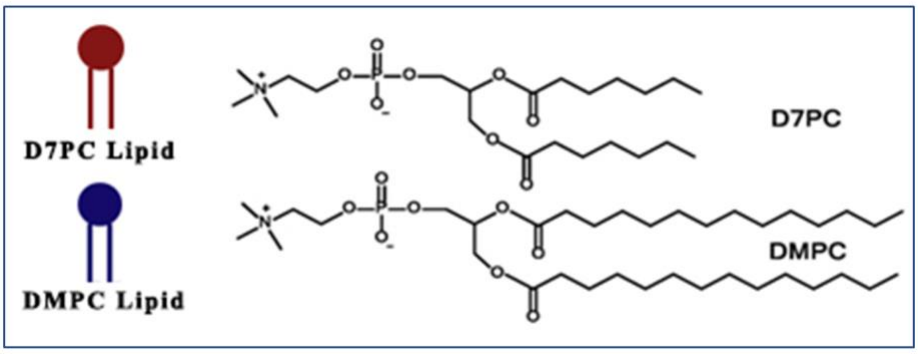

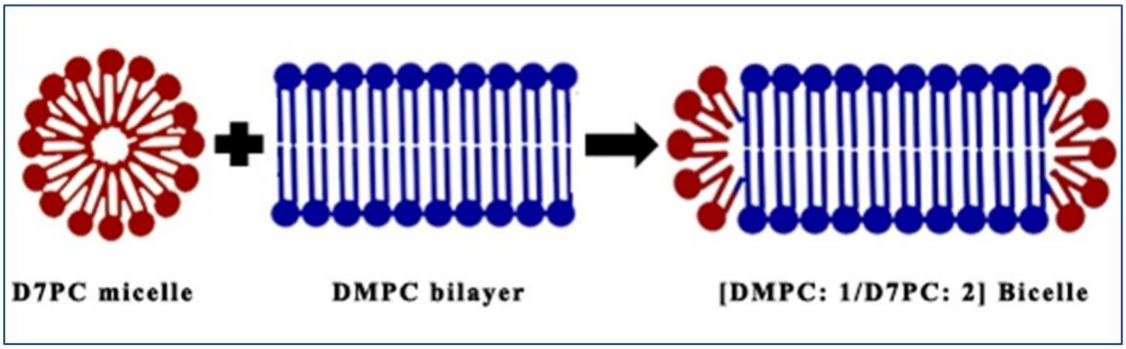

Figure III.3 Gel permeation chromatography of the assembled nanodiscs comprised of DMPC and MSP1D1.

The elution profiles for several hydrodynamic standards are superimposed onto the chromatogram for the nanodiscs. The nanodiscs migrated with an apparent molecular weight that was less than that of γ-globulin (158 kDa) on a Superdex 200 10/300 GL column. The major peaks comprised uniformly assembled nanodiscs while a significantly smaller peak corresponding to incomplete assemblies was also observed.

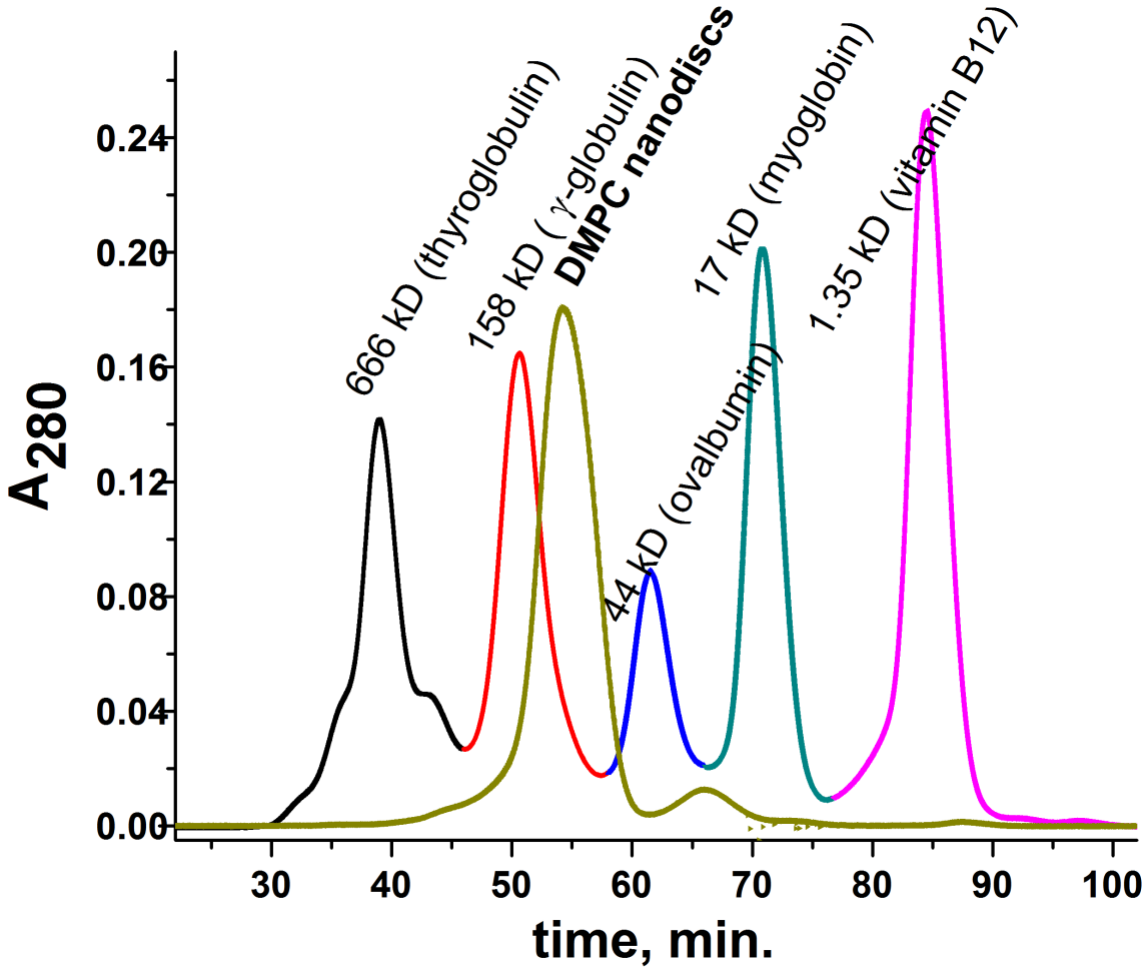

Figure III.4 Options for the location of doxyl substitution on phosphatidylcholine (PC) inserted into the membrane bilayer.

Doxyl substitution at the 5-position is the closest choice in the acyl chain to the head group. It introduces more numerous PREs to the protein interacting peripherally. Doxyl substitution at the 14-position deep in the bilayer results in fewer PREs in the protein, but which are more likely to be central to the interface. The blue ribbon depicts MMP-12. Interfacial residues are plotted by ball-and-stick.

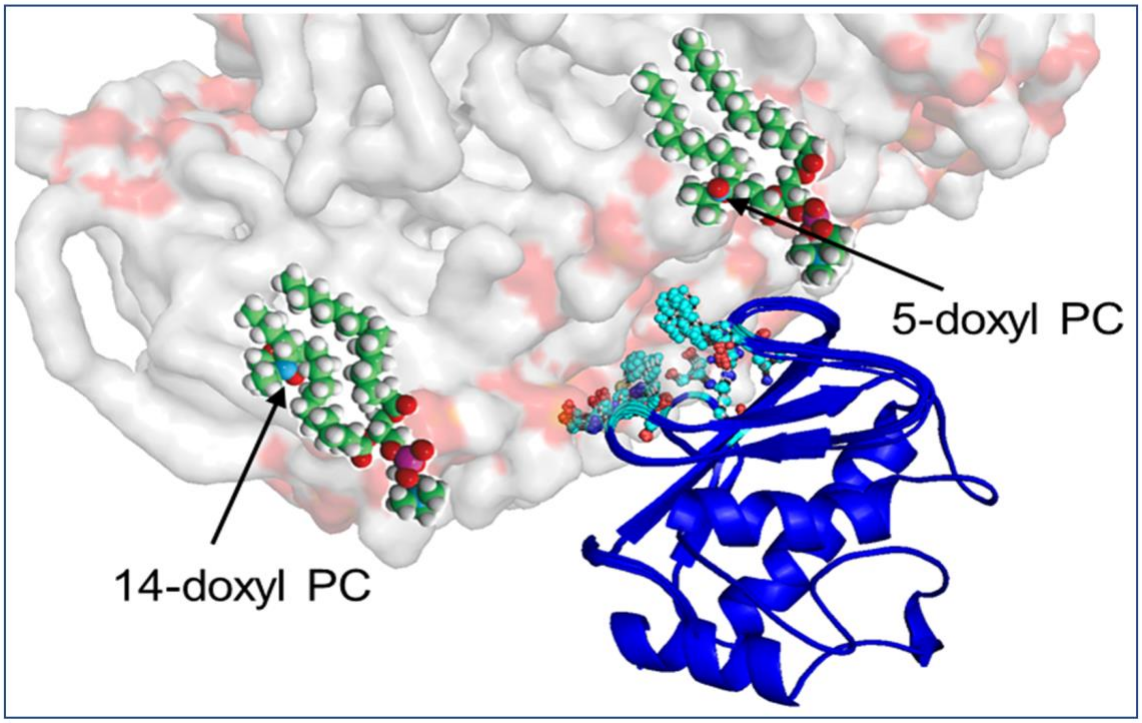

Figure III.5 The site-directed fluor labeling (SDFL) approach for defining peripheral membrane binding-sites for a protein.

When the IANBD (red) conjugated to the protein (blue) inserts in a hydrophobic compartment such as the bilayer, its fluorescence emission increases.

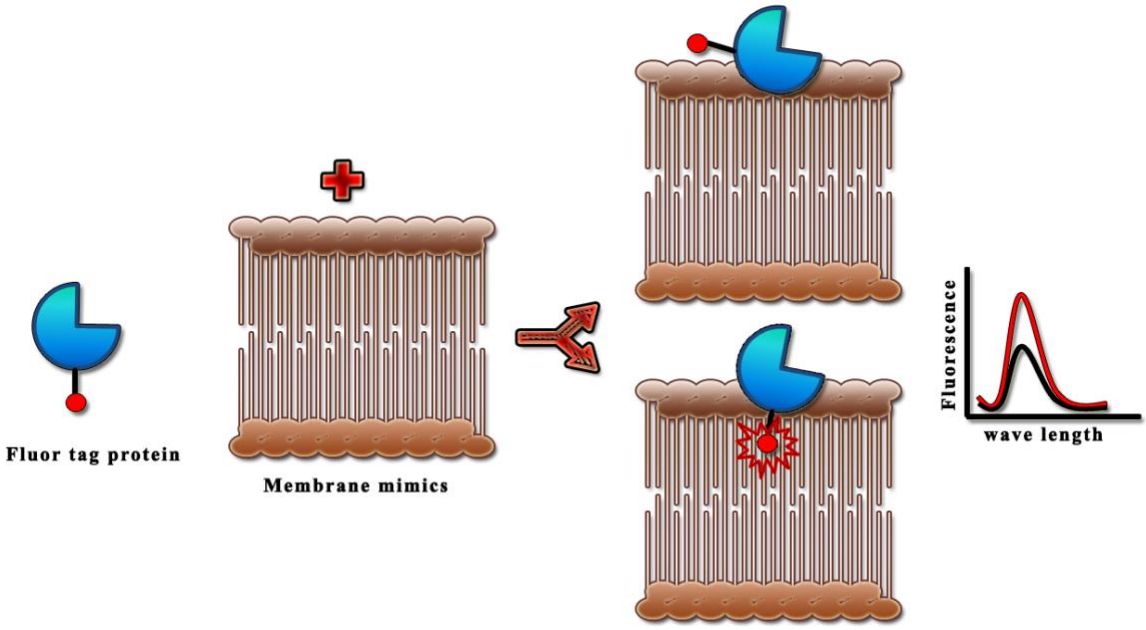

Figure III.6 IANBD Conjugation

Conjugation of the iodoacetamide-containing, environment-sensitive NBD fluorochrome (IANBD) to a single surface-exposed, reactive cysteine thiol.

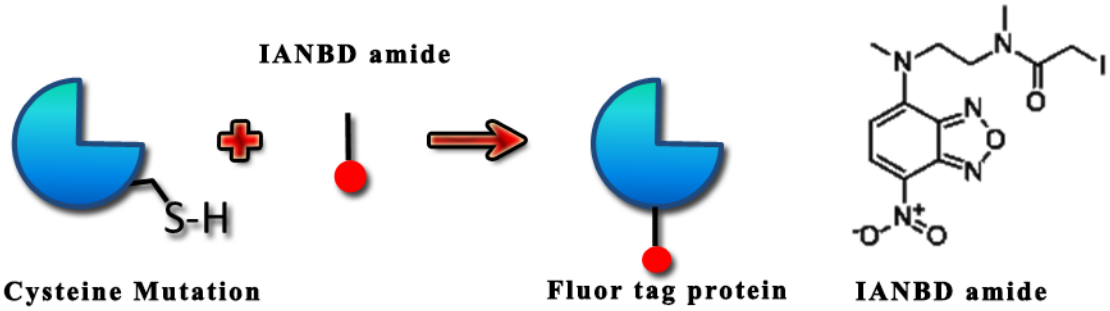

III.8 REFERENCES

1. Moravcevic, K., Oxley, C. L., and Lemmon, M. A. (2012) Conditional peripheral membrane proteins: facing up to limited specificity. *Structure* **20**, 15-27

2. Sternlicht, M. D., and Werb, Z. (2001) How matrix metalloproteinases regulate cell behavior. *Annu Rev Cell Dev Biol* **17**, 463-516

3. Clark, P. (2014) Protease-mediated ectodomain shedding. *Thorax* **69**, 682-684

4. Rose-John, S. (2013) ADAM17, shedding, TACE as therapeutic targets. *Pharmacol Res* **71**, 19-22

5. Edwards, D. R., Handsley, M. M., and Pennington, C. J. (2008) The ADAM metalloproteinases. *Mol Aspects Med* **29**, 258-289

6. Sato, H., Takino, T., Okada, Y., Cao, J., Shinagawa, A., Yamamoto, E., and Seiki, M. (1994) A matrix metalloproteinase expressed on the surface of invasive tumour cells. *Nature* **370**, 61-65

7. Strongin, A. Y., Collier, I., Bannikov, G., Marmer, B. L., Grant, G. A., and Goldberg, G. I. (1995) Mechanism of cell surface activation of 72-kDa type IV collagenase. Isolation of the activated form of the membrane metalloprotease. *J Biol Chem* **270**, 5331-5338

8. Yu, W. H., Woessner, J. F., Jr., McNeish, J. D., and Stamenkovic, I. (2002) CD44 anchors the assembly of matrilysin/MMP-7 with heparin-binding epidermal growth factor precursor and ErbB4 and regulates female reproductive organ remodeling. *Genes Dev* **16**, 307-323

9. Berton, A., Selvais, C., Lemoine, P., Henriet, P., Courtoy, P. J., Marbaix, E., and Emonard, H. (2007) Binding of matrilysin-1 to human epithelial cells promotes its activity. *Cell Mol Life Sci* **64**, 610-620

10. Owen, C. A., Hu, Z., Lopez-Otin, C., and Shapiro, S. D. (2004) Membrane-Bound Matrix Metalloproteinase-8 on Activated Polymorphonuclear Cells Is a Potent,

Tissue Inhibitor of Metalloproteinase-Resistant Collagenase and Serpinase. *J Immunol* **172**, 7791-7803

11. Owen, C. A., Hu, Z., Barrick, B., and Shapiro, S. D. (2003) Inducible Expression of Tissue Inhibitor of Metalloproteinases–Resistant Matrix Metalloproteinase-9 on the Cell Surface of Neutrophils. *Am. J. Respir. Cell Mol. Biol.* **29**, 283-294

12. Cobos-Correa, A., Trojanek, J. B., Diemer, S., Mall, M. A., and Schultz, C. (2009) Membrane-bound FRET probe visualizes MMP12 activity in pulmonary inflammation. *Nat Chem Biol* **5**, 628-630

13. Koppisetti, R. K., Fulcher, Y. G., Jurkevich, A., Prior, S. H., Xu, J., Lenoir, M., Overduin, M., and Van Doren, S. R. (2014) Ambidextrous binding of cell and membrane bilayers by soluble matrix metalloproteinase-12. *Nat Commun* **5**, 5552

14. Prior, S. H., Fulcher, Y. G., Koppisetti, R. K., Jurkevich, A., and Van Doren, S. R. (2015) Charge-Triggered Membrane Insertion of Matrix Metalloproteinase-7, Supporter of Innate Immunity and Tumors. *Structure* **23**, 2099-2110

15. Kutateladze, T. G., Capelluto, D. G., Ferguson, C. G., Cheever, M. L., Kutateladze, A. G., Prestwich, G. D., and Overduin, M. (2004) Multivalent mechanism of membrane insertion by the FYVE domain. *J Biol Chem* **279**, 3050-3057

16. Hilty, C., Wider, G., Fernandez, C., and Wuthrich, K. (2004) Membrane protein-lipid interactions in mixed micelles studied by NMR spectroscopy with the use of paramagnetic reagents. *Chembiochem* **5**, 467-473

17. Arumugam, S., and Van Doren, S. R. (2003) Global orientation of bound MMP-3 and N-TIMP-1 in solution via residual dipolar couplings. *Biochemistry* **42**, 7950-7958

18. Arumugam, S., Hemme, C. L., Yoshida, N., Suzuki, K., Nagase, H., Berjanskii, M., Wu, B., and Van Doren, S. R. (1998) TIMP-1 contact sites and perturbations of stromelysin 1 mapped by NMR and a paramagnetic surface probe. *Biochemistry* **37**, 9650-9657.

19. Takeda, M., Terasawa, H., Sakakura, M., Yamaguchi, Y., Kajiwara, M., Kawashima, H., Miyasaka, M., and Shimada, I. (2003) Hyaluronan recognition

mode of CD44 revealed by cross-saturation and chemical shift perturbation experiments. *J Biol Chem* **278**, 43550-43555

20. Garimella, R., Liu, X., Qiao, W., Liang, X., Zuiderweg, E. R., Riley, M. I., and Van Doren, S. R. (2006) Hsc70 contacts helix III of the J domain from polyomavirus T antigens: addressing a dilemma in the chaperone hypothesis of how they release E2F from pRb. *Biochemistry* **45**, 6917-6929

21. Palmier, M. O., Fulcher, Y. G., Bhaskaran, R., Duong, V. Q., Fields, G. B., and Van Doren, S. R. (2010) NMR and bioinformatics discovery of exosites that tune metalloelastase specificity for solubilized elastin and collagen triple helices. *J Biol Chem* **285**, 30918-30930

22. Gobl, C., Madl, T., Simon, B., and Sattler, M. (2014) NMR approaches for structural analysis of multidomain proteins and complexes in solution. *Prog Nucl Magn Reson Spectrosc* **80**, 26-63

23. Hennig, J., Warner, L. R., Simon, B., Geerlof, A., Mackereth, C. D., and Sattler, M. (2015) Chapter Eleven - Structural Analysis of Protein–RNA Complexes in Solution Using NMR Paramagnetic Relaxation Enhancements. in *Methods Enzymol.* (Sarah, A. W., and Frédéric, H. T. A. eds.), Academic Press. pp 333-362

24. Prior, S. H., Byrne, T. S., Tokmina-Roszyk, D., Fields, G. B., and Van Doren, S. R. (2016) Path to Collagenolysis: Collagen V Triple-Helix Model Bound Productively and in Encounters by Matrix Metalloproteinase-12. *J Biol Chem*

25. Iwahara, J., and Clore, G. M. (2006) Detecting transient intermediates in macromolecular binding by paramagnetic NMR. *Nature* **440**, 1227-1230

26. Fawzi, N. L., Doucleff, M., Suh, J. Y., and Clore, G. M. (2010) Mechanistic details of a protein-protein association pathway revealed by paramagnetic relaxation enhancement titration measurements. *Proc Natl Acad Sci U S A* **107**, 1379-1384

27. Schilder, J., and Ubbink, M. (2013) Formation of transient protein complexes. *Curr Opin Struct Biol* **23**, 911-918

28. Bashir, Q., Volkov, A. N., Ullmann, G. M., and Ubbink, M. (2010) Visualization of the Encounter Ensemble of the Transient Electron Transfer Complex of

Cytochrome c and Cytochrome c Peroxidase. *Journal of the American Chemical Society* **132**, 241-247

29. Dancea, F., Kami, K., and Overduin, M. (2008) Lipid interaction networks of peripheral membrane proteins revealed by data-driven micelle docking. *Biophys J* **94**, 515-524

30. Glover, K. J., Whiles, J. A., Wu, G., Yu, N., Deems, R., Struppe, J. O., Stark, R. E., Komives, E. A., and Vold, R. R. (2001) Structural evaluation of phospholipid bicelles for solution-state studies of membrane-associated biomolecules. *Biophys J* **81**, 2163-2171

31. Morrison, E. A., DeKoster, G. T., Dutta, S., Vafabakhsh, R., Clarkson, M. W., Bahl, A., Kern, D., Ha, T., and Henzler-Wildman, K. A. (2012) Antiparallel EmrE exports drugs by exchanging between asymmetric structures. *Nature* **481**, 45-50

32. Liu, Y., Kahn, R. A., and Prestegard, J. H. (2010) Dynamic structure of membrane-anchored Arf*GTP. *Nat Struct Mol Biol* **17**, 876-881

33. Lu, Z., Van Horn, W. D., Chen, J., Mathew, S., Zent, R., and Sanders, C. R. (2012) Bicelles at low concentrations. *Mol Pharm* **9**, 752-761

34. Song, Y., Mittendorf, K. F., Lu, Z., and Sanders, C. R. (2014) Impact of bilayer lipid composition on the structure and topology of the transmembrane amyloid precursor C99 protein. *J Am Chem Soc* **136**, 4093-4096

35. Schuler, M. A., Denisov, I. G., and Sligar, S. G. (2013) Nanodiscs as a new tool to examine lipid-protein interactions. *Methods Mol Biol* **974**, 415-433

36. Denisov, I. G., and Sligar, S. G. (2016) Nanodiscs for structural and functional studies of membrane proteins. *Nat Struct Mol Biol* **23**, 481-486

37. Raschle, T., Hiller, S., Yu, T. Y., Rice, A. J., Walz, T., and Wagner, G. (2009) Structural and functional characterization of the integral membrane protein VDAC-1 in lipid bilayer nanodiscs. *J Am Chem Soc* **131**, 17777-17779

38. Gluck, J. M., Wittlich, M., Feuerstein, S., Hoffmann, S., Willbold, D., and Koenig, B. W. (2009) Integral membrane proteins in nanodiscs can be studied by solution NMR spectroscopy. *J Am Chem Soc* **131**, 12060-12061

39. Yu, T. Y., Raschle, T., Hiller, S., and Wagner, G. (2012) Solution NMR spectroscopic characterization of human VDAC-2 in detergent micelles and lipid bilayer nanodiscs. *Biochim Biophys Acta* **1818**, 1562-1569

40. Hagn, F., Etzkorn, M., Raschle, T., and Wagner, G. (2013) Optimized phospholipid bilayer nanodiscs facilitate high-resolution structure determination of membrane proteins. *J Am Chem Soc* **135**, 1919-1925

41. Studier, F. W. (2005) Protein production by auto-induction in high-density shaking cultures. *Protein Expression and Purification* **41**, 207-234

42. Denisov, I. G., Grinkova, Y. V., Lazarides, A. A., and Sligar, S. G. (2004) Directed self-assembly of monodisperse phospholipid bilayer Nanodiscs with controlled size. *J Am Chem Soc* **126**, 3477-3487

43. Kufareva, I., Lenoir, M., Dancea, F., Sridhar, P., Raush, E., Bissig, C., Gruenberg, J., Abagyan, R., and Overduin, M. (2014) Discovery of novel membrane binding structures and functions. *Biochem Cell Biol* **92**, 555-563

44. Lomize, M. A., Pogozheva, I. D., Joo, H., Mosberg, H. I., and Lomize, A. L. (2012) OPM database and PPM web server: resources for positioning of proteins in membranes. *Nucleic Acids Res* **40**, D370-376

45. Lomize, M. A., Lomize, A. L., Pogozheva, I. D., and Mosberg, H. I. (2006) OPM: orientations of proteins in membranes database. *Bioinformatics* **22**, 623-625

46. Lomize, A. L., Pogozheva, I. D., Lomize, M. A., and Mosberg, H. I. (2007) The role of hydrophobic interactions in positioning of peripheral proteins in membranes. *BMC Struct Biol* **7**, 44

47. Lomize, A. L., Pogozheva, I. D., Lomize, M. A., and Mosberg, H. I. (2006) Positioning of proteins in membranes: a computational approach. *Protein Sci* **15**, 1318-1333

48. Kufareva, I., and Overduin, M. (2015) http://www.slideshare.net/overduin/moda-slideshare.

49. Spurlino, J. C., Smallwood, A. M., Carlton, D. D., Banks, T. M., Vavra, K. J., Johnson, J. S., Cook, E. R., Falvo, J., Wahl, R. C., Pulvino, T. A., and et al. (1994) 1.56 A structure of mature truncated human fibroblast collagenase. *Proteins* **19**, 98-109

50. Bertini, I., Fragai, M., Luchinat, C., Melikian, M., Mylonas, E., Sarti, N., and Svergun, D. I. (2009) Interdomain flexibility in full-length matrix metalloproteinase-1 (MMP-1). *J Biol Chem* **284**, 12821-12828

51. Ye, Q.-Z., Johnson, L. J., and Baragi, V. (1992) Gene Synthesis and Expression in *E. coli* for PUMP, a Human Matrix Metalloproteinase. *Biochemical and Biophysics Research Communications* **186**, 143-149

52. Fulcher, Y. G., Sanganna Gari, R. R., Frey, N. C., Zhang, F., Linhardt, R. J., King, G. M., and Van Doren, S. R. (2014) Heparinoids activate a protease, secreted by mucosa and tumors, via tethering supplemented by allostery. *ACS Chem Biol* **9**, 957-966

53. Zheng, X., Ou, L., Tong, X., Zhu, J., and Wu, H. (2007) Over-expression and refolding of isotopically labeled recombinant catalytic domain of human macrophage elastase (MMP-12) for NMR studies. *Protein Expr Purif* **56**, 160-166

54. Bertini, I., Calderone, V., Fragai, M., Jaiswal, R., Luchinat, C., Melikian, M., Mylonas, E., and Svergun, D. I. (2008) Evidence of reciprocal reorientation of the catalytic and hemopexin-like domains of full-length MMP-12. *J Am Chem Soc* **130**, 7011-7021

55. Lovejoy, B., Welch, A. R., Carr, S., Luong, C., Broka, C., Hendricks, R. T., Campbell, J. A., Walker, K. A., Martin, R., Van Wart, H., and Browner, M. F. (1999) Crystal structures of MMP-1 and -13 reveal the structural basis for selectivity of collagenase inhibitors. *Nat Struct Biol* **6**, 217-221.

56. Zhao, Y., Marcink, T. C., Sanganna Gari, R. R., Marsh, B. P., King, G. M., Stawikowska, R., Fields, G. B., and Van Doren, S. R. (2015) Transient collagen triple helix binding to a key metalloproteinase in invasion and development. *Structure* **23**, 257-269

57. Udi, Y., Fragai, M., Grossman, M., Mitternacht, S., Arad-Yellin, R., Calderone, V., Melikian, M., Toccafondi, M., Berezovsky, I. N., Luchinat, C., and Sagi, I. (2013) Unraveling hidden regulatory sites in structurally homologous metalloproteases. *J Mol Biol* **425**, 2330-2346

58. Lee, W., Cornilescu, G., Dashti, H., Eghbalnia, H. R., Tonelli, M., Westler, W. M., Butcher, S. E., Henzler-Wildman, K. A., and Markley, J. L. (2016) Integrative NMR for biomolecular research. *J Biomol NMR* **64**, 307-332

59. Lee, W., Tonelli, M., and Markley, J. L. (2015) NMRFAM-SPARKY: enhanced software for biomolecular NMR spectroscopy. *Bioinformatics* **31**, 1325-1327

60. Lee, W., Kim, J. H., Westler, W. M., and Markley, J. L. (2011) PONDEROSA, an automated 3D-NOESY peak picking program, enables automated protein structure determination. *Bioinformatics* **27**, 1727-1728

61. Lee, W., Stark, J. L., and Markley, J. L. (2014) PONDEROSA-C/S: client-server based software package for automated protein 3D structure determination. *J Biomol NMR* **60**, 73-75

62. Ruschak, A. M., and Kay, L. E. (2010) Methyl groups as probes of supra-molecular structure, dynamics and function. *J Biomol NMR* **46**, 75-87

63. Tugarinov, V., and Kay, L. E. (2003) Ile, Leu, and Val methyl assignments of the 723-residue malate synthase G using a new labeling strategy and novel NMR methods. *J Am Chem Soc* **125**, 13868-13878

64. Sprangers, R., and Kay, L. E. (2007) Quantitative dynamics and binding studies of the 20S proteasome by NMR. *Nature* **445**, 618-622

65. Sinha, K., Jen-Jacobson, L., and Rule, G. S. (2013) Divide and conquer is always best: sensitivity of methyl correlation experiments. *J Biomol NMR* **56**, 331-335

66. Chao, F. A., Kim, J., Xia, Y., Milligan, M., Rowe, N., and Veglia, G. (2014) FLAMEnGO 2.0: an enhanced fuzzy logic algorithm for structure-based assignment of methyl group resonances. *J Magn Reson* **245**, 17-23

67. Poget, S. F., Cahill, S. M., and Girvin, M. E. (2007) Isotropic bicelles stabilize the functional form of a small multidrug-resistance pump for NMR structural studies. *J Am Chem Soc* **129**, 2432-2433

68. Bayburt, T. H., Grinkova, Y. V., and Sligar, S. G. (2002) Self-assembly of discoidal phospholipid bilayer nanoparticles with membrane scaffold proteins. *Nano Letters* **2**, 853-856

69. Bayburt, T. H., Dennisov, I. G., Grinkova, Y. V., and Sligar, S. G. Nanodisc Technology: Protocols for Preparation of Nanodiscs. http://sligarlab.life.uiuc.edu/nanodisc/protocols.html. University of Illinois, Urbana-Champaign, Illinois

70. Liu, Y., and Prestegard, J. H. (2008) Direct measurement of dipole-dipole/CSA cross-correlated relaxation by a constant-time experiment. *J Magn Reson* **193**, 23-31

71. Lee, D., Hilty, C., Wider, G., and Wuthrich, K. (2006) Effective rotational correlation times of proteins from NMR relaxation interference. *J Magn Reson* **178**, 72-76

72. Aguilar, J. A., Nilsson, M., Bodenhausen, G., and Morris, G. A. (2012) Spin echo NMR spectra without J modulation. *Chemical Communications* **48**, 811-813

73. Schulz, T. A., Choi, M. G., Raychaudhuri, S., Mears, J. A., Ghirlando, R., Hinshaw, J. E., and Prinz, W. A. (2009) Lipid-regulated sterol transfer between closely apposed membranes by oxysterol-binding protein homologues. *J Cell Biol* **187**, 889-903

74. Kim, Y. E., Chen, J., Chan, J. R., and Langen, R. (2010) Engineering a polarity-sensitive biosensor for time-lapse imaging of apoptotic processes and degeneration. *Nat Methods* **7**, 67-73

75. Song, Y., Hustedt, E. J., Brandon, S., and Sanders, C. R. (2013) Competition between homodimerization and cholesterol binding to the C99 domain of the amyloid precursor protein. *Biochemistry* **52**, 5051-5064

76. Löhr, F., Tumulka, F., Bock, C., Abele, R., and Dötsch, V. (2015) An extended combinatorial 15N, 13Cα, and $$ ^{13} {\text{C}}^{\prime } $$ 13 C ′ labeling

approach to protein backbone resonance assignment. *J. Biomol. NMR* **62**, 263-279

77. Ikeya, T., Takeda, M., Yoshida, H., Terauchi, T., Jee, J. G., Kainosho, M., and Guntert, P. (2009) Automated NMR structure determination of stereo-array isotope labeled ubiquitin from minimal sets of spectra using the SAIL-FLYA system. *J Biomol NMR* **44**, 261-272

78. Hefke, F., Bagaria, A., Reckel, S., Ullrich, S. J., Dotsch, V., Glaubitz, C., and Guntert, P. (2011) Optimization of amino acid type-specific 13C and 15N labeling for the backbone assignment of membrane proteins by solution- and solid-state NMR with the UPLABEL algorithm. *J Biomol NMR* **49**, 75-84

79. Opitz, C., Isogai, S., and Grzesiek, S. (2015) An economic approach to efficient isotope labeling in insect cells using homemade 15N-, 13C- and 2H-labeled yeast extracts. *J Biomol NMR* **62**, 373-385

80. Sattler, M., and Fesik, S. W. (1996) Use of deuterium labeling in NMR: overcoming a sizeable problem. *Structure* **4**, 1245-1249

81. Tugarinov, V., Muhandiram, R., Ayed, A., and Kay, L. E. (2002) Four-dimensional NMR spectroscopy of a 723-residue protein: chemical shift assignments and secondary structure of malate synthase g. *J Am Chem Soc* **124**, 10025-10035

82. Revington, M., and Zuiderweg, E. R. (2004) TROSY-driven NMR backbone assignments of the 381-residue nucleotide-binding domain of the Thermus Thermophilus DnaK molecular chaperone. *J Biomol NMR* **30**, 113-114

83. Lescop, E., Schanda, P., and Brutscher, B. (2007) A set of BEST triple-resonance experiments for time-optimized protein resonance assignment. *J Magn Reson* **187**, 163-169

84. Schanda, P., Van Melckebeke, H., and Brutscher, B. (2006) Speeding up three-dimensional protein NMR experiments to a few minutes. *J Am Chem Soc* **128**, 9042-9043

85. Velyvis, A., Ruschak, A. M., and Kay, L. E. (2012) An economical method for production of (2)H, (13)CH3-threonine for solution NMR studies of large

protein complexes: application to the 670 kDa proteasome. *PLoS One* **7**, e43725

86. Gennis, R. B. (1989) *Biomembranes: Molecular Structure and Function*, Springer-Verlag, New York

87. Palmier, M. O., and Van Doren, S. R. (2007) Rapid determination of enzyme kinetics from fluorescence: overcoming the inner filter effect. *Anal Biochem* **371**, 43-51

88. Li, L., Shi, X., Guo, X., Li, H., and Xu, C. (2014) Ionic protein-lipid interaction at the plasma membrane: what can the charge do? *Trends Biochem Sci* **39**, 130-140

IV. MT1-MMP Family Interactions: Finding Insights From The Other Members

IV.1 INTRODUCTION

IV.1.1 MMP-1 and MT1-MMP: A Structural Comparison

MMP-1 (collagenase-1) was the first studied enzyme from the MMP family and has many similarities to MT1-MMP including activation of MMP-2, MMP-9 (1,2). MMP-1 is one of four members of the MMP family (along with MT1-MMP, MMP-8, and MMP-13) that degrade fibrillary collagens, leaving them unstable and prone to degradation by other MMPs (3). MMP-1 is a soluble MMP. Proteolysis of the PRO domain is required for activation of the enzyme. Although the linker between MMP-1 catalytic and HPX domains is among the shortest in the family, it has a large degree of flexibility suggesting that all MMPs have sizable conformational freedom between domains (4). Overall, the structure of the productive complex of MMP-1 has been seen as a model for other collagenase productive complexes (5).

Previously it was shown that the HPX blade I of MMP-1 was implicated in collagen binding by hydrogen-deuterium exchange (6) even though the HPX domain lacks binding pockets or clefts for a peptide substrate (7). Later it was discovered that MMP-1's catalytic and HPX domains adopt a compact productive complex where collagen binds (8). The crystal structure of this complex was uncovered a year later (5) showing the HPX domain binding 10 residues from the

site of collagenolysis (scissile bond). Further work on the MMP-1 compact complex showed multiple conformations between the catalytic and HPX domains (9). Although the HPX and catalytic domain interactions are somewhat transient, they lead to conformations that position the HPX collagen binding site to the solvent.

The HPX domain of MT1-MMP binds collagen in a very similar trajectory as MMP-1 (10). The difference between the two structures is the position where the HPX domains bind the strands of the collagen mimic. MT1-MMP HPX domain binds alongside the scissile bond of collagen whereas MMP-1 HPX domain binds 10 residues upstream from the site of collagenolysis. To explain this difference, two models of interdomain collagen binding where proposed for MT1-MMP. One model posits that the HPX domain undergoes a sliding motion axial to the collagen allowing the catalytic domain to slide towards the scissile bond. The other is a clasping model where the catalytic domain reaches above the HPX domain and cuts at the scissile bond sandwiching the two domains with the collagen in between (10). Discussed here is the possibility of MT1-MMP adopting a similar compact conformation as MMP-1 during the proposed sliding model allowing for collagenolysis on the membrane.

Another similarity of these two enzymes is the GYPK loop in blade II of the HPX domain that is described in Marcink et al (submitted); see chapter 2 (11). While no work has been done on MMP-1's interactions with membranes, this loop could be implicated in binding the membrane surface in MMP-1. Furthermore, it has been shown that the catalytic domain of MT1-MMP binds membranes (12). Shown here is the preliminary NMR results of the catalytic domain interaction with

bicelles and nanodiscs along with a proposal that the compact conformation of MMP-1 might play a part in a productive complex of MT1-MMP with a collagen triple-helix on the cell surface.

IV.1.2 MT1-MMP Structural Comparison with MMP-12 and its Antimicrobial Loop

The HPX domain is required for collagenolysis by the true collagenases of the MMP family (13,14), but this does not include MMP-12. Membrane interactions of MMP-12 catalytic domain were already reported (15). Recent work discussed below shows NMR peak broadenings of MMP-12 HPX domain induced by the addition of nanodiscs (12,15).

The HPX domain of MMP-12 plays a bactericidal role in phagolysosomes of macrophages (16). While the catalytic domain is likely to be unfolded by the low pH of phagolysosomes, the HPX domain remains intact and was shown to disrupt bacterial membranes by a specific KDDK loop motif (12,16). It was proposed that MMP-12 antimicrobial properties could occur through a cell disruption at the membrane surface (12). This loop motif is adjacent to a proposed blade II membrane binding loop discovered by Marcink et al (submitted); see chapter 2 (11). While MT1-MMP has not been shown to have antimicrobial properties (16,17), it has a similar loop motif (KDEK) as MMP-12 (KDDK). Understanding how these two important loops and how their proximity impact each other could

increase understanding of the mechanism of bacterial killing by the HPX domain of MMP-12.

IV.2 MATERIAL AND METHODS

IV.2.1 Catalytic and HPX Sample Preparation

The MT1-MMP HPX domain and MMP-12 were both expressed and purified as previously described (10,18). For the catalytic domain, cells were sonicated, and the resulting inclusion bodies were dissolved in 6 M urea and centrifuged to remove precipitate. An NTA affinity column was used to purify the catalytic domain with a buffer of 20 mM Tris (pH 7.2), 6 M urea, and 500 mM NaCl. After 5 column volumes a 20 mM imidazole wash, protein was eluted with 3 column volumes of 300 mM imidazole. The eluate was diluted to 0.05 mg/ml with 20 mM Tris (pH 7.2), 150 mM NaCl, and 3M urea. The resulting solution was dialyzed once against 10 column volumes of 1M urea and then twice against 0 M urea to remove all excess salt and denaturant. The final sample was concentrated and stored with 0.02% sodium azide.

IV.2.2 Ultracentrifugation Membrane Interaction Assay

Large unilamellar vesicles (LUVs) were formed by suspending DMPC monomers in 20 mM Tris (pH 7.2). After an hour at 37°C for the hydration of lipids, the solution was subjected to multiple freeze-thaw cycles in liquid nitrogen. The resulting LUVs were incubated at concentration of 1 mM in DMPC monomers for

1 hour at 25 °C with both the HPX and catalytic domains of MT1-MMP. The resulting mixtures were pelleted through ultracentrifugation at 180,000 x g at 4 °C for 20 min (12). Pellets were resuspended in 1/8 of the original volume. The resuspended pellets and supernatant were both run on SDS-PAGE and analyzed using imageJ.

IV.2.3 Assay of Membrane Interactions using Intrinsic Tryptophan Fluorescence

SUVs were made by same protocol used in Chapter II (11).

IV.2.4 Mapping of Interface for Bilayers using NMR Peak Broadenings

TROSY NMR spectra of the catalytic domain of MT1-MMP were recorded in the absence and presence of an equimolar concentration of nanodiscs or bicelles. This was performed in 20 mM Tris (pH 7.2), 150 mM NaCl, and 10 mM CaCl2. Peak heights were analyzed through CCPNMR software. The largest peak intensity decreases upon the addition of the membrane mimics (> 20%) were plotted upon the crystal structure of the MT1-MMP catalytic domain (2bqq).

IV.2.5 Full Length MMP-12 And E. coli Induced NMR Peak Broadenings

TROSY spectra were recorded with additions of 0, 100, 1,000 and 10,000 E. coli bacterial cells (measured by OD600) added to 200 μM MMP-12 in 20 mM Tris, 150 mM NaCl, 10 mM $CaCl_2$, 100 μM ZnCl at pH 7.2. Peak heights were

analyzed with CCPNMR Analysis and the largest addition of bacteria was used for subsequent broadening results. Largest peak height decreases (> 20%) upon the addition of bacteria where plotted on the crystal structure of full-length MMP-12 (PDB ID: 3BA0).

IV.3 RESULTS

IV.3.1 Membrane Interactions with the HPX And Catalytic Domains of MT1-MMP

Utilizing intrinsic tryptophan fluorescence along with high speed centrifugation assays (Fig. 1A,B), it has been shown the catalytic domain and HPX domain of MT1-MMP has an affinity for the membrane and at least is transiently bound (12). Furthermore, using MODA membrane interaction prediction software, there are many residues on the catalytic domain that may be favorable for membrane binding (Fig. 2).

NMR studies have measured regions of membrane interactions. Bicelles and nanodiscs both introduced broadenings to residues on the catalytic domain. Most of these residues centered around the active site. Nanodisc -induced broadenings were more concentrated near the active site and towards α-helices B and C (Fig 2). Broadenings induced by DMPC/DHPC bicelles (q=0.5) were for the most part located in the loop opposite of the α-helices above the beta sheet (Fig 2).

IV.3.2 Similarities of MT1-MMP and MMP-1's Compact Conformation

It has been previously shown that MMP-1 adopts a compact formation wherein the catalytic domain positions itself up against blade one of the HPX domain (Fig. 3A) (8). Two of these residues on the HPX domain of MMP-1 jut out to make contact with the catalytic domain (Fig.3B). They are conserved in MT1-MMP Superposition of the MT1-MMP catalytic domain on the HPX domain showed a similar structure to the MMP-1 compact orientation.

To understand how this compact orientation could be possible on the surface of the plasma membrane, this compact structure was compared to previous HPX:nanodisc binding orientations discussed earlier. Aligned with blade IV at the membrane surface, the compact conformation allowed for the catalytic domain residues broadened by membranes to come in contact with membranes (Fig. 4A). However, if TIMP were bound, the TIMP would clash with the membrane (Fig. 4B). When docked with blade II at the bilayer surface, the residues of peaks broadened away by the membrane mimics face away from the membrane and towards the solvent (Fig 4c). This orientation on the membrane allows TIMP binding the catalytic and HPX domains packed with the ball-and-socket arrangement proposed in MMP-1 by Arnold et al. (8). Some of the residues near the active site potentially involved in membrane binding (Fig. 2) may be covered by the TIMP.

IV.3.3 Interactions of *E. coli* with MMP-12 Detected By NMR

To understand the effects that MMP-12 has on bacterial cells, NMR was used. There was a broadening of NMR peak heights upon the addition of increasing *E. coli* BL21 DE3 cells in both the catalytic and HPX domains (Fig. 5A). In the catalytic domain these broadenings were scattered throughout (Fig. 5A). In the HPX domain, the greatest broadenings (> 20% reduction from original peak height) occurred mainly in blades 1 and 2 (Fig. 5B). Many of these broadenings are near the bactericidal KDDK loop, as well as near the blade II loop that was discovered to bind membranes in MT1-MMP.

IV.3.4 Potential Membrane Binding Interface of MMP-12 Based on MT1-MMP Results

MMP-12 has the sequence EPNYPK bulging from blade II which is very similar to the membrane binding sequence EPGYPK in the MT1-MMP HPX domain (Fig. 6A). Overlay of the two models show high structural similarities in this loop region (Fig. 6B). The microbial KDDK loop can be seen interacting with the membrane surface in the MMP-12 overlay (Fig. 6C). Further structural data is needed to further understand these interactions.

IV.4 DISCUSSION

IV.4.1 Membrane Interactions with the MT1-MMP Catalytic Domain

The catalytic domain of MT1-MMP binds bilayers (Figs. 1, 2), in contrast to cartoons in the literature that portray it as distant from the membrane. Both bicelles and nanodiscs induce broadenings of NMR peaks of residues in similar areas. These residues overlap with some of the sites predicted by MODA to bind bilayers (Fig 2). These results suggest that the catalytic domain is at least transiently in contact with the membrane.

This result, along with the previous insights into membrane binding by the HPX domain, calls into question the idea that MT1-MMP branches straight out into the extracellular space (19,20). There should be periods of time both domains are bound to the membrane. The question remains if this membrane interaction is biologically significant? Results from chapter II show an increase in collagenolysis upon the addition of lipids indicated the membrane plays a role in collagen degradation. Earlier work on the HPX domain and collagen raised the question of side-by-side vs. clasping modes of collagen binding in collagenolysis (10). The membrane might play an important role in determining which is correct. The active site is where most of the bilayer-induced peak broadenings occur in the catalytic domain. HPX membrane binding could induce a conformational change that flips the catalytic domain off the membrane, exposing the active site. This conformational change could favor the clasping model. Further in-depth analysis is required to understand the interactions of MT1-MMP on the membrane.

Little is known on the interactions between the HPX and catalytic domains of MT1-MMP. Work shown here proposes a similar compact orientation between the two domains as found in MMP-1 with the ball and socket model (8,21,22). This model had two main residues that protrude from the MMP-1 HPX domain (Arg300 and Phe301) which are similar to MT1-MMP residues Arg339 and Trp340 (Fig 3). When the MT1-MMP domains are oriented in similar fashion as the MMP-1 domains, there are no steric clashes between expected at the surface of the bilayer (Fig 4A). Moreover, this hypothesis positions the catalytic domain where it can easily reach the bilayer surface via surfaces suggested by NMR to bind surfaces (Fig. 4A).

It can be hypothesized that this close positioning of the two domains of MT1-MMP accommodates its binding bilayers by either of its interfaces at blade II or blade IV of the HPX domain. With blade IV bound to the membrane, the TIMP inhibitor of MT1-MMP is unlikely to bind due to the steric clash with the membrane surface (Fig 4B). Collagen binding to the HPX domain could potentially disrupt the close association of HPX and catalytic domains to allow the catalytic domain to reposition its active site to cleave collagen in a clasping orientation. Binding of blade II to the membrane could turn the membrane binding surfaces of the catalytic domain away from the bilayer when the catalytic domain is closely associated in the orientation hypothesized (Fig 4C). This orientation might be less favorable in that it exposes hydrophobic residues to the extracellular space. Interestingly, this orientation allows for TIMP-2 binding which covers these hydrophobic areas when it inactivates the enzyme (Fig. 4C). Furthermore, this orientation could promote the

capture of proMMP-2, for which TIMP-2 is required (23). The trimeric proMMP-2:TIMP-2:MT1-MMP complex initiates the activation of MMP-2 (24,25). These predictions gained from peak broadenings and structural comparisons with MMP-1 suggest hypothesis for testing by future experiments to explore these complex interactions on membrane surfaces.

IV.4.2 Bacterial-Induced Broadenings of NMR Peaks of Full-length MMP-12

The MMP-12 HPX domain was shown to bind and kill bacteria in phagolysozomes of macrophages (16). This activity by MMP-12's HPX domain could occur at the membrane protein interface since most antimicrobial peptides disturb the bacterial membrane (16,26,27). NMR line broadening studies with MMP-12 and nanodiscs have shown the highest density of affected residues around blades III and IV (12). Peak broadenings induced by bacterial cells show a concentration of affected residues in blades I and II (Fig 5). These results seem in conflict with each other. However, the recent results on membrane binding by MT1-MMP and sequence similarities can offer some preliminary guidance.

MMP-12 has in blade II a highly similar membrane binding loop motif (EPNYPK) as MT1-MMP (EPGYPK). This loop motif sits adjacent to the antimicrobial KDDK motif. MT1-MMP has a very similar motif (KDEK) (fig 6A) and when these two structures are overlaid the MMP-12 KDDK motif makes contact with the phospholipid head groups on the membrane surface (Fig. 6B,C). Could MMP-12 use this same membrane loop as MT1-MMP and make contact with the bacterial cell membrane surface? The membrane and protein interface could play

a large role in the bactericidal activity of MMP-12. Further studies still need to be done to confirm which orientation MMP-12 binds membranes and this preliminary work is a step forward in the experimental design to uncover these important interactions.

IV.5 FIGURES

Figure IV.1 Soluble domains of MT1-MMP bind vesicles.

(A) SDS-PAGE gels of the catalytic and (C) HPX domains of MT1-MMP that sedimented with large unilamellar vesicles during high speed centrifugation. Pellet fractions were reconstituted in 1/8 the original sample volume. (B,D) Intrinsic tryptophan quenching assays of the catalytic (B) and HPX (D) domains upon the addition of small unilamellar vesicles with 2% PyPE, a tryptophan quencher. (Figure taken with permission from Van Doren et al., 2010) (12)

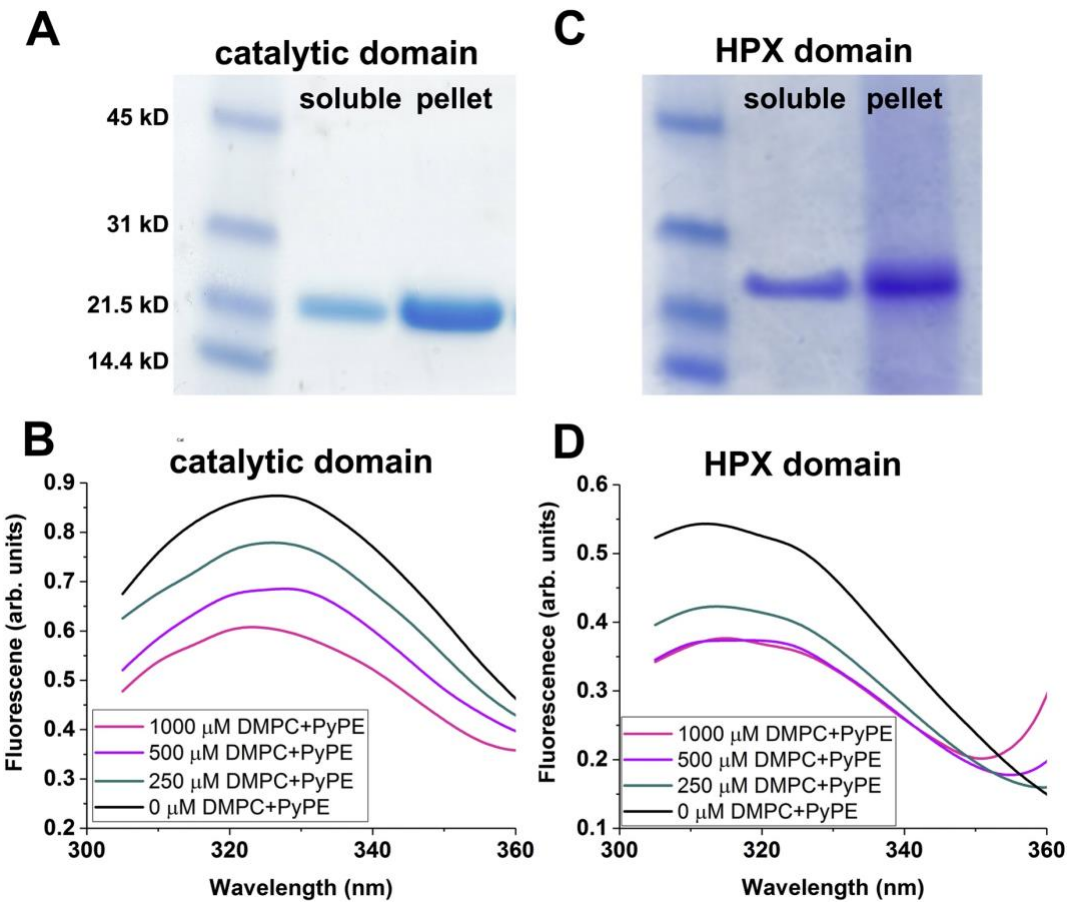

Figure IV.2 Membrane interactions of MT1-MMP catalytic domain.

(A) The catalytic domain of MMP was predicted to bind membranes by MODA with the contacts shown in orange dots. Residues whose intensity decreased upon the addition of a 1:1 complex of protein with bicelles (blue spheres) or nanodiscs (pink spheres) surround the active site cleft. (B) This 90-degree rotation of panel A also shows the overlap of MODA-predicted sites with bicelle-induced broadenings.

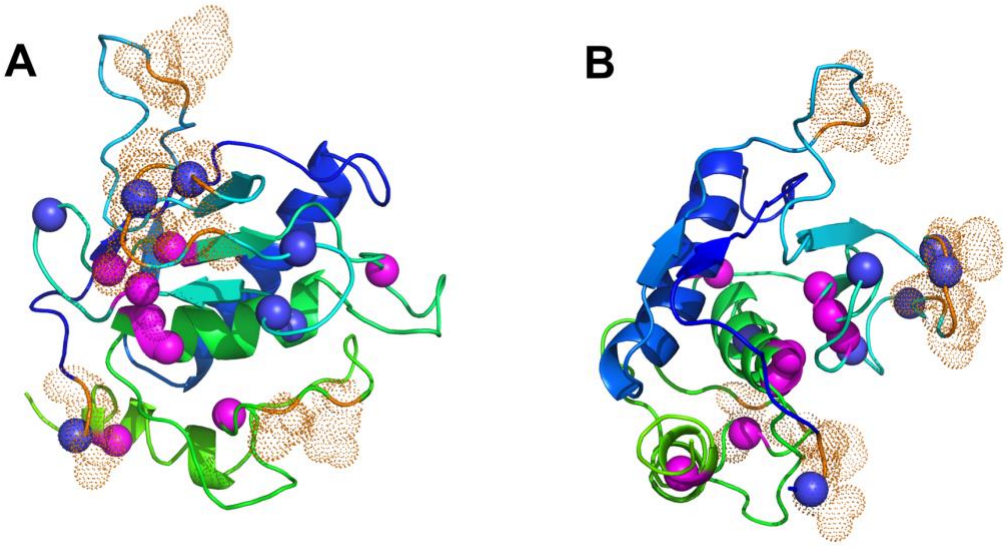

Figure IV.3 The ball and socket model of MMP-1 might apply to MT1-MMP.

(A) MMP-1 ball and socket model where the catalytic domain (green) interacts with the HPX domain (blue) in a compact orientation. (B) MT1-MMP HPX domain has a similarly charged binding ball on the HPX where the catalytic domain can bind. (Panel A used with permission from Arnold, L.H. et al., 2011) (8)

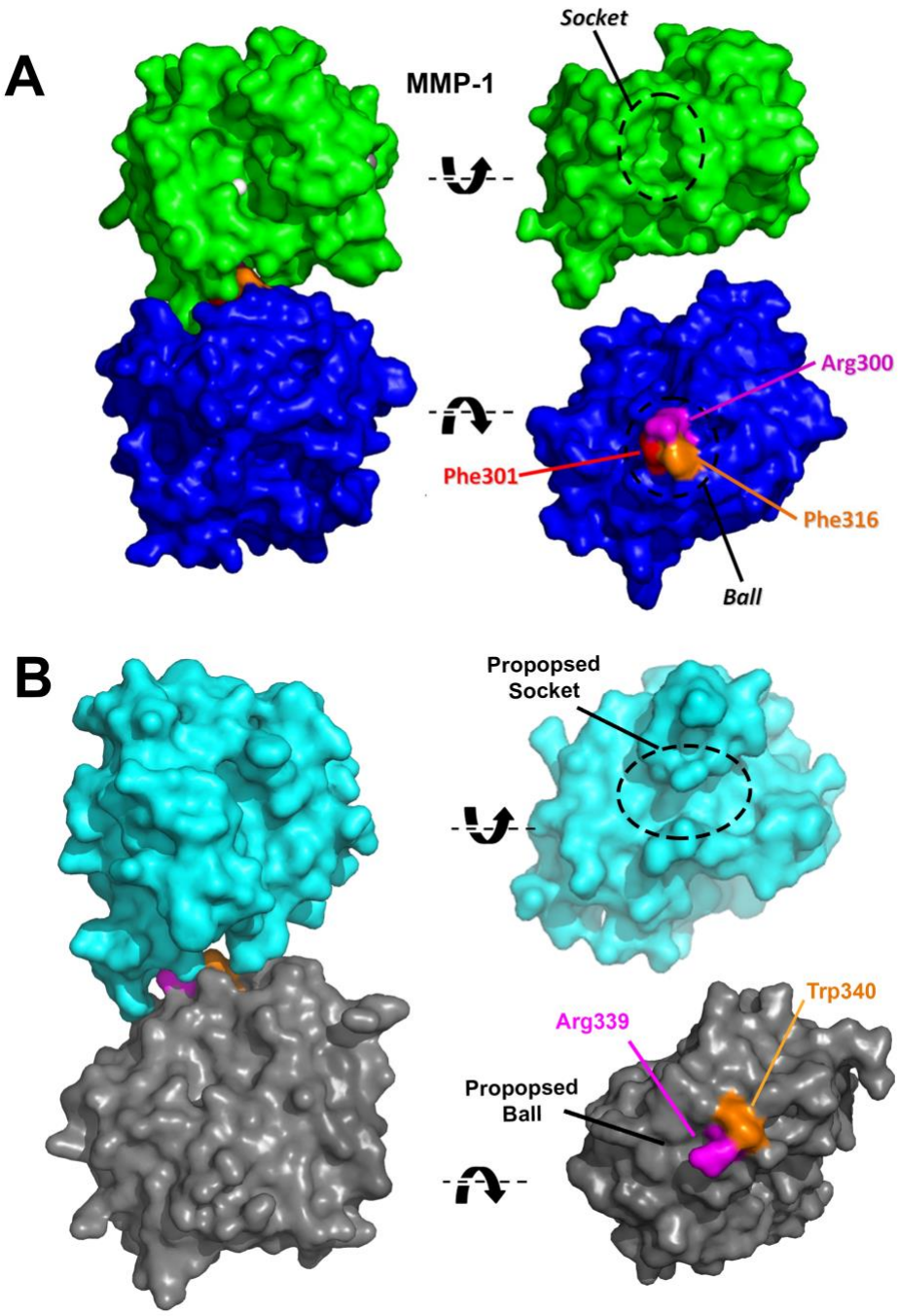
A
MMP-1
Socket
Arg300
Phe301
Phe316
Ball
B
Propopsed
Socket
Trp340
Arg339
Propopsed
Ball

Figure IV.4 Proposed functional orientations of both MT1-MMPsoluble domains in relation to the membrane.

(A,B) Proposed binding orientation of the catalytic (cartoon) and HPX (grey surface) domains without (A) and with (B) TIMP-2 (yellow) bound according to the crystal structure (1BQQ)(28). Both of these structures were overlaid with the blade IV of the HPX domain bound to the nanodisc. This shows TIMP clashing with the membrane surface (B). (C,D) Same proposed compact orientation without (C) and with (D) TIMP. However, the blade II side is bound to the nanodiscs in the structural overlay. There is no clash of TIMP with the membrane surface in this orientation (D).

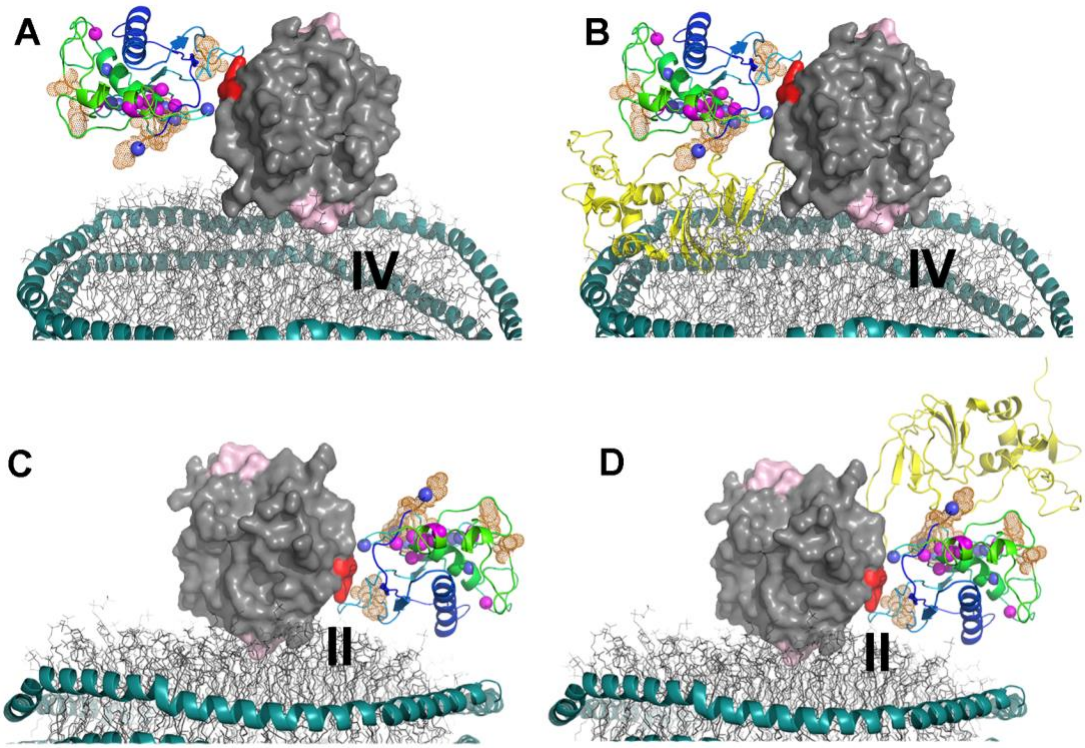

Figure IV.5 Bacterial induced NMR peak broadenings of the full length MMP-12.

(A) Relative peak intensities upon addition of 10,000 *E. coli* cells with MMP-12. Peak heights reduced by 20% or more are considered significant. Those in the HPX domain region colored in purple. (B) Peak heights of significance in the HPX domain plotted on the crystal structure as purple spheres. Thanks to Rama Koppisetti for expression and purification of the full length MMP-12 along with collecting the NMR data.

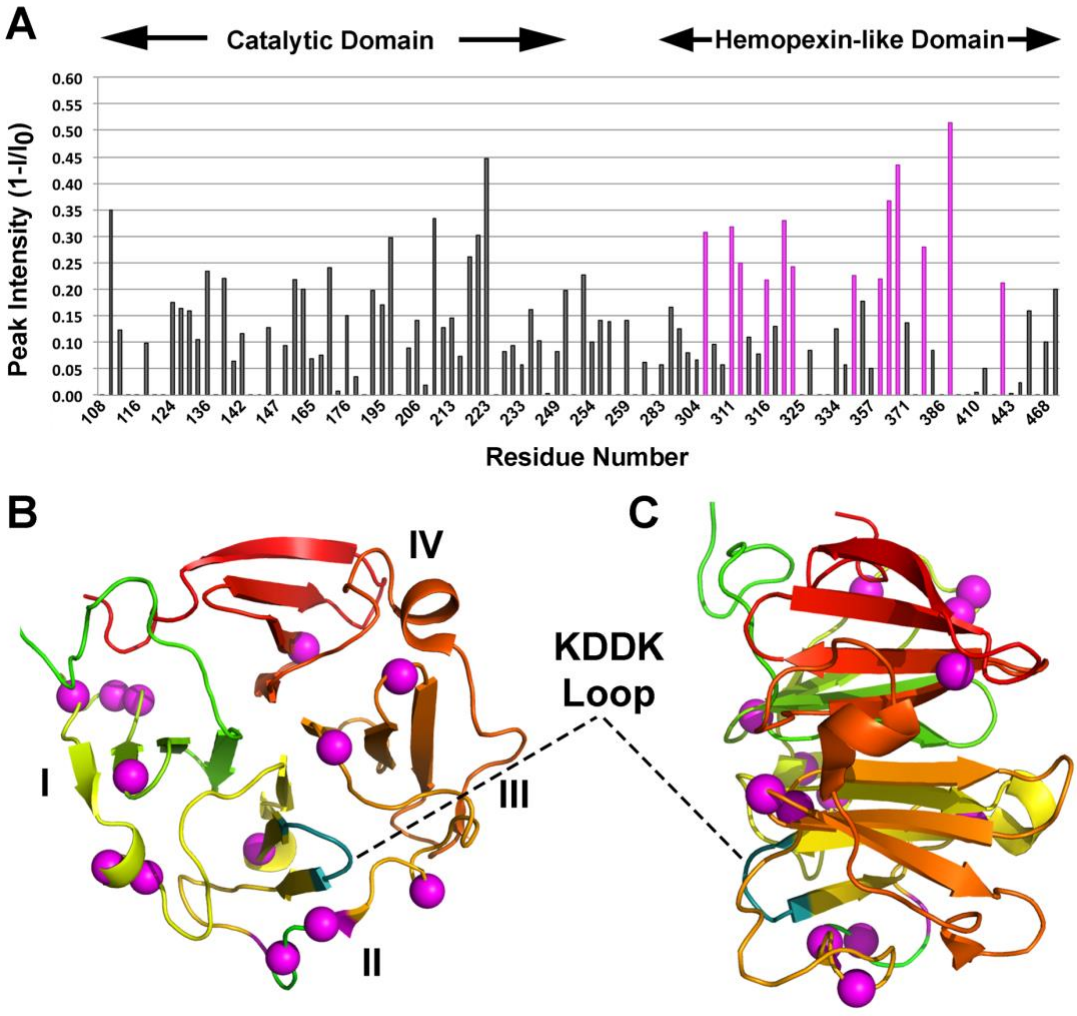

Figure IV.6 Overlay of both the bilayer-binding and antimicrobial loops of MT1-MMP and MMP-12.

(A) MT1-MMP bound to nanodiscs with the membrane binding loop shown in purple (PDB ID 6CM1). The peptide sequence corresponding to the antimicrobial peptide fragment from MMP-12 is colored teal with the antimicrobial loop at the magenta surface. (B,C) Overlay of MMP-12 with the experimental model of the MT1-MMP HPX domain bound to a DMPC bilayer by blade II. The magenta surface suggests the proximity of the KDDK loop to the membrane.

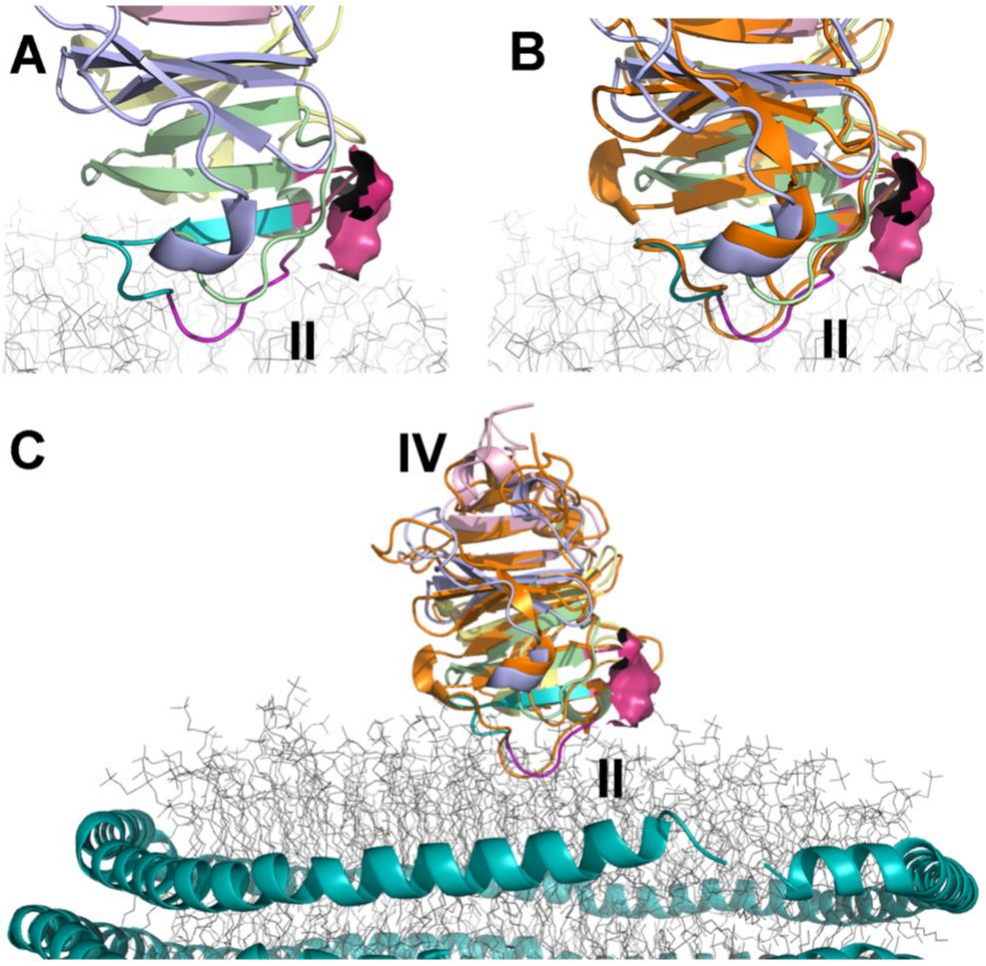

IV.6 REFERENCES

1. Gross, J., and Lapiere, C. M. (1962) COLLAGENOLYTIC ACTIVITY IN AMPHIBIAN TISSUES: A TISSUE CULTURE ASSAY. *Proceedings of the National Academy of Sciences of the United States of America* **48**, 1014-1022

2. Rao, B. G. (2005) Recent developments in the design of specific Matrix Metalloproteinase inhibitors aided by structural and computational studies. *Curr Pharm Des* **11**, 295-322

3. Pardo, A., and Selman, M. (2005) MMP-1: the elder of the family. *Int J Biochem Cell Biol* **37**, 283-288

4. Bertini, I., Fragai, M., Luchinat, C., Melikian, M., Mylonas, E., Sarti, N., and Svergun, D. I. (2009) Interdomain flexibility in full-length matrix metalloproteinase-1 (MMP-1). *J Biol Chem* **284**, 12821-12828

5. Manka, S. W., Carafoli, F., Visse, R., Bihan, D., Raynal, N., Farndale, R. W., Murphy, G., Enghild, J. J., Hohenester, E., and Nagase, H. (2012) Structural insights into triple-helical collagen cleavage by matrix metalloproteinase 1. *Proc. Natl. Acad. Sci. U. S. A.*

6. Lauer-Fields, J. L., Chalmers, M. J., Busby, S. A., Minond, D., Griffin, P. R., and Fields, G. B. (2009) Identification of specific hemopexin-like domain residues that facilitate matrix metalloproteinase collagenolytic activity. *J Biol Chem* **284**, 24017-24024

7. Iyer, S., Visse, R., Nagase, H., and Acharya, K. R. (2006) Crystal structure of an active form of human MMP-1. *J Mol Biol* **362**, 78-88

8. Arnold, L. H., Butt, L. E., Prior, S. H., Read, C. M., Fields, G. B., and Pickford, A. R. (2011) The Interface between Catalytic and Hemopexin Domains in Matrix Metalloproteinase-1 Conceals a Collagen Binding Exosite. *J. Biol. Chem.* **286**, 45073-45082

9. Cerofolini, L., Fields, G. B., Fragai, M., Geraldes, C. F., Luchinat, C., Parigi, G., Ravera, E., Svergun, D. I., and Teixeira, J. M. (2013) Examination of matrix

metalloproteinase-1 in solution: a preference for the pre-collagenolysis state. *J Biol Chem* **288**, 30659-30671

10. Zhao, Y., Marcink, T. C., Sanganna Gari, R. R., Marsh, B. P., King, G. M., Stawikowska, R., Fields, G. B., and Van Doren, S. R. (2015) Transient collagen triple helix binding to a key metalloproteinase in invasion and development. *Structure* **23**, 257-269

11. Marcink, T. C., Simoncic, J. A., An, B., Knapinska, A. M., Fields, G. B., and Van Doren, S. R. (2018) MT1-MMP Binds Membranes by Opposite Tips of its β-Propeller to Position it for Pericellular Proteolysis. *In Submission*

12. Van Doren, S. R., Marcink, T. C., Koppisetti, R. K., Jurkevich, A., and Fulcher, Y. G. (2017) Peripheral membrane associations of matrix metalloproteinases. *Biochim Biophys Acta*

13. Hurst, D. R., Schwartz, M. A., Jin, Y., Ghaffari, M. A., Kozarekar, P., Cao, J., and Sang, Q. X. (2005) Inhibition of enzyme activity of and cell-mediated substrate cleavage by membrane type 1 matrix metalloproteinase by newly developed mercaptosulphide inhibitors. *Biochem J* **392**, 527-536

14. Shapiro, S. D., and Hartzell, W. O. (2003) Matrix metalloproteinase-12 from human and mouse and their antimicrobial C-terminal peptides, and related methods and compositions for preventing and treating microbial infections. (The Brigham and Women's Hospital, Inc., USA). Application: WO

    WO

15. Koppisetti, R. K., Fulcher, Y. G., Jurkevich, A., Prior, S. H., Xu, J., Lenoir, M., Overduin, M., and Van Doren, S. R. (2014) Ambidextrous binding of cell and membrane bilayers by soluble matrix metalloproteinase-12. *Nat Commun* **5**, 5552

16. Houghton, A. M., Hartzell, W. O., Robbins, C. S., Gomis-Ruth, F. X., and Shapiro, S. D. (2009) Macrophage elastase kills bacteria within murine macrophages. *Nature* **460**, 637-641

17. Talmi-Frank, D., Altboum, Z., Solomonov, I., Udi, Y., Jaitin, D. A., Klepfish, M., David, E., Zhuravlev, A., Keren-Shaul, H., Winter, D. R., Gat-Viks, I., Mandelboim,

M., Ziv, T., Amit, I., and Sagi, I. (2016) Extracellular Matrix Proteolysis by MT1-MMP Contributes to Influenza-Related Tissue Damage and Mortality. *Cell Host Microbe* **20**, 458-470

18. Bertini, I., Calderone, V., Fragai, M., Jaiswal, R., Luchinat, C., Melikian, M., Mylonas, E., and Svergun, D. I. (2008) Evidence of reciprocal reorientation of the catalytic and hemopexin-like domains of full-length MMP-12. *J Am Chem Soc* **130**, 7011-7021

19. Deryugina, E. I., and Quigley, J. P. (2011) The Role of Matrix Metalloproteinases in Cellular Invasion and Metastasis. in *Extracellular Matrix Degradation* (Parks, W. C., and Mecham, R. P. eds.), Springer-Verlag, Berlin. pp 145-191

20. Turunen, S. P., Tatti-Bugaeva, O., and Lehti, K. (2017) Membrane-type matrix metalloproteases as diverse effectors of cancer progression. *Biochimica et Biophysica Acta (BBA) - Molecular Cell Research* **1864**, 1974-1988

21. Bhaskaran, R., Palmier, M. O., Lauer-Fields, J. L., Fields, G. B., and Van Doren, S. R. (2008) MMP-12 Catalytic Domain Recognizes Triple Helical Peptide Models of Collagen V with Exosites and High Activity. *J Biol Chem* **283**, 21779-21788

22. Bertini, I., Fragai, M., Luchinat, C., Melikian, M., Toccafondi, M., Lauer, J. L., and Fields, G. B. (2012) Structural Basis for Matrix Metalloproteinase 1-Catalyzed Collagenolysis. *Journal of the American Chemical Society* **134**, 2100-2110

23. Rapti, M., Knauper, V., Murphy, G., and Williamson, R. A. (2006) Characterization of the AB loop region of TIMP-2. Involvement in pro-MMP-2 activation. *J Biol Chem* **281**, 23386-23394

24. Overall, C. M., Tam, E., McQuibban, G. A., Morrison, C., Wallon, U. M., Bigg, H. F., King, A. E., and Roberts, C. R. (2000) Domain interactions in the gelatinase A.TIMP-2.MT1-MMP activation complex. The ectodomain of the 44-kDa form of membrane type-1 matrix metalloproteinase does not modulate gelatinase A activation. *J Biol Chem* **275**, 39497-39506

25. Jo, M., Thomas, L. E., Wheeler, S. E., and Curry, T. E., Jr. (2004) Membrane type 1-matrix metalloproteinase (MMP)-associated MMP-2 activation increases in the rat ovary in response to an ovulatory dose of human chorionic gonadotropin. *Biol Reprod* **70**, 1024-1032

26. Epand, R. F., Epand, R. M., Monaco, V., Stoia, S., Formaggio, F., Crisma, M., and Toniolo, C. (1999) The antimicrobial peptide trichogin and its interaction with phospholipid membranes. *Eur J Biochem* **266**, 1021-1028

27. Nguyen, L., and Vogel, H. (2012) Structural perspectives on antimicrobial chemokines. *Frontiers in Immunology* **3**

28. Fernandez-Catalan, C., Bode, W., Huber, R., Turk, D., Calvete, J. J., Lichte, A., Tschesche, H., and Maskos, K. (1998) Crystal structure of the complex formed by the membrane type 1-matrix metalloproteinase with the tissue inhibitor of metalloproteinases-2, the soluble progelatinase A receptor. *Embo J* **17**, 5238-5248.

V. APPENDIX 1: Molecular Dynamics Protocol for Membrane Binding

A.1 INTRODUCTION

Peripheral protein-membrane structural simulations have been developed recently including discussions in this work (1-3). My purpose in using molecular dynamics simulations was to test the cellular feasibility of an interaction between a protein and its partner and gain structural insights of this interaction. There is currently no established method for executing molecular dynamics simulations of peripheral protein interactions with membranes.

Presented here is a strategy that relies upon distance restraints based upon PREs measured by NMR of spin-labeled assemblies of nanodiscs with a peripherally bound protein. Initial docking is performed with the HADDOCK program designed for rigid body docking of proteins, originally with other proteins or nuclei acids (4,5). However, HADDOCK rigid body docking does not have an adequate force field for understanding molecular interactions. In fact, steric clashes can remain in its structural results. In order to obtain a highly refined structural model, the strategy proceeds to novel incorporation of PRE-based distance restraints on the subsequent refinement step using molecular dynamics

with an atomistic model of a nanodisc. After initial docking with HADDOCK (1,2), one can transpose their findings into molecular dynamics through NAMD (6) using the CHARMM36 force field (7,8). This full atomistic force field can help refine the structural rigid body docking presenting a more accurate representation of the peripheral proteins interaction with the membrane surface. Through the use of these new developments, one can now undertake peripheral membrane simulations with more ease of use. Presented here is a protocol for successfully running such a molecular dynamics simulation using NAMD. It is outlined in Figure 1.

A.2 METHODS

A2.1 Detailed Outline of steps for obtaining lowest energy structures of peripheral membrane proteins

1. Setup for HADDOCK using NMR restraints (see Figure 2)
    a. PREs are set as restraints to resname SPIN lipids
        i. All distances based on PREs or other distance measurements (NOEs, line broadenings, etc.) are restrained to the appropriate lipid carbon.
        ii. For PREs, the Γ_2 values are used to estimate the distance from the spin label to the residue of interest by the following equation: $\Gamma_2 = 4\kappa\tau_c / r^6$ where κ =1.23e-44 $m^6 s^{-2}$ and τ_c is the

rotational correlation time determined from an amide ^{15}N NMR transverse cross-correlation rate experiment (8,9).

iii. For PREs, raise the upper bound to at 10% greater than the estimated distance, plus an estimated fluctuation of the relevant depth of the spin label and ambiguity in proS vs proR methyl groups. (2.9 Å)

b. CSPs and line broadenings are set up as ambiguous restraints per HADDOCK guidelines.

c. 6 Å Repulsive restraints are added to the lower leaflet distal to the cage.

d. 10 Å repulsive restraints were added to the edges of the membrane cage. These restrict the protein to the middle within the cage on the correct side of the membrane.

e. Edit the CNS file using www.bonvinlab.org/software/haddock2.2/haddock-start

i. Replace topology, linkage, and energy parameter files with those files at the end of this chapter

ii. Calculate at least 300 structures

2. Analysis of HADDOCK structures after simulations

a. Structures are analyzed for violations of distance restraints via PyMOL

b. All structures with no violations were aligned and hand selected for further analysis

Note that variations in the angle of insertion into the bilayer in the structural models are expected since MD will allow for variations

3. Uses of the CHARMM-GUI software
    a. Generate empty nanodiscs via the CHARMM-GUI Membrane Builder
    b. Align the lipids of the empty nanodisc with the lipids of the HADDOCK-derived structural model of the assembly
    c. Input final protein and membrane assembly PDB in the CHARMM-GUI Quick MD Simulator
    d. Output files for NAMD with Charmm36 force field
4. Molecular dynamics in NAMD
    a. NAMD restraint parameter setup
        i. Colvar restraints set up as xy-distance plane restraints
            1. Distance restraint values are the same as used in HADDOCK
            2. Identify peripheral lipid atoms around the nanodiscs at the same depth used in HADDOCK. Through this process of using multiple lipids around the periphery, an XY plane will be created for which the restraints are tethered to.
        ii. harmonic force restraints
            1. Force constant for unambiguous restraints = 1.0

2. Force constant for ambiguous restraints = 0.1

b. NAMD run (see Figure 3)

i. Minimize the HADDOCK-docked models using at least 10,000 steps. In the case of hand-docked starting structures, use 100,000 steps of minimization.

ii. Equilibration until misc (restraint) energies level out. Misc energies will jump up significantly now that minimization has completed, and restraints are introduced. Use at least 2 ns for HADDOCK docked structures and 4 ns for hand-docked structures

iii. Restrained refinement (production) run with a minimum of 4 ns

iv. Unrestrained production run for a similar length as the restrained portion of the simulation

5. Final Structure Analysis

a. Quality checks via the VMD suite

i. RMSD

ii. Lowest energy structures determined through log files and misc (restraint) energies.

iii. Alignment of structures by the membrane

A.3 FIGURES

Figure A.1 Flowchart from HADDOCK to NAMD

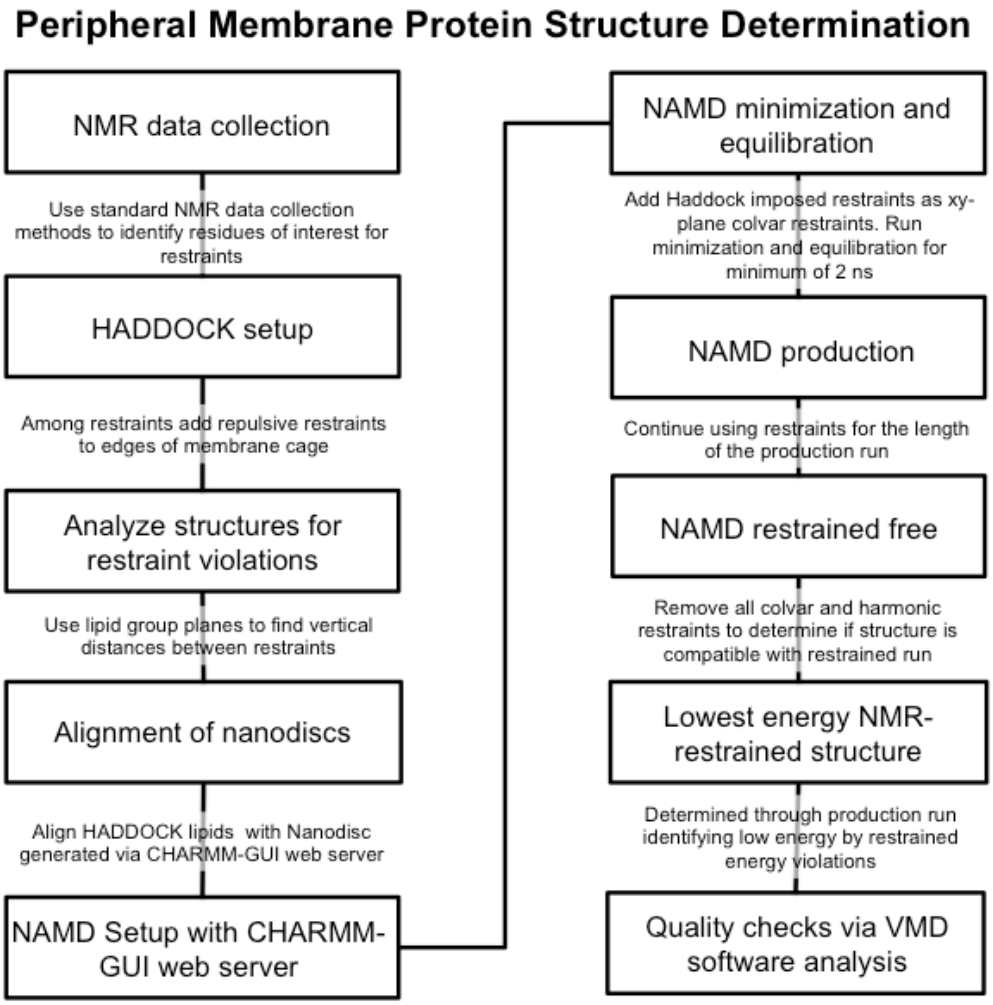

Figure A.2 HADDOCK Peripheral Protein Set-up

(A) Lipid membrane cage (LMC) that confines protein of interest within the boundaries. (B) Overview of the LMC. (C) HPX of MT1-MMP after HADDOCK calculations docked with LMC. (D) Close-up view of the HPX domain of MT1-MMP showing insertion depth of protein

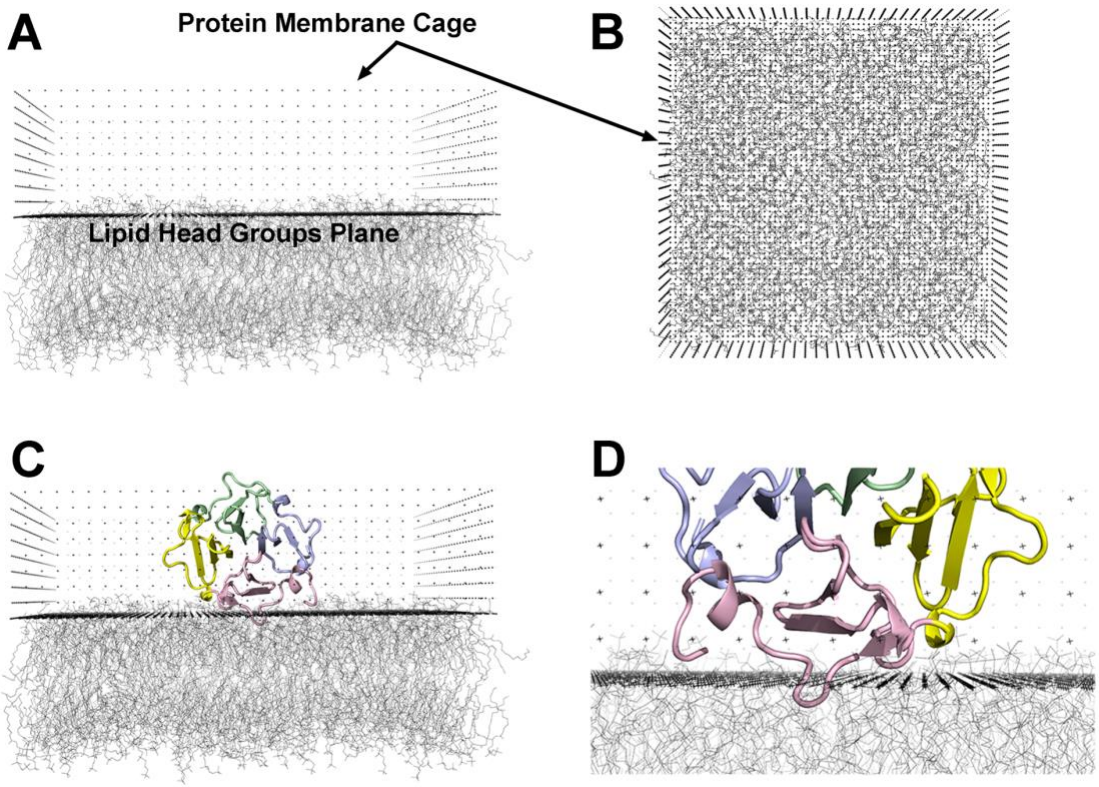

Figure A.3 NAMD Setup and Execution

(A) Cut away view of a box of water and ion molecules surrounding the MT1-MMP HPX domain peripherally bound to a nanodisc. (B) Steps involved in a NAMD production run. The assembly is prepared for MD by minimization for ≥ 2 ps, followed by ≥ 2 ns of equilibration where restrained are turned on. Next there is a section of NMR-based restraints used during the production run. Finally, a production run without NMR restraints is used to determine whether or not the structural model persists without the restraints.

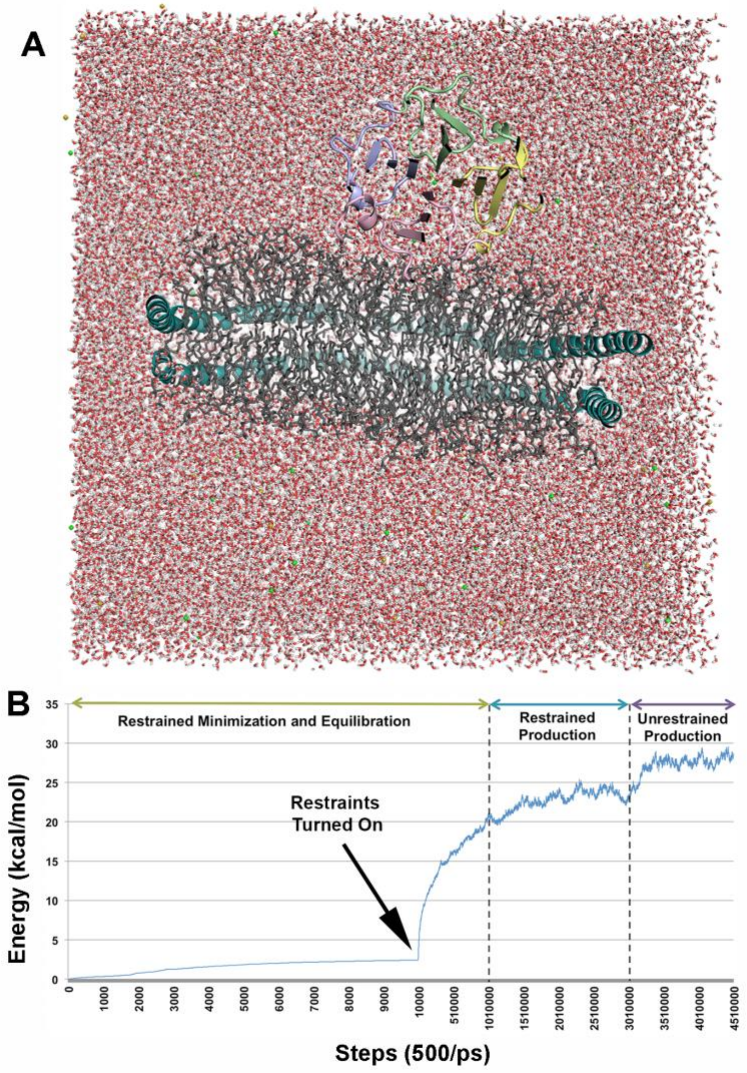

A.4 REFERENCES

1. Prior, S. H., Fulcher, Y. G., Koppisetti, R. K., Jurkevich, A., and Van Doren, S. R. (2015) Charge-Triggered Membrane Insertion of Matrix Metalloproteinase-7, Supporter of Innate Immunity and Tumors. *Structure* **23**, 2099-2110

2. Koppisetti, R. K., Fulcher, Y. G., Jurkevich, A., Prior, S. H., Xu, J., Lenoir, M., Overduin, M., and Van Doren, S. R. (2014) Ambidextrous binding of cell and membrane bilayers by soluble matrix metalloproteinase-12. *Nat Commun* **5**, 5552

3. Mazhab-Jafari, M. T., Marshall, C. B., Smith, M. J., Gasmi-Seabrook, G. M., Stathopulos, P. B., Inagaki, F., Kay, L. E., Neel, B. G., and Ikura, M. (2015) Oncogenic and RASopathy-associated K-RAS mutations relieve membrane-dependent occlusion of the effector-binding site. *Proc Natl Acad Sci U S A* **112**, 6625-6630

4. de Vries, S. J., van Dijk, A. D., Krzeminski, M., van Dijk, M., Thureau, A., Hsu, V., Wassenaar, T., and Bonvin, A. M. (2007) HADDOCK versus HADDOCK: new features and performance of HADDOCK2.0 on the CAPRI targets. *Proteins* **69**, 726-733

5. Dominguez, C., Boelens, R., and Bonvin, A. M. (2003) HADDOCK: a protein-protein docking approach based on biochemical or biophysical information. *J Am Chem Soc* **125**, 1731-1737

6. Phillips, J. C., Braun, R., Wang, W., Gumbart, J., Tajkhorshid, E., Villa, E., Chipot, C., Skeel, R. D., Kale, L., and Schulten, K. (2005) Scalable molecular dynamics with NAMD. *J Comput Chem* **26**, 1781-1802

7. Huang, J., and MacKerell, A. D., Jr. (2013) CHARMM36 all-atom additive protein force field: validation based on comparison to NMR data.

8. Lee, S., Tran, A., Allsopp, M., Lim, J. B., Hénin, J., and Klauda, J. B. (2014) CHARMM36 United Atom Chain Model for Lipids and Surfactants. *The Journal of Physical Chemistry B* **118**, 547-556

9. Lee, D., Hilty, C., Wider, G., and Wuthrich, K. (2006) Effective rotational correlation times of proteins from NMR relaxation interference. *J Magn Reson* **178**, 72-76

10. Liu, Y., and Prestegard, J. H. (2008) Direct measurement of dipole-dipole/CSA cross-correlated relaxation by a constant-time experiment. *J Magn Reson* **193**, 23-31

A1.5 PARAMETER FILES FOR HADDOCK

File 1: Lipid Linkage File

```
!Linker file for DMPC+SPIN
!filename=SPIN.linker

REMARKS  dpc.cns.linker - macro for linking dpc molecules
SET ECHO=FALSE END

! link  DL2  head - *   tail + CEN end
! link  DL1  head - *   tail + *   end

! evaluate ($counter=1)
! evaluate ($dpcm=54)
! while ( $counter <= $dpcm ) loop dpcm
!  patch DPCL
!    reference=1=(segid B and resid $counter)
!    reference=2=(segid B and resid $dpcm+1)
!  end
!  evaluate ($counter=$counter+1)
! end loop dpcm

SET ECHO=TRUE END
```

File 2: Lipid Energy Parameter File

```
!Parameter file for DMPC
!filename=SPIN.param
!
  BOND CH3p NL   899.7   1.470
  BOND CH3p NL   899.7   1.470
  BOND CH3p NL   899.7   1.470
  BOND NL   CH2  899.7   1.470
  BOND CH2  CH2  800.0   1.530
  BOND CH2  OA   799.6   1.430
  BOND OA   P,SI 599.7   1.610
  BOND P,SI OM   900.4   1.480
  BOND P,SI OM   900.4   1.480
  BOND P,SI OA   599.7   1.610
  BOND OA   CH2  799.6   1.430
  BOND CH2  CH1  800.0   1.530
  BOND CH1  OE   799.6   1.430
  BOND CH1  CH2  800.0   1.530
  BOND OE   C    997.7   1.330
  BOND C    O    1200.5  1.230
  BOND C    CH2  799.9   1.480
  BOND CH2  CH2  800.0   1.530
  BOND CH2  CH2  800.0   1.530
  BOND CH2  CH2  800.0   1.530
  BOND CH2  CH2  800.0   1.530
  BOND CH2  CH2  800.0   1.530
  BOND CH2  CH2  800.0   1.530
  BOND CH2  CH2  800.0   1.530
  BOND CH2  CH2  800.0   1.530
  BOND CH2  CH2  800.0   1.530
  BOND CH2  CH2  800.0   1.530
  BOND CH2  CH2  800.0   1.530
  BOND CH2  CH3  800.0   1.530
  BOND CH2  OE   799.6   1.430
  BOND OE   C    997.7   1.330
  BOND C    O    1200.5  1.230
  BOND C    CH2  799.9   1.480
  BOND CH2  CH2  800.0   1.530
  BOND CH2  CH2  800.0   1.530
  BOND CH2  CH2  800.0   1.530
  BOND CH2  CH2  800.0   1.530
  BOND CH2  CH2  800.0   1.530
  BOND CH2  CH2  800.0   1.530
  BOND CH2  CH2  800.0   1.530
  BOND CH2  CH2  800.0   1.530
  BOND CH2  CH2  800.0   1.530
  BOND CH2  CH2  800.0   1.530
  BOND CH2  CH2  800.0   1.530
  BOND CH2  CH2  800.0   1.530
  BOND CH2  CH3  800.0   1.530
  BOND CH3  DUM    0.0   1.530
  BOND DUM  DUM    0.0   1.530

  ANGLe CH3p NL   CH3p 124.3   109.5
```

```
ANGLe CH3p NL   CH3p 124.3   109.5
ANGLe CH3p NL   CH2  124.3   109.5
ANGLe CH3p NL   CH3p 124.3   109.5
ANGLe CH3p NL   CH2  124.3   109.5
ANGLe CH3p NL   CH2  124.3   109.5
ANGLe NL   CH2  CH2  126.7   111.0
ANGLe CH2  CH2  OA   126.7   111.0
ANGLe CH2  OA   P,SI 126.7   120.0
ANGLe OA   P,SI OM   107.6   109.6
ANGLe OA   P,SI OM   107.6   109.6
ANGLe OA   P,SI OA   100.4   103.0
ANGLe P,SI OA   CH2  126.7   120.0
ANGLe OM   P,SI OM   186.4   120.0
ANGLe OM   P,SI OA   107.6   109.6
ANGLe OM   P,SI OA   107.6   109.6
ANGLe OA   CH2  CH1  126.7   111.0
ANGLe CH2  CH1  OE   124.3   109.5
ANGLe CH2  CH1  CH2  124.3   109.5
ANGLe CH1  OE   C    151.8   117.0
ANGLe CH1  CH2  OE   126.7   111.0
ANGLe OE   CH1  CH2  124.3   109.5
ANGLe OE   C    O    167.3   122.0
ANGLe OE   C    CH2  130.3   113.0
ANGLe C    CH2  CH2  126.7   111.0
ANGLe O    C    CH2  179.3   125.0
ANGLe CH2  CH2  CH2  126.7   111.0
ANGLe CH2  CH2  CH2  126.7   111.0
ANGLe CH2  CH2  CH2  126.7   111.0
ANGLe CH2  CH2  CH2  126.7   111.0
ANGLe CH2  CH2  CH2  126.7   111.0
ANGLe CH2  CH2  CH2  126.7   111.0
ANGLe CH2  CH2  CH2  126.7   111.0
ANGLe CH2  CH2  CH2  126.7   111.0
ANGLe CH2  CH2  CH2  126.7   111.0
ANGLe CH2  CH2  CH3  126.7   111.0
ANGLe CH2  OE   C    151.8   117.0
ANGLe OE   C    O    167.3   122.0
ANGLe OE   C    CH2  130.3   113.0
ANGLe C    CH2  CH2  126.7   111.0
ANGLe O    C    CH2  179.3   125.0
ANGLe CH2  CH2  CH2  126.7   111.0
ANGLe CH2  CH2  CH2  126.7   111.0
ANGLe CH2  CH2  CH2  126.7   111.0
ANGLe CH2  CH2  CH2  126.7   111.0
ANGLe CH2  CH2  CH2  126.7   111.0
ANGLe CH2  CH2  CH2  126.7   111.0
ANGLe CH2  CH2  CH2  126.7   111.0
ANGLe CH2  CH2  CH2  126.7   111.0
ANGLe CH2  CH2  CH2  126.7   111.0
ANGLe CH2  CH2  CH2  126.7   111.0
ANGLe CH2  CH2  CH3  126.7   111.0
ANGLe CH2  CH3  DUM    0.0   111.0
ANGLe CH3  DUM  DUM    0.0   111.0
ANGLe DUM  DUM  DUM    0.0   111.0
```

```
DIHEdral CH3p NL   CH2  CH2  0.9    1  43.4
DIHEdral NL   CH2  CH2  OA   1.4    1  61.6
DIHEdral NL   CH2  CH2  OA   2.1    1  61.6
DIHEdral CH2  CH2  OA   P,SI 0.9    1  173.6
DIHEdral CH2  OA   P,SI OA   1.2    1  162.1
DIHEdral CH2  OA   P,SI OA   0.8    1  162.1
DIHEdral OA   P,SI OA   CH2  1.2    1  60.8
DIHEdral OA   P,SI OA   CH2  0.8    1  60.8
DIHEdral P,SI OA   CH2  CH1  0.9    1  168.7
DIHEdral OA   CH2  CH1  CH2  1.4    1  75.2
DIHEdral CH2  CH1  OE   C    0.9    1  143.8
DIHEdral CH2  CH1  CH2  OE   1.4    1  54.3
DIHEdral CH1  OE   C    CH2  5.7    1  156.7
DIHEdral CH1  CH2  OE   C    0.9    1  112.9
DIHEdral OE   C    CH2  CH2  0.2    1  141.9
DIHEdral C    CH2  CH2  CH2  1.4    1  177.9
DIHEdral CH2  CH2  CH2  CH2  1.4    1  145.7
DIHEdral CH2  CH2  CH2  CH2  1.4    1  16.7
DIHEdral CH2  CH2  CH2  CH2  1.4    1  176.4
DIHEdral CH2  CH2  CH2  CH2  1.4    1  66.8
DIHEdral CH2  CH2  CH2  CH2  1.4    1  153.8
DIHEdral CH2  CH2  CH2  CH2  1.4    1  156.5
DIHEdral CH2  CH2  CH2  CH2  1.4    1  140.9
DIHEdral CH2  CH2  CH2  CH2  1.4    1  164.0
DIHEdral CH2  CH2  CH2  CH2  1.4    1  162.6
DIHEdral CH2  CH2  CH2  CH3  1.4    1  165.6
DIHEdral CH2  OE   C    CH2  5.7    1  178.2
DIHEdral OE   C    CH2  CH2  0.2    1  178.0
DIHEdral C    CH2  CH2  CH2  1.4    1  72.1
DIHEdral CH2  CH2  CH2  CH2  1.4    1  82.0
DIHEdral CH2  CH2  CH2  CH2  1.4    1  142.5
DIHEdral CH2  CH2  CH2  CH2  1.4    1  83.9
DIHEdral CH2  CH2  CH2  CH2  1.4    1  90.9
DIHEdral CH2  CH2  CH2  CH2  1.4    1  96.0
DIHEdral CH2  CH2  CH2  CH2  1.4    1  144.5
DIHEdral CH2  CH2  CH2  CH2  1.4    1  162.2
DIHEdral CH2  CH2  CH2  CH2  1.4    1  120.5
DIHEdral CH2  CH2  CH2  CH2  1.4    1  177.1
DIHEdral CH2  CH2  CH2  CH3  1.4    1  174.2
!  DIHEdral CH2  CH2  CH3  DUM  1.4    1  174.2
!  DIHEdral CH2  CH3  DUM  DUM  1.4    1  174.2
!  DIHEdral CH3  DUM  DUM  DUM  1.4    1  174.2
!  DIHEdral DUM  DUM  DUM  DUM  1.4    1  174.2

IMPRoper CH1  OE   CH2  CH2  0.0    0  35.3
IMPRoper C    OE   O    CH2  0.0    0  0.0
IMPRoper C    OE   O    CH2  0.0    0  0.0

NONBONDED        C      0.06935        0.36     0.06935        0.36
NONBONDED        NL     0.1599  0.31   0.1599  0.31
NONBONDED        OE     0.2643  0.28   0.2643  0.28
NONBONDED        OM     0.4313  0.26   0.4313  0.26
NONBONDED        OA     0.2643  0.28   0.2643  0.28
NONBONDED        CH1    0.02372        0.5      0.02372        0.5
NONBONDED        CH2    0.1026  0.41   0.1026  0.41
NONBONDED        CH3    0.2168  0.37   0.2168  0.37
```

```
  NONBONDED        O       0.3198  0.28    0.3198  0.28
  NONBONDED        P,SI    0.6117  0.34    0.6117  0.34
  NONBONDED        CH3p    0.2168  0.37    0.2168  0.37
  NONBONDED        DUM     0.0000  0.00    0.0000  0.00

!SEGMent
!   name=DMPC
!   molecule number=1 name=DMPC end
!END
```

File 3: Lipid Topology File

```
!DMPC Topology File
!Filename=SPIN.top
!
! Parameters for DMPC (1,2-dimyristoyl-sn-glycero3-phosphocholine)
! To be used in conjunction with the GROMOS 54a7 forcefield files.
! Please cite the following references when using this topology:
! Poger D, van Gunsteren WF & Mark AE (2010) J. Comput. Chem. 31(6), 1117-1125
! Poger D & Mark AE (2010) J. Chem. Theory Comput. 6(1), 325-336
!           Topology file created by lipidATB at 23:48 on 2010-07-07
!
!TOPOLOGY
!     GROUP
  RESIdue SPIN
     ATOM CN1  TYPE=CH3p CHARge=0.400    MASS=15.0350  END
     ATOM CN3  TYPE=CH3p CHARge=0.400    MASS=15.0350  END
     ATOM CN2  TYPE=CH3p CHARge=0.400    MASS=15.0350  END
     ATOM NTM  TYPE=NL   CHARge=-0.500   MASS=14.0067  END
     ATOM CA   TYPE=CH2  CHARge=0.300    MASS=14.0270  END
     ATOM CB   TYPE=CH2  CHARge=0.400    MASS=14.0270  END
     ATOM OA   TYPE=OA   CHARge=-0.800   MASS=15.9994  END
     ATOM P    TYPE=P,SI CHARge=1.700    MASS=30.9738  END
     ATOM OC   TYPE=OM   CHARge=-0.800   MASS=15.9994  END
     ATOM OB   TYPE=OM   CHARge=-0.800   MASS=15.9994  END
     ATOM OD   TYPE=OA   CHARge=-0.700   MASS=15.9994  END
     ATOM CC   TYPE=CH2  CHARge=0.400    MASS=14.0270  END
     ATOM CD   TYPE=CH1  CHARge=0.300    MASS=13.0190  END
     ATOM OE   TYPE=OE   CHARge=-0.700   MASS=15.9994  END
     ATOM C1A  TYPE=C    CHARge=0.700    MASS=12.0110  END
     ATOM OF   TYPE=O    CHARge=-0.700   MASS=15.9994  END
     ATOM C1B  TYPE=CH2  CHARge=0.000    MASS=14.0270  END
     ATOM C1C  TYPE=CH2  CHARge=0.000    MASS=14.0270  END
     ATOM C1D  TYPE=CH2  CHARge=0.000    MASS=14.0270  END
     ATOM C1E  TYPE=CH2  CHARge=0.000    MASS=14.0270  END
     ATOM C1F  TYPE=CH2  CHARge=0.000    MASS=14.0270  END
     ATOM C1G  TYPE=CH2  CHARge=0.000    MASS=14.0270  END
     ATOM C1H  TYPE=CH2  CHARge=0.000    MASS=14.0270  END
     ATOM C1I  TYPE=CH2  CHARge=0.000    MASS=14.0270  END
     ATOM C1J  TYPE=CH2  CHARge=0.000    MASS=14.0270  END
     ATOM C1K  TYPE=CH2  CHARge=0.000    MASS=14.0270  END
     ATOM C1L  TYPE=CH2  CHARge=0.000    MASS=14.0270  END
     ATOM C1M  TYPE=CH2  CHARge=0.000    MASS=14.0270  END
     ATOM C1N  TYPE=CH3  CHARge=0.000    MASS=15.0350  END
     ATOM CE   TYPE=CH2  CHARge=0.500    MASS=14.0270  END
     ATOM OG   TYPE=OE   CHARge=-0.700   MASS=15.9994  END
     ATOM C2A  TYPE=C    CHARge=0.800    MASS=12.0110  END
     ATOM OH   TYPE=O    CHARge=-0.600   MASS=15.9994  END
     ATOM C2B  TYPE=CH2  CHARge=0.000    MASS=14.0270  END
     ATOM C2C  TYPE=CH2  CHARge=0.000    MASS=14.0270  END
     ATOM C2D  TYPE=CH2  CHARge=0.000    MASS=14.0270  END
     ATOM C2E  TYPE=CH2  CHARge=0.000    MASS=14.0270  END
     ATOM C2F  TYPE=CH2  CHARge=0.000    MASS=14.0270  END
     ATOM C2G  TYPE=CH2  CHARge=0.000    MASS=14.0270  END
```

```
ATOM C2H  TYPE=CH2  CHARge=0.000   MASS=14.0270  END
ATOM C2I  TYPE=CH2  CHARge=0.000   MASS=14.0270  END
ATOM C2J  TYPE=CH2  CHARge=0.000   MASS=14.0270  END
ATOM C2K  TYPE=CH2  CHARge=0.000   MASS=14.0270  END
ATOM C2L  TYPE=CH2  CHARge=0.000   MASS=14.0270  END
ATOM C2M  TYPE=CH2  CHARge=0.000   MASS=14.0270  END
ATOM C2N  TYPE=CH3  CHARge=0.000   MASS=15.0350  END
ATOM XAA  TYPE=DUM  CHARge=0.000   MASS=15.0350  END
ATOM XAB  TYPE=DUM  CHARge=0.000   MASS=15.0350  END
ATOM XAC  TYPE=DUM  CHARge=0.000   MASS=15.0350  END
ATOM XAD  TYPE=DUM  CHARge=0.000   MASS=15.0350  END
ATOM XBA  TYPE=DUM  CHARge=0.000   MASS=15.0350  END
ATOM XBB  TYPE=DUM  CHARge=0.000   MASS=15.0350  END
ATOM XBC  TYPE=DUM  CHARge=0.000   MASS=15.0350  END
ATOM XBD  TYPE=DUM  CHARge=0.000   MASS=15.0350  END
ATOM XCA  TYPE=DUM  CHARge=0.000   MASS=15.0350  END
ATOM XCB  TYPE=DUM  CHARge=0.000   MASS=15.0350  END
ATOM XCC  TYPE=DUM  CHARge=0.000   MASS=15.0350  END
ATOM XCD  TYPE=DUM  CHARge=0.000   MASS=15.0350  END
ATOM XDA  TYPE=DUM  CHARge=0.000   MASS=15.0350  END
ATOM XDB  TYPE=DUM  CHARge=0.000   MASS=15.0350  END
ATOM XDC  TYPE=DUM  CHARge=0.000   MASS=15.0350  END
ATOM XDD  TYPE=DUM  CHARge=0.000   MASS=15.0350  END
ATOM YAA  TYPE=DUM  CHARge=0.000   MASS=15.0350  END
ATOM YAB  TYPE=DUM  CHARge=0.000   MASS=15.0350  END
ATOM YAC  TYPE=DUM  CHARge=0.000   MASS=15.0350  END
ATOM YAD  TYPE=DUM  CHARge=0.000   MASS=15.0350  END
ATOM YBA  TYPE=DUM  CHARge=0.000   MASS=15.0350  END
ATOM YBB  TYPE=DUM  CHARge=0.000   MASS=15.0350  END
ATOM YBC  TYPE=DUM  CHARge=0.000   MASS=15.0350  END
ATOM YBD  TYPE=DUM  CHARge=0.000   MASS=15.0350  END
ATOM YCA  TYPE=DUM  CHARge=0.000   MASS=15.0350  END
ATOM YCB  TYPE=DUM  CHARge=0.000   MASS=15.0350  END
ATOM YCC  TYPE=DUM  CHARge=0.000   MASS=15.0350  END
ATOM YCD  TYPE=DUM  CHARge=0.000   MASS=15.0350  END
ATOM YDA  TYPE=DUM  CHARge=0.000   MASS=15.0350  END
ATOM YDB  TYPE=DUM  CHARge=0.000   MASS=15.0350  END
ATOM YDC  TYPE=DUM  CHARge=0.000   MASS=15.0350  END
ATOM YDD  TYPE=DUM  CHARge=0.000   MASS=15.0350  END
ATOM ZAA  TYPE=DUM  CHARge=0.000   MASS=15.0350  END
ATOM ZAB  TYPE=DUM  CHARge=0.000   MASS=15.0350  END
ATOM ZAC  TYPE=DUM  CHARge=0.000   MASS=15.0350  END
ATOM ZAD  TYPE=DUM  CHARge=0.000   MASS=15.0350  END
ATOM ZBA  TYPE=DUM  CHARge=0.000   MASS=15.0350  END
ATOM ZBB  TYPE=DUM  CHARge=0.000   MASS=15.0350  END
ATOM ZBC  TYPE=DUM  CHARge=0.000   MASS=15.0350  END
ATOM ZBD  TYPE=DUM  CHARge=0.000   MASS=15.0350  END
ATOM ZCA  TYPE=DUM  CHARge=0.000   MASS=15.0350  END
ATOM ZCB  TYPE=DUM  CHARge=0.000   MASS=15.0350  END
ATOM ZCC  TYPE=DUM  CHARge=0.000   MASS=15.0350  END
ATOM ZCD  TYPE=DUM  CHARge=0.000   MASS=15.0350  END
ATOM ZDA  TYPE=DUM  CHARge=0.000   MASS=15.0350  END
ATOM ZDB  TYPE=DUM  CHARge=0.000   MASS=15.0350  END
ATOM ZDC  TYPE=DUM  CHARge=0.000   MASS=15.0350  END
ATOM ZDD  TYPE=DUM  CHARge=0.000   MASS=15.0350  END
```

```
BOND CN1  NTM
BOND CN3  NTM
BOND CN2  NTM
BOND NTM  CA
BOND CA   CB
BOND CB   OA
BOND OA   P
BOND P    OC
BOND P    OB
BOND P    OD
BOND OD   CC
BOND CC   CD
BOND CD   OE
BOND CD   CE
BOND OE   C1A
BOND C1A  OF
BOND C1A  C1B
BOND C1B  C1C
BOND C1C  C1D
BOND C1D  C1E
BOND C1E  C1F
BOND C1F  C1G
BOND C1G  C1H
BOND C1H  C1I
BOND C1I  C1J
BOND C1J  C1K
BOND C1K  C1L
BOND C1L  C1M
BOND C1M  C1N
BOND CE   OG
BOND OG   C2A
BOND C2A  OH
BOND C2A  C2B
BOND C2B  C2C
BOND C2C  C2D
BOND C2D  C2E
BOND C2E  C2F
BOND C2F  C2G
BOND C2G  C2H
BOND C2H  C2I
BOND C2I  C2J
BOND C2J  C2K
BOND C2K  C2L
BOND C2L  C2M
BOND C2M  C2N
BOND C2N  XAA
BOND XAA  XAB
BOND XAB  XAC
BOND XAC  XAD
BOND XAD  XBA
BOND XBA  XBB
BOND XBB  XBC
BOND XBC  XBD
BOND XBD  XCA
BOND XCA  XCB
BOND XCB  XCC
```

```
BOND XCC  XCD
BOND XCD  XDA
BOND XDA  XDB
BOND XDB  XDC
BOND XDC  XDD
BOND XDD  YAA
BOND YAA  YAB
BOND YAB  YAC
BOND YAC  YAD
BOND YAD  YBA
BOND YBA  YBB
BOND YBB  YBC
BOND YBC  YBD
BOND YBD  YCA
BOND YCA  YCB
BOND YCB  YCC
BOND YCC  YCD
BOND YCD  YDA
BOND YDA  YDB
BOND YDB  YDC
BOND YDC  YDD
BOND YDD  ZAA
BOND ZAA  ZAB
BOND ZAB  ZAC
BOND ZAC  ZAD
BOND ZAD  ZBA
BOND ZBA  ZBB
BOND ZBB  ZBC
BOND ZBC  ZBD
BOND ZBD  ZCA
BOND ZCA  ZCB
BOND ZCB  ZCC
BOND ZCC  ZCD
BOND ZCD  ZDA
BOND ZDA  ZDB
BOND ZDB  ZDC
BOND ZDC  ZDD

ANGLe CN1  NTM  CN3
ANGLe CN1  NTM  CN2
ANGLe CN1  NTM  CA
ANGLe CN3  NTM  CN2
ANGLe CN3  NTM  CA
ANGLe CN2  NTM  CA
ANGLe NTM  CA   CB
ANGLe CA   CB   OA
ANGLe CB   OA   P
ANGLe OA   P    OC
ANGLe OA   P    OB
ANGLe OA   P    OD
ANGLe P    OD   CC
ANGLe OC   P    OB
ANGLe OC   P    OD
ANGLe OB   P    OD
ANGLe OD   CC   CD
ANGLe CC   CD   OE
```

ANGLe CC CD CE
ANGLe CD OE C1A
ANGLe CD CE OG
ANGLe OE CD CE
ANGLe OE C1A OF
ANGLe OE C1A C1B
ANGLe C1A C1B C1C
ANGLe OF C1A C1B
ANGLe C1B C1C C1D
ANGLe C1C C1D C1E
ANGLe C1D C1E C1F
ANGLe C1E C1F C1G
ANGLe C1F C1G C1H
ANGLe C1G C1H C1I
ANGLe C1H C1I C1J
ANGLe C1I C1J C1K
ANGLe C1J C1K C1L
ANGLe C1K C1L C1M
ANGLe C1L C1M C1N
ANGLe CE OG C2A
ANGLe OG C2A OH
ANGLe OG C2A C2B
ANGLe C2A C2B C2C
ANGLe OH C2A C2B
ANGLe C2B C2C C2D
ANGLe C2C C2D C2E
ANGLe C2D C2E C2F
ANGLe C2E C2F C2G
ANGLe C2F C2G C2H
ANGLe C2G C2H C2I
ANGLe C2H C2I C2J
ANGLe C2I C2J C2K
ANGLe C2J C2K C2L
ANGLe C2K C2L C2M
ANGLe C2L C2M C2N
ANGLE C2M C2N XAA
ANGLE C2N XAA XAB
ANGLE XAA XAB XAC
ANGLE XAB XAC XAD
ANGLE XAC XAD XBA
ANGLE XAH XBA XBB
ANGLE XBA XBB XBC
ANGLE XBB XBC XBD
ANGLE XBC XBD XCA
ANGLE XBH XCA XCB
ANGLE XCA XCB XCC
ANGLE XCB XCC XCD
ANGLE XCC XCD XDA
ANGLE XCH XDA XDB
ANGLE XDA XDB XDC
ANGLE XDB XDC XDD
ANGLE XDC XDD YAA
ANGLE XHH YAA YAB
ANGLE YAA YAB YAC
ANGLE YAB YAC YAD
ANGLE YAC YAD YBA

ANGLE YAH YBA YBB
ANGLE YBA YBB YBC
ANGLE YBB YBC YBD
ANGLE YBC YBD YCA
ANGLE YBH YCA YCB
ANGLE YCA YCB YCC
ANGLE YCB YCC YCD
ANGLE YCC YCD YDA
ANGLE YCH YDA YDB
ANGLE YDA YDB YDC
ANGLE YDB YDC YDD
ANGLE YDC YDD ZAA
ANGLE YHH ZAA ZAB
ANGLE ZAA ZAB ZAC
ANGLE ZAB ZAC ZAD
ANGLE ZAC ZAD ZBA
ANGLE ZAH ZBA ZBB
ANGLE ZBA ZBB ZBC
ANGLE ZBB ZBC ZBD
ANGLE ZBC ZBD ZCA
ANGLE ZBH ZCA ZCB
ANGLE ZCA ZCB ZCC
ANGLE ZCB ZCC ZCD
ANGLE ZCC ZCD ZDA
ANGLE ZCH ZDA ZDB
ANGLE ZDA ZDB ZDC
ANGLE ZDB ZDC ZDD

DIHEdral CN2 NTM CA CB
DIHEdral NTM CA CB OA
DIHEdral NTM CA CB OA
DIHEdral CA CB OA P
DIHEdral CB OA P OD
DIHEdral CB OA P OD
DIHEdral OA P OD CC
DIHEdral OA P OD CC
DIHEdral P OD CC CD
DIHEdral OD CC CD CE
DIHEdral CC CD OE C1A
DIHEdral CC CD CE OG
DIHEdral CD OE C1A C1B
DIHEdral CD CE OG C2A
DIHEdral OE C1A C1B C1C
DIHEdral C1A C1B C1C C1D
DIHEdral C1B C1C C1D C1E
DIHEdral C1C C1D C1E C1F
DIHEdral C1D C1E C1F C1G
DIHEdral C1E C1F C1G C1H
DIHEdral C1F C1G C1H C1I
DIHEdral C1G C1H C1I C1J
DIHEdral C1H C1I C1J C1K
DIHEdral C1I C1J C1K C1L
DIHEdral C1J C1K C1L C1M
DIHEdral C1K C1L C1M C1N
DIHEdral CE OG C2A C2B
DIHEdral OG C2A C2B C2C

```
  DIHEdral C2A  C2B  C2C  C2D
  DIHEdral C2B  C2C  C2D  C2E
  DIHEdral C2C  C2D  C2E  C2F
  DIHEdral C2D  C2E  C2F  C2G
  DIHEdral C2E  C2F  C2G  C2H
  DIHEdral C2F  C2G  C2H  C2I
  DIHEdral C2G  C2H  C2I  C2J
  DIHEdral C2H  C2I  C2J  C2K
  DIHEdral C2I  C2J  C2K  C2L
  DIHEdral C2J  C2K  C2L  C2M
  DIHEdral C2K  C2L  C2M  C2N

  IMPRoper CD   OE   CE   CC
  IMPRoper C1A  OE   OF   C1B
  IMPRoper C2A  OG   OH   C2B
END

RESIdue DMPC
  ATOM CN1  TYPE=CH3p CHARge=0.400    MASS=15.0350  END
  ATOM CN3  TYPE=CH3p CHARge=0.400    MASS=15.0350  END
  ATOM CN2  TYPE=CH3p CHARge=0.400    MASS=15.0350  END
  ATOM NTM  TYPE=NL   CHARge=-0.500   MASS=14.0067  END
  ATOM CA   TYPE=CH2  CHARge=0.300    MASS=14.0270  END
  ATOM CB   TYPE=CH2  CHARge=0.400    MASS=14.0270  END
  ATOM OA   TYPE=OA   CHARge=-0.800   MASS=15.9994  END
  ATOM P    TYPE=P,SI CHARge=1.700    MASS=30.9738  END
  ATOM OC   TYPE=OM   CHARge=-0.800   MASS=15.9994  END
  ATOM OB   TYPE=OM   CHARge=-0.800   MASS=15.9994  END
  ATOM OD   TYPE=OA   CHARge=-0.700   MASS=15.9994  END
  ATOM CC   TYPE=CH2  CHARge=0.400    MASS=14.0270  END
  ATOM CD   TYPE=CH1  CHARge=0.300    MASS=13.0190  END
  ATOM OE   TYPE=OE   CHARge=-0.700   MASS=15.9994  END
  ATOM C1A  TYPE=C    CHARge=0.700    MASS=12.0110  END
  ATOM OF   TYPE=O    CHARge=-0.700   MASS=15.9994  END
  ATOM C1B  TYPE=CH2  CHARge=0.000    MASS=14.0270  END
  ATOM C1C  TYPE=CH2  CHARge=0.000    MASS=14.0270  END
  ATOM C1D  TYPE=CH2  CHARge=0.000    MASS=14.0270  END
  ATOM C1E  TYPE=CH2  CHARge=0.000    MASS=14.0270  END
  ATOM C1F  TYPE=CH2  CHARge=0.000    MASS=14.0270  END
  ATOM C1G  TYPE=CH2  CHARge=0.000    MASS=14.0270  END
  ATOM C1H  TYPE=CH2  CHARge=0.000    MASS=14.0270  END
  ATOM C1I  TYPE=CH2  CHARge=0.000    MASS=14.0270  END
  ATOM C1J  TYPE=CH2  CHARge=0.000    MASS=14.0270  END
  ATOM C1K  TYPE=CH2  CHARge=0.000    MASS=14.0270  END
  ATOM C1L  TYPE=CH2  CHARge=0.000    MASS=14.0270  END
  ATOM C1M  TYPE=CH2  CHARge=0.000    MASS=14.0270  END
  ATOM C1N  TYPE=CH3  CHARge=0.000    MASS=15.0350  END
  ATOM CE   TYPE=CH2  CHARge=0.500    MASS=14.0270  END
  ATOM OG   TYPE=OE   CHARge=-0.700   MASS=15.9994  END
  ATOM C2A  TYPE=C    CHARge=0.800    MASS=12.0110  END
  ATOM OH   TYPE=O    CHARge=-0.600   MASS=15.9994  END
  ATOM C2B  TYPE=CH2  CHARge=0.000    MASS=14.0270  END
  ATOM C2C  TYPE=CH2  CHARge=0.000    MASS=14.0270  END
  ATOM C2D  TYPE=CH2  CHARge=0.000    MASS=14.0270  END
  ATOM C2E  TYPE=CH2  CHARge=0.000    MASS=14.0270  END
  ATOM C2F  TYPE=CH2  CHARge=0.000    MASS=14.0270  END
```

```
ATOM C2G  TYPE=CH2  CHARge=0.000    MASS=14.0270  END
ATOM C2H  TYPE=CH2  CHARge=0.000    MASS=14.0270  END
ATOM C2I  TYPE=CH2  CHARge=0.000    MASS=14.0270  END
ATOM C2J  TYPE=CH2  CHARge=0.000    MASS=14.0270  END
ATOM C2K  TYPE=CH2  CHARge=0.000    MASS=14.0270  END
ATOM C2L  TYPE=CH2  CHARge=0.000    MASS=14.0270  END
ATOM C2M  TYPE=CH2  CHARge=0.000    MASS=14.0270  END
ATOM C2N  TYPE=CH3  CHARge=0.000    MASS=15.0350  END

BOND CN1  NTM
BOND CN3  NTM
BOND CN2  NTM
BOND NTM  CA
BOND CA   CB
BOND CB   OA
BOND OA   P
BOND P    OC
BOND P    OB
BOND P    OD
BOND OD   CC
BOND CC   CD
BOND CD   OE
BOND CD   CE
BOND OE   C1A
BOND C1A  OF
BOND C1A  C1B
BOND C1B  C1C
BOND C1C  C1D
BOND C1D  C1E
BOND C1E  C1F
BOND C1F  C1G
BOND C1G  C1H
BOND C1H  C1I
BOND C1I  C1J
BOND C1J  C1K
BOND C1K  C1L
BOND C1L  C1M
BOND C1M  C1N
BOND CE   OG
BOND OG   C2A
BOND C2A  OH
BOND C2A  C2B
BOND C2B  C2C
BOND C2C  C2D
BOND C2D  C2E
BOND C2E  C2F
BOND C2F  C2G
BOND C2G  C2H
BOND C2H  C2I
BOND C2I  C2J
BOND C2J  C2K
BOND C2K  C2L
BOND C2L  C2M
BOND C2M  C2N

ANGLe CN1  NTM  CN3
```

ANGLe CN1 NTM CN2
ANGLe CN1 NTM CA
ANGLe CN3 NTM CN2
ANGLe CN3 NTM CA
ANGLe CN2 NTM CA
ANGLe NTM CA CB
ANGLe CA CB OA
ANGLe CB OA P
ANGLe OA P OC
ANGLe OA P OB
ANGLe OA P OD
ANGLe P OD CC
ANGLe OC P OB
ANGLe OC P OD
ANGLe OB P OD
ANGLe OD CC CD
ANGLe CC CD OE
ANGLe CC CD CE
ANGLe CD OE C1A
ANGLe CD CE OG
ANGLe OE CD CE
ANGLe OE C1A OF
ANGLe OE C1A C1B
ANGLe C1A C1B C1C
ANGLe OF C1A C1B
ANGLe C1B C1C C1D
ANGLe C1C C1D C1E
ANGLe C1D C1E C1F
ANGLe C1E C1F C1G
ANGLe C1F C1G C1H
ANGLe C1G C1H C1I
ANGLe C1H C1I C1J
ANGLe C1I C1J C1K
ANGLe C1J C1K C1L
ANGLe C1K C1L C1M
ANGLe C1L C1M C1N
ANGLe CE OG C2A
ANGLe OG C2A OH
ANGLe OG C2A C2B
ANGLe C2A C2B C2C
ANGLe OH C2A C2B
ANGLe C2B C2C C2D
ANGLe C2C C2D C2E
ANGLe C2D C2E C2F
ANGLe C2E C2F C2G
ANGLe C2F C2G C2H
ANGLe C2G C2H C2I
ANGLe C2H C2I C2J
ANGLe C2I C2J C2K
ANGLe C2J C2K C2L
ANGLe C2K C2L C2M
ANGLe C2L C2M C2N

DIHEdral CN2 NTM CA CB
DIHEdral NTM CA CB OA
DIHEdral NTM CA CB OA

```
  DIHEdral CA   CB   OA   P
  DIHEdral CB   OA   P    OD
  DIHEdral CB   OA   P    OD
  DIHEdral OA   P    OD   CC
  DIHEdral OA   P    OD   CC
  DIHEdral P    OD   CC   CD
  DIHEdral OD   CC   CD   CE
  DIHEdral CC   CD   OE   C1A
  DIHEdral CC   CD   CE   OG
  DIHEdral CD   OE   C1A  C1B
  DIHEdral CD   CE   OG   C2A
  DIHEdral OE   C1A  C1B  C1C
  DIHEdral C1A  C1B  C1C  C1D
  DIHEdral C1B  C1C  C1D  C1E
  DIHEdral C1C  C1D  C1E  C1F
  DIHEdral C1D  C1E  C1F  C1G
  DIHEdral C1E  C1F  C1G  C1H
  DIHEdral C1F  C1G  C1H  C1I
  DIHEdral C1G  C1H  C1I  C1J
  DIHEdral C1H  C1I  C1J  C1K
  DIHEdral C1I  C1J  C1K  C1L
  DIHEdral C1J  C1K  C1L  C1M
  DIHEdral C1K  C1L  C1M  C1N
  DIHEdral CE   OG   C2A  C2B
  DIHEdral OG   C2A  C2B  C2C
  DIHEdral C2A  C2B  C2C  C2D
  DIHEdral C2B  C2C  C2D  C2E
  DIHEdral C2C  C2D  C2E  C2F
  DIHEdral C2D  C2E  C2F  C2G
  DIHEdral C2E  C2F  C2G  C2H
  DIHEdral C2F  C2G  C2H  C2I
  DIHEdral C2G  C2H  C2I  C2J
  DIHEdral C2H  C2I  C2J  C2K
  DIHEdral C2I  C2J  C2K  C2L
  DIHEdral C2J  C2K  C2L  C2M
  DIHEdral C2K  C2L  C2M  C2N

  IMPRoper CD   OE   CE   CC
  IMPRoper C1A  OE   OF   C1B
  IMPRoper C2A  OG   OH   C2B
END
```

VITA

Tara Marcink was born in New York, USA. She received her Bachelor's of Science degree in Chemistry at Missouri State University in 2012. Afterward she enrolled in the University of Missouri to pursue a PhD in Biochemistry under the guidance of Dr. Steven Van Doren. She defended her Thesis in April of 2018 and received her PhD.